NASA
Technical
Paper
2273

AVSCOM
Technical
Report
83-A-17

February 1984

Airfoil Interaction With an Impinging Vortex

K. W. McAlister
and C. Tung

NASA

NASA Technical Paper 2273

AVSCOM Technical Report 83-A-17

1984

Airfoil Interaction With an Impinging Vortex

K. W. McAlister
and C. Tung

Aeromechanics Laboratory
USAAVSCOM Research and Technology Laboratories
Ames Research Center
Moffett Field, California

NASA
National Aeronautics
and Space Administration

Scientific and Technical Information Branch

SYMBOLS

C chord of downstream airfoil, m

C_d drag coefficient

C_ℓ lift coefficient

C_m quarter-chord pitching-moment coefficient

c chord of generator airfoil, m

Re Reynolds number, $U_\infty C/\nu$

r radial distance from the vortex center, m

U_∞ free-stream velocity, m/sec

w circumferential-velocity component, m/sec

α airfoil incidence, deg

$\tilde{\alpha}$ generator incidence, deg

Γ circulation

ν kinematic viscosity, m^2/sec

SUMMARY

The tip of a finite-span airfoil was used to generate a streamwise vortical flow, the strength of which could be varied by changing the incidence of the airfoil. The vortex that was generated traveled downstream and interacted with a second airfoil on which measurements of lift, drag, and pitching moment were made. The flow field, including the vortex core, was visualized in order to study the structural alterations to the vortex resulting from various levels of encounter with the downstream airfoil. These observations were also used to evaluate the accuracy of a theoretical model.

1. INTRODUCTION

The vortices that are generated by missiles, canards, wings, and rotor-blade tips often have a detrimental effect on the flow fields of other control or lifting surfaces. One of the most elementary models of this type of flow interaction is provided by the passage of a streamwise vortex near a downstream lifting airfoil. For an accurate calculation of this flow field, it is necessary to correctly account for (1) the time-varying viscous structure of the vortex; (2) the three-dimensional viscous flow over the airfoil, including the shedding of its own wake; and (3) the nonlinear path of the vortex resulting from its interaction with the airfoil. From the experimenters' point of view, the challenge is (1) to produce a fully developed, steady, and well-defined vortex in the flow, without the attendant wake of the generator, (2) to correctly scale the vortex-airfoil interaction, and (3) to provide suitable measurements in sufficient detail to meet the level of evaluation required.

The mathematical model for the impinging vortex has ranged in complexity from that of an inviscid-line vortex fixed along a rectilinear path, to a viscous-core vortex developing along an unprescribed path. Similarly, the mathematical model for the interacting airfoil has evolved from a simple lifting-line theory to a dense vortex-lattice representation (refs. 1-3). Numerous experiments have been performed to assess the value of various combinations of these computational models, as well as to define the flow field and resultant loads on the airfoil during the interaction. These studies have shown that when details of the flow are required (such as airfoil pressure distribution) during a close vortex encounter (roughly within one core diameter), only the most comprehensive models are capable of providing calculations with acceptable accuracy. In those cases in which the vortex interaction is severe enough to cause separation on the airfoil, the choice of models must be narrowed to the few that include the boundary layer. Furthermore, the boundary-layer model must be three dimensional to account for the strong spanwise flow component caused by the interaction (ref. 4). Recognition of the boundary layer is an important factor in determining the full effect of the vortex-airfoil interaction since vortex-induced separation on the airfoil has been found to substantially limit the extent of the induced loads (ref. 5). Only recently have codes become available that are capable of treating the vortex interaction problem where flow separation is present (ref. 6), and the results from one of these will be examined in light of the present experiment.

Although many noteworthy vortex interaction studies have preceded this investigation, some aspects of the problem have not been sufficiently addressed and therefore remain in question. Specifically, these questions concern the alterations to both the trajectory and stability of the vortex, as well as the overall performance of the airfoil resulting from the interaction. This subject can be most simply addressed by considering the case for a streamwise-oriented vortex encountering a two-dimensional lifting airfoil. Those questions pertaining to the vortex are (1) Does the path of the vortex essentially conform to the streamline pattern existing for the airfoil alone? (2) To what extent does the strength of the vortex influence its trajectory? and (3) Is proximity to the airfoil sufficient to cause an appreciable diffusion or breakdown of the vortex? Those questions regarding airfoil performance are (1) How does the presence of a nearby vortex (either passing above or below the airfoil) affect the airfoil stall? and (2) To what extent are the total pre-stall loads on the airfoil affected by a direct vortex impingement? These questions were to be addressed in the present experiment by visualizing the vortex and the airfoil boundary layer, along with direct measurements of airfoil lift, drag, and pitching moment.

In addition to obtaining certain physical insights into the subject of vortex-airfoil interactions, there was an interest in comparing the results of the experiment with the calculations of a promising mathematical model. This comparison would not only provide an opportunity to evaluate the accuracy of

the model, but would also form the basis on which any refinements to the model are made.

The authors would like to acknowledge and express their appreciation to Rabindra Mehta, T. T. Lim, and Raymond Piziali, who reviewed the original manuscript. They provided valuable challenges to various technical issues raised by the authors, and in so doing, contributed greatly to the readability and accuracy of the final report. The authors would also like to thank Brian Maskew (Analytical Methods, Inc.) for contributing the theoretical model, for supporting the comparison with the experimental results in an unbiased manner, and for so kindly providing counsel whenever it was required.

2. DESCRIPTION OF THE EXPERIMENT

This study was conducted in the 4000-liter, closed-circuit water tunnel facility at the Aeromechanics Laboratory, Ames Research Center (fig. 1). This was a particularly suitable facility for this investigation because of the ease of obtaining definitive visualizations of the vortex and the advantage of examining on-line the resultant loads on the airfoil during the interactions. The technique for visualizing the flow was based on the generation of minute hydrogen bubbles through electrolysis of a weak solution of sodium sulfate and water. Loads were measured directly by an external apparatus that served as both support and balance for the airfoil.

The airfoil selected for this study was a NACA 0012 having a two-dimensional planform of 10 cm (chord) by 21 cm (span). The test section measures 31 cm (height) by 21 cm (width), and the airfoil was positioned so that it spanned the width of the section to within 0.015 cm on either side. The airfoil was cast of an electrically nonconducting fiber resin, with platinum electrodes placed at nine chordwise locations along the upper surface. The bubbles that were generated at these electrodes were transported downstream by the fluid in the boundary layer and wake, thus enabling the thickness and eventual separation of the boundary layer to be observed.

The vortex was generated by placing a semispan airfoil at incidence in the free stream ahead of the NACA 0012 airfoil. The vortex generator was a NACA 0015 airfoil with a rectangular planform and a 5-cm chord (fig. 2). Two vortex generators were constructed from an electrically nonconducting fiber resin. When installed, in turn, on the upper test section wall (fig. 3), the tip of one generator would extend to the centerline of the tunnel and therefore be on line with the pitch axis of the downstream airfoil (generator aspect ratio of 3); the tip of the other generator would be 0.5 c above the downstream airfoil (generator aspect ratio of 2). Two electrodes were placed on each vortex generator. One of the electrodes was located on the pressure side of the generator; it extended over 80% of the chord in a streamwise direction and was inboard from the tip a distance of 0.1 c. This electrode was used to visualize the tip vortex. By generating bubbles on the pressure side and allowing them to be advected around the tip to the suction side, the authors believe that a more accurate picture of the coalescing and shedding behavior of the tip-vortex core is obtained. The second electrode was located on the suction side of the generator, extended over 1.3 cm in a spanwise direction, and was upstream from the trailing edge a distance of 0.2 c. This electrode was used to monitor flow separation on the generator. A third electrode was attached to the tip of the generator at the quarter-chord location, and was stretched across the flow to a connection point on the lower test-section window. The purpose of this electrode was to visualize the helical structure of the vortex outside of the core region. The pitch axes of both the generator and the airfoil were located at their respective quarter-chords, and a distance of four generator-chord lengths separated the two axes (fig. 4). This arrangement provided a vortex maturation distance of 2.75 c from the trailing edge of the generator to the leading edge of the airfoil.

The spar of the airfoil extended through the test-section windows and was supported by lift and drag transducers on both sides (fig. 5). One end of the spar was adjoined to an instrumented drive shaft through a torsionally stiff coupling so that airfoil incidence could be set and the pitching moment measured. Static frictional moments imparted by the support bearings and seals were also measured and later treated as load tares. Only quantities relating to the airfoil were electrically instrumented: incidence, lift (both sides), drag (both sides), total pitching moment, and the bearing and seal moments (both sides). After amplification, the signals were either appropriately summed (i.e., total pitching moment minus both frictional moments) and displayed on local monitors or they were transmitted to a remote data acquisition system where they were digitized, averaged, and stored for later processing. It is estimated that both airfoil and generator incidence were set to an accuracy of 0.2° during the test. Lift and drag measurements are considered to be accurate to 0.01 N and the pitching moments to 0.002 N•m.

The bubbles were illuminated by a sheet of light (about 5 cm wide) directed through the upper test-section window and covering a length of 30 cm in the free-stream direction (fig. 6). Both continuous and flash sources of light were produced over this length. The continuous source of light was provided by a single 1000-W quartz-halogen lamp; the lamp was used for general viewing, as well as for long-duration exposures (20 sec in this experiment). The flash source of light was obtained from a 10,000-W xenon lamp that could either be synchronized to the shutter of a high-speed camera or operated in a single-flash mode with a view camera. A second xenon lamp (not shown in fig. 6) was directed upward through the lower test-section window to provide an equal amount of illumination from below the airfoil.

The tunnel was operated at two fixed drive speeds during this experiment. With the airfoil set at zero incidence, the dynamic pressures for these two speeds were 0.10 lb/in.^{2} and 0.025 lb/in.^{2}; they are equivalent to Reynolds numbers of 120,000 and 60,000, respectively, based on an airfoil chord of 10 cm. Some reduction in tunnel speed is thought to have occurred when the airfoil was stalled; however, no attempt was made either to measure or account for this degradation.

The scope of the experiment was limited to discrete values of incidence for the generator and airfoil. The airfoil was placed at both positive and negative values of incidence, and at angles ranging from 0° to beyond stall (in 1° increments). Three free-stream conditions ahead of the airfoil were considered. First, a control case in which no vortex generator was present. Second, a mild interaction case resulting from a short vortex generator (tip off centerline) being placed in the stream at angles of 0°, 5°, and 10°. Third, a severe interaction case resulting from a long vortex generator (tip on centerline) being placed in the stream at angles of 0°, 5°, and 10°. Lift, drag, and pitching moment measurements on the airfoil were made at Re = 120,000. Flow visualizations were made at both Re = 60,000 and Re = 120,000, with corresponding velocities of 0.58 m/sec (1.9 ft/sec) and 1.16 m/sec (3.82 ft/sec).

3. DESCRIPTION OF THE THEORY

The particular theoretical model to be used for comparison with the experimental data is a panel method formulation using Green's theorem. The code is capable of calculating the trajectory of the vortex, as well as the resulting loads on the airfoil arising from the interaction. A detailed description of the method is given in reference 7; however, a brief discussion will be presented here for convenience.

The surface of the wing is approximated by a set of flat panels consisting of uniform sources and doublets. The source strength of each panel is determined by the local external Neumann boundary condition and the strength of each doublet distribution is determined from a set of simultaneous linear equations explicitly specifying the internal Dirichlet boundary condition of zero perturbation potential. The wake generated by the flow over the airfoil is also represented by flat panels of uniform doublet singularities. All wake panels along a streamwise column have the same doublet strength as determined by the zero-load condition at the trailing edge heading that column. When the flow is separated from the leading edge, the wake is enclosed by a pair of free-shear surfaces, each having a doublet distribution of linear strength in the streamwise direction and of constant strength in the crossflow direction. The code also provides for a fully coupled boundary-layer calculation in order to account for the viscous-inviscid interaction.

4. DISCUSSION OF RESULTS

Flow Visualization at Re = 60,000

The tip of the vortex generator was located on the centerline of the tunnel and was, therefore, geometrically on line with the pitch axis of the downstream airfoil. The vortex generator was set to three angles of incidence, $\tilde{\alpha}$ = 0°, 5°, and 10°; and for each of these angles the downstream airfoil was varied from -16° to +16° (figs. 7-9). By placing the generator at 0° incidence, a control case (fig. 7) was established against which the effects of the vortex on the streamlines around the airfoil could be evaluated. For brevity, the upstream airfoil that was responsible for producing the tip vortex will be referred to simply as the "generator" while the downstream airfoil that interacted with the vortex will be referred to as the "airfoil."

Rotating the generator to 5° incidence caused a weak vortex to be produced (fig. 8). The hydrogen bubbles that were formed along the electrode on the pressure side of the generator were swept around the tip to form a relatively large vortex core. The bubbles that were produced along the free-stream electrode near the generator tip are seen to form the outer helical structure of the vortex. Since the core of the vortex leaves the trailing edge of the generator at a slightly inboard location, the central portion of the vortex passes above the airfoil even when the airfoil is at a small negative incidence. Furthermore, it appears that the vortex survives its encounter with the airfoil over an incidence range from about -2° to +8°. At +9° incidence, however, the buffeting effects of the separated flow over the trailing edge of the airfoil causes the vortex to become unstable. At +10° incidence the flow separates from the leading edge and causes the vortex to become unstable before reaching the trailing edge of the airfoil. This instability appears to grow until the vortex becomes unrecognizable after passing about one airfoil-chord length into the wake. As the airfoil incidence increases further, the distance over which the vortex can still be recognized behind the trailing edge of the airfoil decreases. Because of the irregular and large-scale structure of the wake behind the airfoil during static stall conditions, the interaction between the vortex and the airfoil should be considered an unsteady process.

The streamlines of the flow ahead of the airfoil are also affected by the presence of the vortex. However, considerable care must be taken when interpreting these results because the vortex imparts a helical component to the flow field, as a result of which the streamline visualizations nowhere represent a two-dimensional cross section of the flow. Accordingly, these results must be interpreted with caution. Considering the airfoil at an incidence of +8°, and comparing the weak-vortex case (fig. 8) with the no-vortex case (fig. 7), it is apparent that two major changes have taken place. First, the vortex (which is rotating counterclockwise

when viewed along a downstream direction) has lifted the neighboring flow ahead of the airfoil (on the upwash side of the vortex) by one streamline; and second, the separated zone over the rear portion of the airfoil has increased greatly. Comparing this flow with that for the case without a vortex (fig. 7), and focusing on the airfoil at +10° incidence, suggests that the effect of the vortex is to induce an increase in the angle of attack by approximately +2° (based on the amount of separation present in each case). Recalling that these observations are applicable only to the upwash side of the helical flow, it is important to note that a similar (though not visible) but opposite condition must be occurring on the downwash side. Since the core of the vortex not only appears as a dense band of bubbles, but is central to the vortical motion, an evaluation of its trajectory is more straightforward. The vortex core seems to move inboard from the generator tip as it approaches the airfoil, cutting across the streamlines that occur in the no-vortex case (see fig. 7 for -8° and +8° incidence); but after reaching the suction peak on the airfoil, the core closely follows the no-vortex streamlines. At an incidence of -2° (fig. 8), the outer part of the vortex interacts strongly with the flow along the pressure side of the airfoil. The vortex core is still visible, but the outer helical streamlines disappear and instead become a cloud of bubbles. At more negative angles of incidence, the vortex becomes even more disorganized as it is pulled toward the airfoil. When the airfoil is at -8° incidence, the vortex nearly impacts on the pressure side of the airfoil close to the leading edge. However, for more negative angles of incidence, the vortex is driven away slightly from the airfoil surface. In addition, an instability of the vortex core progresses upstream from the wake (at -10° incidence), to the trailing edge (-11°), and finally to a point ahead of the airfoil (-12°).

Rotating the generator to 10° incidence causes a much stronger vortex to be produced (fig. 9). Although the trend is essentially the same as that observed for the weak-vortex case, certain features can be described with greater clarity because of the more conspicuous behavior of the flow. In comparing the weak-vortex flow field (fig. 8) with that occurring for the strong vortex (fig. 9) when the airfoil is at zero incidence, several observations can be readily made. First, the bubbles comprising the vortex core are confined to a more slender filament, no doubt a result of a greatly reduced static pressure along the vortex core. Second, and in keeping with a vortex of greater strength, the streamlines that form the outer helical portion of the vortex are clearly twisting at a much higher angular rate. Third, the core of the vortex continues to leave the generator at about the same slightly inboard position (0.09 c above centerline-grid line), in spite of the difference in vortex strength. With regard to the stability of the vortex core over the positive incidence range of the airfoil, there is no significant difference between the weak and strong vortex cases. The main difference between the two cases occurs in the streamlines ahead of the airfoil. Referring to the +8° of incidence case, for example, the strong vortex (fig. 9) causes the neighboring flow ahead of the airfoil (on the upwash side of the vortex) to be lifted by two streamlines (compared to the no-vortex case, fig. 7), whereas the weak vortex (fig. 8) shifted the flow by only one streamline. In terms of induced separation over the airfoil, the sequence of flows shown in figures 7-9 indicates that separation occurs at slightly over 9° in the presence of a strong vortex, at slightly under 10° for a weak vortex, and probably at about 11° when no vortex is present.

With regard to the trajectory of the core of the vortex in the +8° of incidence case, for example, there appears to be no difference between the weak- and strong-vortex cases. Although core instabilities were observed in the weak-vortex case for -4° of airfoil incidence, their appearance is even more striking during the strong-vortex interactions. Whereas the core never quite collided with the airfoil in the weak-vortex case, a direct impingement occurs at -6° of incidence in the strong-vortex case. Direct impingement causes a wide band of bubbles, with no apparent organized structure, to appear in the wake of the airfoil. Continuing to focus on the strong-vortex case, at -8° of incidence some degree of periodicity can be seen in the wake flow after passing over the suction side of the airfoil, and, at -10°, the scale of this periodicity increases. At -11° of incidence, a particularly interesting event occurs. The core of the vortex just ahead of the airfoil appears to undergo a helical distortion that is characteristic of an unstable vortex. After colliding with the airfoil, the flow breaks down over the pressure side of the airfoil and is shed into the wake with a clearly periodic organization (about 11.5 Hz). At -12° of incidence, the location of this presumed vortex instability moves upstream about one half of a generator-chord length ahead of the airfoil. A similar breakdown of the vortex has been reported in a smoke visualization test (ref. 8) of a vortex impinging on a downstream airfoil.

Flow Visualization at Re = 120,000

The tip of the vortex generator was located on the centerline of the tunnel, as well as offset from the centerline a distance equal to one half of the generator chord. The vortex generator was set to three angles of incidence, $\tilde{\alpha}$ = 0°, 5°, and 10°; and for each of these angles the downstream airfoil was again varied from -16° to +16° (figs. 10-12). The increase in Reynolds number for these results was obtained by doubling the free-stream velocity. Since the duration of the light pulse was not changed during this test, the particle-path lengths at this higher speed will appear twice as long. Although this streaking effect tends to lessen the clarity of the inviscid portion of the flow field, it will aid in the identification of turbulent and rotational motions that occur in the viscous portion of the flow field. In addition to the short-duration exposures obtained using the strobe, long-time exposures (20 sec) of the flow were made using a continuous

light source. The main purpose of the long exposures was to obtain an accumulated visual record of the trajectory of the vortex core in order to distinguish between regions having a concentrated and well-defined vortex path and those where lateral excursions and possible instabilities are present. Included in these visualizations is a section of the boundary layer exposed by hydrogen bubbles that were generated along the chord of the airfoil. These bubbles are believed to have had no measurable effect on the interaction. Although the evidence is not conclusive, it was observed that as the number of bubbles was increased (by increasing the voltage on the electrodes) for photographic purposes, no change was observed in either the thickness of the boundary layer or in the proximity of the vortex to the airfoil. However, the meaning of these visualizations requires some consideration. Since the region of the interaction between the vortex and boundary layer is known to be highly three dimensional, the fact that only a narrow spanwise portion of the boundary layer was visualized should be kept in mind when interpreting the results. In the following discussions, the short-exposure results will be addressed first, and in more detail.

Vortex generator on centerline– Once again, by placing the generator at 0° incidence, a control case (fig. 10) was produced against which comparisons could be made. There are essentially no differences between these results and those obtained at the lower Reynolds number, except that a more definite Karman-vortex street can be detected in the bubbles emanating from the trailing edge of the generator.

Rotating the generator to 5° incidence produces a vortex core that is more visible (fig. 11) than the one obtained under the same conditions at the lower Reynolds number (fig. 8). The presence of a more visible core could be caused by either a vortex of greater strength (therefore attracting more bubbles because of the lower static pressure) or a visual reinforcement of the core filament because of the streaking allowed by the finite-time exposure. Another distinction is that the neighboring flow ahead of the airfoil is shifted upward by about one additional streamline (compare, for example, the +8° of incidence flows in figs. 8 and 11). This additional uplifting of the streamlines could be a result of either a vortex of greater *local* strength (to be discussed momentarily) or an increase in the size of the vortex so that the region of high rotational velocity has moved farther away from the center. In all other respects, however, the trends observed earlier at the lower Reynolds number with regard to the stability of the vortex core and the induced separation over the airfoil remain essentially the same. One interesting behavior that appears to be more distinct at the higher Reynolds number concerns the vortex instability over the airfoil. When the airfoil stalls at +10° of incidence (fig. 11), the vortex core appears to undergo a more obvious helical twisting motion.

The explanations given above for the additional uplifting of the streamlines when the free-stream velocity was increased may require some further discussion. Based on classic aerodynamic theory, the swirl angle of a fully developed vortex can be argued to be independent of the free-stream velocity. To demonstrate this point, consider the expressions for the circulation on the generator, $\Gamma = C_Q U_\infty c/2$, and the circumferential velocity component of an inviscid vortex, $w = \Gamma/4\pi r$. These two equations can be combined to obtain $w = C_Q U_\infty c/8\pi r$. An approximation for the swirl angle can, therefore, be given by $\theta \approx w/U_\infty = C_Q c/8\pi r$, which is independent of the free-stream velocity. To some extent this conclusion is inexact because of the neglect of viscous effects. It is more significant, however, that the arguments given cannot be strictly applied in the vortex-development region behind the generator. The extent of this development region for a rectangular planform has been shown to be about 4 chord lengths behind the generator (ref. 9). During that time, reported measurements of the maximum circumferential velocity of the vortex indicated that the swirl angle decayed approximately 50% before the roll-up was complete.

Rotating the generator to 10° incidence produces a flow (fig. 12) that, except for the differences noted above for the 5° case, is quite similar to that observed at the lower Reynolds number (fig. 9). The maximum theoretical circulation on the generator for this case is $\Gamma = 0.28$. Some of the events that are more obvious in the higher Reynolds number visualizations (fig. 12) concern the vortex impingement at angles below -9° incidence. The region of vortex instability ahead of the airfoil from -9° through -16° incidence is much more pronounced. In addition, the breakdown of the flow on the pressure side of the airfoil into periodically shedding structures (about 23 Hz) is even more evident.

The same range of conditions for the generator and airfoil were considered for the long-exposure visualizations (figs. 13-15). When the generator is placed at 0° of incidence, the bubbles that were produced near the tip (side opposite from view) are observed to leave the trailing edge over a broad band (fig. 13), instead of in a straight line directly downstream of the electrode. This band can also be seen in the short-exposure results (although less distinctly) and is due to the slight spanwise-pressure gradient that drives the bubbles inboard over the generator surface and away from the tip. It may be useful to note that this band of bubbles provides a white background against which the black trailing edge of the generator can be easily identified in the photographs. Keeping in mind that these bubbles are all produced on the pressure side of the generator, the influence of the vortex on the flow near the tip can be better appreciated when it is realized that nearly all of these bubbles are drawn around the tip and become a part of the vortex core on the upper surface just as it leaves the trailing edge (fig. 14). This sweeping of fluid around the tip is even more dramatic when the strength of the vortex is increased (fig. 15). This increase in swirl angle is probably caused by the upstream movement of the origin of the vortex on the upper surface of the generator (ref. 10).

Aside from the helical trajectory of the path of the strong-vortex core (fig. 15) that extends over a distance of 1.5 c downstream of the generator, the path of the vortex core *appears* to be well defined and two dimensional as long as the viscous region around the airfoil is avoided (from 0° to +8° incidence in figs. 14 and 15). Although the path of the vortex seems to be two dimensional over this distance, it is actually more likely that some amount of transverse movement (normal to the plane of view) is present as the vortex encounters the circulation field around the airfoil. In fact, this type of transverse distortion of the path of the vortex is clearly evident in the results obtained in a similar experiment (ref. 11), which included a side view and a plan view of the vortex-airfoil interaction.

At -4° incidence the vortex can be distinguished from the boundary layer in the weak-vortex case (fig. 14); however, a large thickening (and probable weakening owing to viscous effects) of the vortex appears to have resulted from the interaction in the strong-vortex case (fig. 15). At more negative values of incidence, some thickening (or meandering) of the vortex can be observed upstream of the airfoil. However, the condition (or even survival) of the vortex after mixing with the highly dissipative flow around the airfoil is not certain. Considering, on the other hand, positive angles of incidence for which the airfoil stalls (at or above +12°), interaction with the separated region clearly produces a wide band of vortex trajectories above the airfoil. This band, which appears to broaden as it moves downstream, is not to be interpreted as a vortex "burst" similar to that occurring over delta wings at high incidence. Short-exposure results (discussed earlier) have already established this to be a region in which the core usually still exists as a filament (although not always a stable one). This band indicates the extent to which the vortex is jostled during its encounter with an inherently unsteady separated zone.

Vortex generator off centerline– By offsetting the tip of the generator from the centerline of the tunnel a distance of one-half the chord of the generator, a relatively mild vortex-interaction environment is produced. Placing the generator at 0° incidence (fig. 16), as before, provides a basis of comparison with other cases. Considering that portion of the flow where streamlines exist for both conditions (that is, below the centerline of the tunnel), the flow appears to be independent of the extent to which the generator and its wake protrude into the test section. Although some disturbance to the flow moving around the generator tip is present in both cases, it has no observable effect on the stall of the downstream airfoil.

Rotating the generator to 5° incidence produces a vortex that passes well above the airfoil for the entire incidence range from -16° to +16° (fig. 17). Judging by the size of the vortex core, as well as by the rotational rate of the streamlines near the core, the vortex corresponding to the off-centerline case (fig. 17) may be weaker than the vortex in the on-centerline case (fig. 11). This reduction in tip-vortex strength could be attributed to an increase in the shedding of vorticity into the wake before reaching the tip (in short, an aspect-ratio effect). Although the vortex in this case is relatively weak and remote from the airfoil, it nevertheless induces the flow ahead of the airfoil to be shifted upward by about one-half streamline on the upwash side of the helical flow (compare, for example, the streamlines at zero incidence in fig. 16 with those in fig. 17). As long as the airfoil is not stalled, the vortex-airfoil interaction has no effect on the stability of the vortex core. Even when the airfoil stalls ($\alpha > 10°$) and the buffeting action of the separated wake interacts strongly with the vortex, there is still no clear evidence of an instability. Rather, the evidence seems to show that as long as a strong shear layer is not encountered, the vortex is able to withstand relatively large transverse pressure gradients without becoming unstable (see, for example, -12° incidence in fig. 17).

Rotating the generator to 10° incidence causes the vortex core and its surrounding helical streamlines to become more distinct (fig. 18). The flow ahead of the airfoil is now shifted upward about one streamline on the upwash side of the helical flow around the vortex core; this shift is about twice that observed for the generator at 5° incidence. Again, once the airfoil stalls, the path of the vortex core can be seen to go through large undulations as it interacts with the separated zone downstream of the airfoil. In some cases (note +14° and +16°), the vortex core appears to experience an instability.

The path of the vortex core during long exposures is shown in figures 19-21. The characteristics of the vortex are essentially the same as those in the close-encounter case with regard to its persistence while moving through the pressure field created by the airfoil. Since the viscous region around the airfoil is completely avoided, the interaction of the vortex with the airfoil is strictly potential. Once again, when the airfoil stalls, the boundary of the separated zone is unsteady and causes the core of the vortex to be buffeted over a band of trajectories.

Load Measurements at Re = 120,000

Lift, drag, and pitching-moment loads were measured at a Reynolds number of 120,000. Data were taken at 1° increments of airfoil incidence over a range from -16° to +16°. Because of the high density of data points, symbols have been omitted from many of the figures in order to allow a better examination of the curves that were constructed using straight-line connections between the points.

Of initial concern was the unavoidable presence of the generator wake and its possible effect on the loads of the downstream airfoil. Although the greatest disturbance to the flow field by the trailing-edge wake is created when the generator is placed at maximum incidence ($\tilde{\alpha}$ = 10°), its

influence on the airfoil loads cannot be separated from the more dominant effects of the tip vortex. The generator was, therefore, placed at zero incidence in order to produce a wake (albeit small), as well as a distortion of the flow around the tip (but without producing a vortex). The results, which are presented in figure 22, show that the presence of the generator in the free stream has essentially no effect on the airfoil loads, even when the generator extends to the centerline of the tunnel. Since some level of disturbance can be expected when the generator is at incidence, the orientation of the generator in the flow field with respect to the downstream airfoil in the present experiment has the advantage of placing the wake farther away from the airfoil than the vortex.

Placing the generator at incidence can be seen to have a definite effect on the airfoil loads, especially when the vortex makes a close encounter with the airfoil (fig. 23). The vortex causes the airfoil to experience an early stall and a reduced (more narrow) drag bucket. Note that only the pitching moment shows any significant change at angles below stall. This is probably caused by the presence of a laminar separation bubble, which becomes distorted so as to cause only a shift in the center of pressure. The behavior of this bubble, which no doubt is responsible for the kink in the lift curve and the non-zero slope in the moment curve over the unstalled range, is thought also to cause the stall to be different from what is observed at higher Reynolds numbers (refs. 12–14). Although the proximity of the vortex to the leading edge of the airfoil is quite dependent on the sense of the airfoil incidence (figs. 11 and 12), the vortex passes over the suction side of the airfoil at the point of stall and causes the same degree of early stall for both positive and negative values of incidence. Based on the onset of lift and moment stall (which appear to be more distinct than drag stall), the interaction causes an early stall by 1.6° in the weak-vortex case and by 2.3° in the strong-vortex case.

When the generator is off centerline, a more modest encounter with the airfoil results (fig. 24). The effects of the vortex interaction are greatly reduced over the unstalled region, but the same trends are observed as in the strong-interaction case (discussed above). Although there is a difference in the post-stall curves depending on whether the airfoil is at positive or negative incidence, it is interesting that the angle at which stall occurs does not appear to be affected by which side of the airfoil (pressure or suction) the vortex is on. The most significant difference probably appears in the sense of the rolling moment; however, this quantity was not measured in this experiment. In the present case the interaction causes an early stall by 0.8° in the weak-vortex case and by 1.7° in the strong-vortex case.

Theory at Re = 120,000

In order to better represent the conditions of the experiment, extra panels were added to the formulation to simulate the presence of the upper and lower tunnel walls. All of the computations were made for the close encounter, strong-vortex case. In other words, the generator tip was considered to be on centerline with an incidence of 10°. Comparisons with the experiment were made at three angles of airfoil incidence: α = +8°, +12°, and +16°. The calculated path of the vortex core will be discussed first.

Considering the case for the airfoil at +8° incidence, the computed results are shown in figure 25(a) in the form of streamlines leaving the trailing edge of the generator and passing over the downstream airfoil. The core of the vortex (shown as a dashed line) was computed to be the centroid of the circulation for the vortices in the tip roll-up. The encircled points were obtained from the experiment by making discrete-coordinate measurements along the mean trajectory of the vortex core (from fig. 21). This comparison shows a rather favorable agreement between theory and experiment.

The computation for the interaction with the airfoil at +12° incidence is shown in figure 25(b). For this calculation, wake-relaxation iterations were required to simulate the flow separation from the leading edge. After three iterations, good agreement with the experimental data was obtained ahead of the airfoil. However, in passing over the airfoil, the agreement remains good only when considering the inner boundary of the band of possible trajectories (the upper and lower boundaries are indicated by the two symbols at each location). Nevertheless, the agreement is classified as being generally good over the entire encounter, since it is beyond the scope of present-day codes to account for this type of unsteady separation behavior. The region of greatest disagreement is just downstream of the trailing edge of the airfoil, where the theoretical core appears to be diverging from that observed in the experiment. This may be attributable to the fact that calculations of the details of the roll-up were terminated before passing downstream of the airfoil.

Examining the results for the final case with the airfoil at +16° incidence (fig. 25(c)), the comparison between theory and experiment is not especially good. The calculations made with a "no-separation" restraint agree reasonably well with the experimental results ahead of the airfoil; however, the agreement is poor in the region over the airfoil. A second calculation, which allowed for separation on the airfoil, shows a very different trend; however, the agreement remains poor. Although some of the differences between the theory and the experiment can be reduced by increasing the panel density on the generator (ref. 15) as well as by accounting for the initial vortex development over the surface of the generator, it may be that the greatest improvement will come from a better separation model for the flow on the downstream airfoil.

Based on the VSAERO code, the computed lift, drag, and pitching-moment coefficients for the three angles of airfoil incidence are shown in figure 26. When the airfoil is stalled, it is clear that the first-iteration calculation (which assumes the flow is fully attached) is incorrect. However, the second-iteration calculation (which allows for flow separation) is in much better agreement with the experiment at $+16^\circ$. With the airfoil at $+12^\circ$, the code predicts a partial span separation over the upper surface, whereas the flow was apparently fully separated in the experiment. This difference is probably a result of the level of free-stream turbulence in the present experiment, as well as the strong buffeting character of the stall observed for this airfoil. A partial span separation can occur under certain conditions, as was the case reported in reference 11.

5. CONCLUSIONS

1. A vortex may survive distortions caused by modest values of transverse and axial pressure gradients more easily than it can shear along its axis.

2. Buffeting from a nearby separated region can initiate a vortex instability, with the path of the core itself assuming a helical shape.

3. An encounter between the vortex and the airfoil boundary layer causes the interacting flow to mix and emerge into the wake with no apparent vortex structure.

4. When the vortex impinges along the stagnation region of an airfoil (and becomes subject to a strong adverse axial pressure gradient), the core of the vortex becomes unstable ahead of the airfoil and is then transformed into a segmented and periodic structure as it moves over the surface of the airfoil.

5. The presence of the vortex was found to cause premature stall in every case in this experiment. The greater the strength of the vortex and the closer the encounter, the earlier the stall.

6. The extent to which early stall occurs appears to be independent of whether the vortex is on the pressure or suction side of the airfoil.

7. The theoretical model considered in this study accurately calculates the vortex trajectory and airfoil loads prior to stall. After stall, calculations for the vortex trajectory do not compare well with the experimental data; however, those for the loads are acceptable.

REFERENCES

1. Smith, W. G.; and Lazzeroni, F. A.: Experimental and Theoretical Study of a Rectangular Wing in a Vortical Wake at Low Speed. NASA TN D-339, 1960.
2. McMillan, O. J.; Schwind, R. G.; Nielsen, J. N.; and Dillenius, M. F. E: Rolling Moments in a Trailing Vortex Flow Field. NASA CR-151961, 1977.
3. Cheeseman, I. C.: Developments in Rotary Wing Aircraft Aerodynamics. Vertica, vol. 6, no. 3, 1982, pp. 181-202.
4. Ham, N. D.: Some Preliminary Results from an Investigation of Blade-Vortex Interaction. AHS J., Apr. 1974.
5. Ham, N. D.: Some Conclusions from an Investigation of Blade-Vortex Interaction. AHS J., Oct. 1975.
6. Maskew, B.; and Rao, B. M.: Calculation of Vortex Flows on Complex Configurations. ICAS-82-6.2.3., 13th Congress of the International Council of the Aeronautical Sciences, 1982.
7. Maskew, B.: Prediction of Subsonic Aerodynamic Characteristics – A Case for Low-Order Panel Methods. AIAA Paper 81-0252, St. Louis, Mo., 1981.
8. Patel, M. H.; and Hancock, G. J.: Some Experimental Results of the Effect of a Streamwise Vortex on a Two-Dimensional Wing. Aeronaut. J., Apr. 1974.
9. Chigier, N. A.; and Corsiglia, V. R.: Tip Vortices-Velocity Distributions. AHS 27th Annual National V/STOL Forum, 1971.
10. Hoffman, J. D.; and Velkoff, H. R.: Vortex Flow over Helicopter Rotor Tips. J. Aircraft, vol. 8, no. 9, 1971.
11. Mehta, R. D.; and Lim, T. T.: Flow Visualization of a Vortex/Wing Interaction. NASA TM-
12. Nakamura, Y.; and Isogai, K.: Stalling Characteristics of the NACA 0012 Section at Low Reynolds Numbers. Technical Report of National Aerospace Laboratory, NAL TR-175, 1969.
13. Nagamatsu, H.; and Cuche, D.: Low Reynolds Number Aerodynamic Characteristics of Low Drag NACA 63-208 Airfoil. AIAA 13th Fluid and Plasma Dynamics Conference, 1980.
14. Mueller, T. J.; and Jansen, B. J., Jr.: Aerodynamic Measurements at Low Reynolds Numbers. AIAA 12th Aerodynamic Testing Conference, 1982.
15. Maskew, B.: Predicting Aerodynamic Characteristics of Vortical Flows on Three-Dimensional Configurations Using a Surface-Singularity Panel Method. AGARD CP-342, 1983.

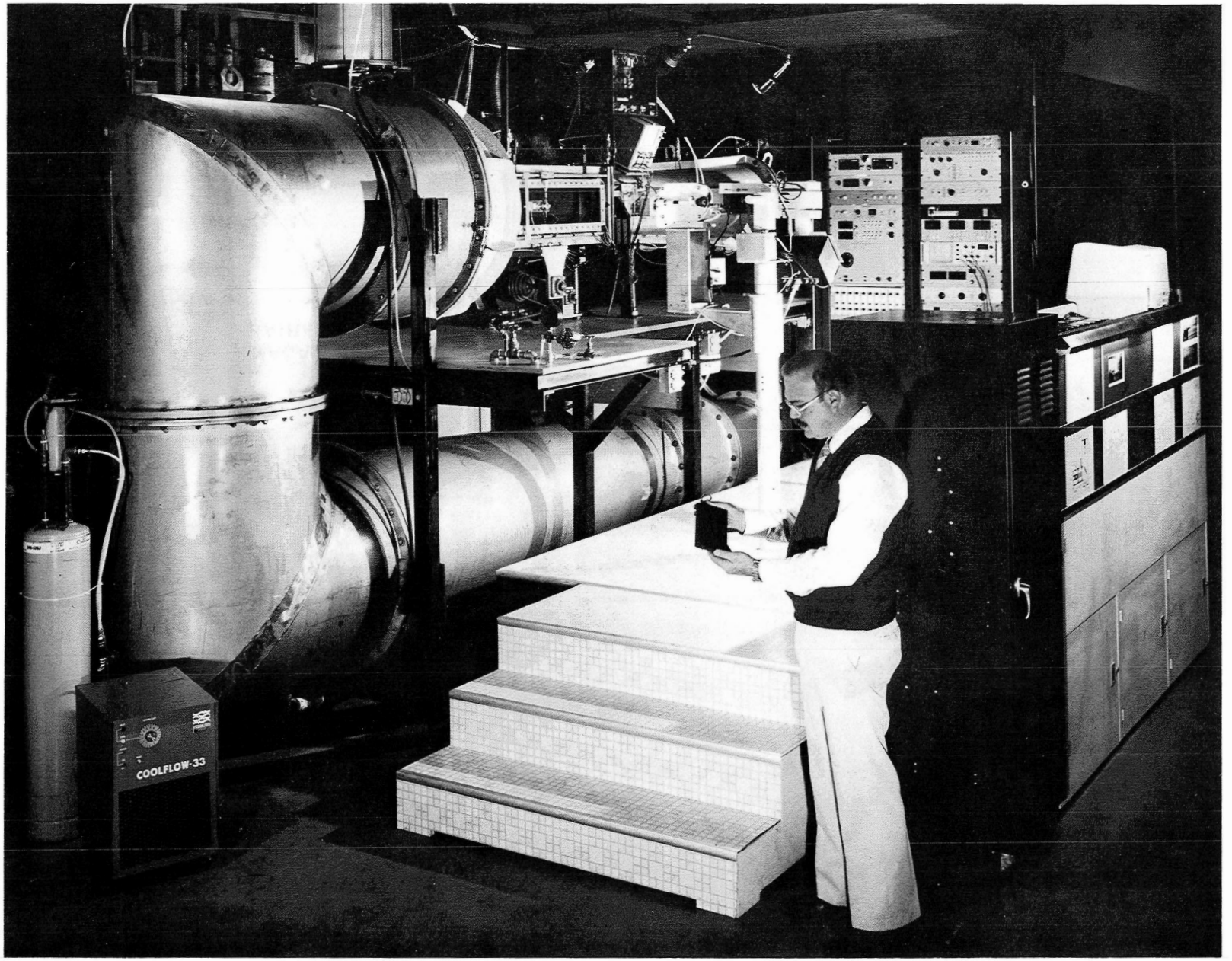

Figure 1.– Aeromechanics Laboratory's 21- by 31-Centimeter Water Tunnel.

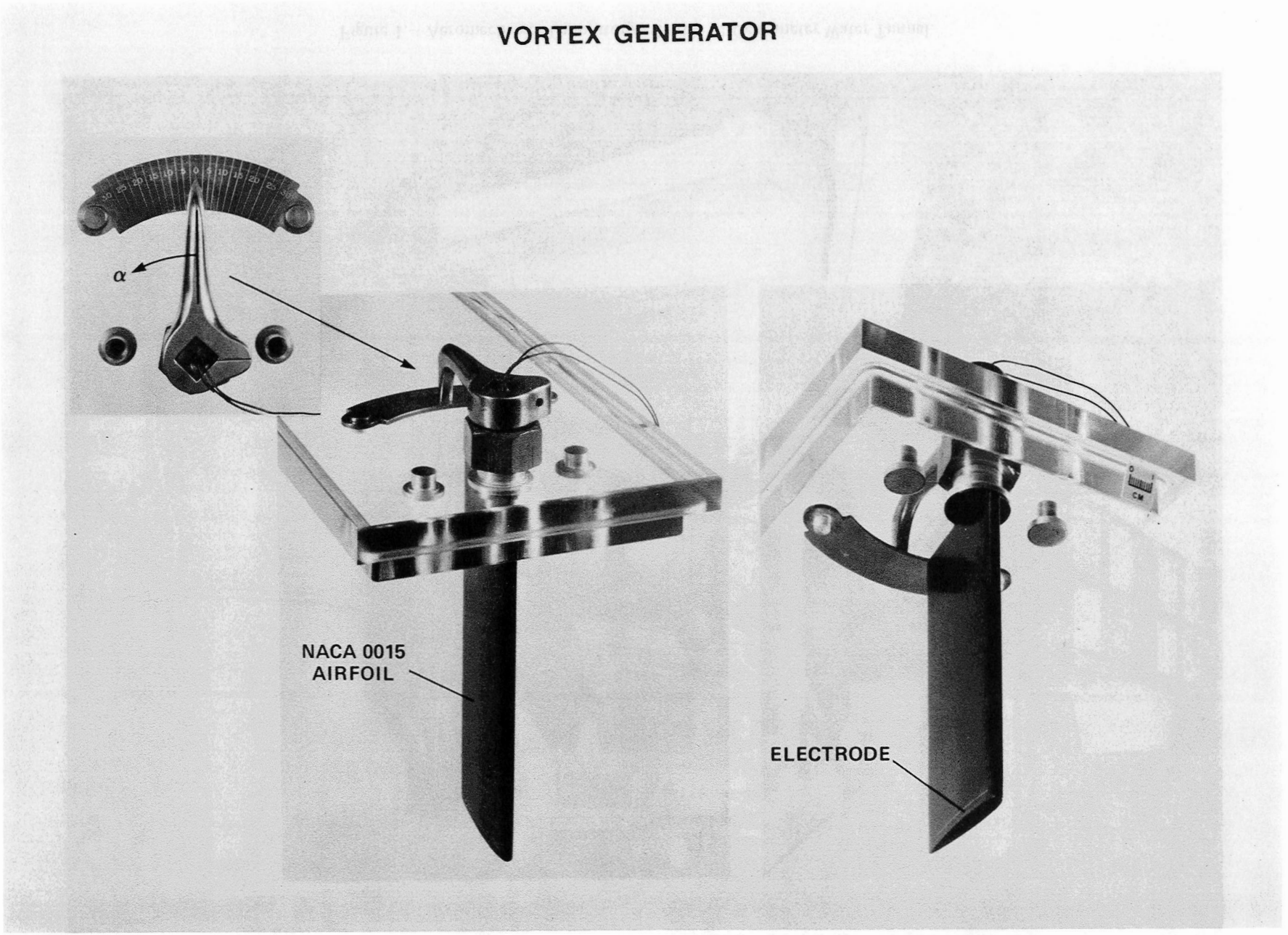

Figure 2.– Mounting of vortex generator on upper test-section window.

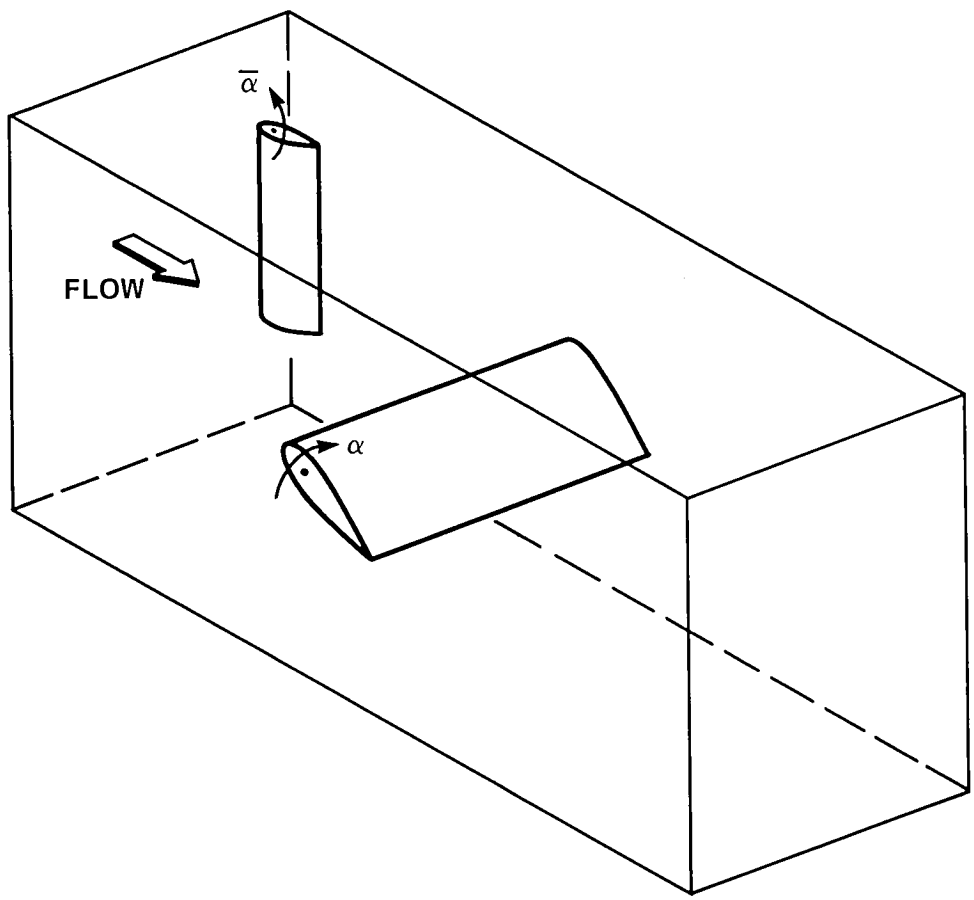

Figure 3.– Orientation of vortex generator and downstream airfoil in test section.

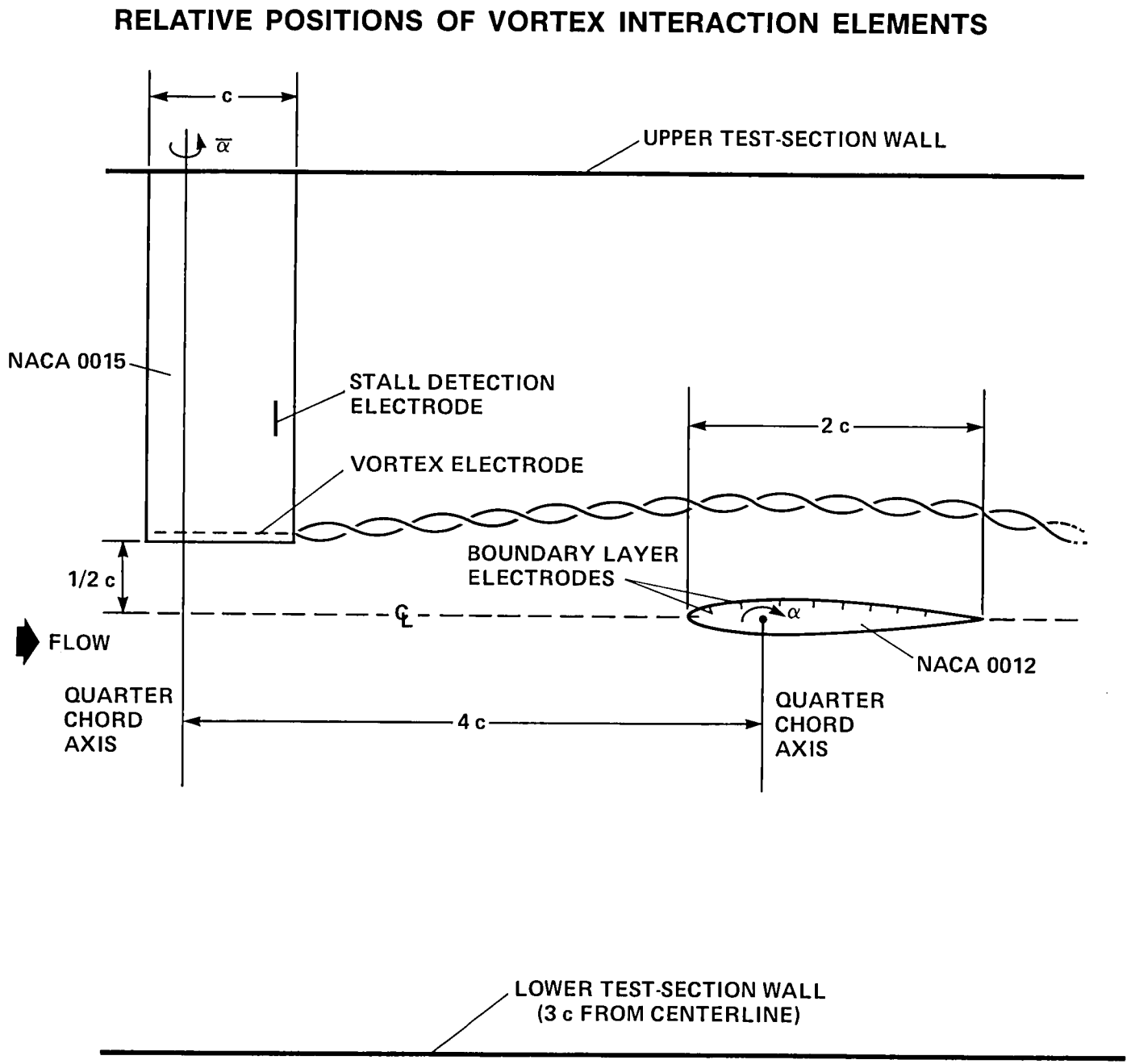

Figure 4.– Relative size and placement of generator and airfoil.

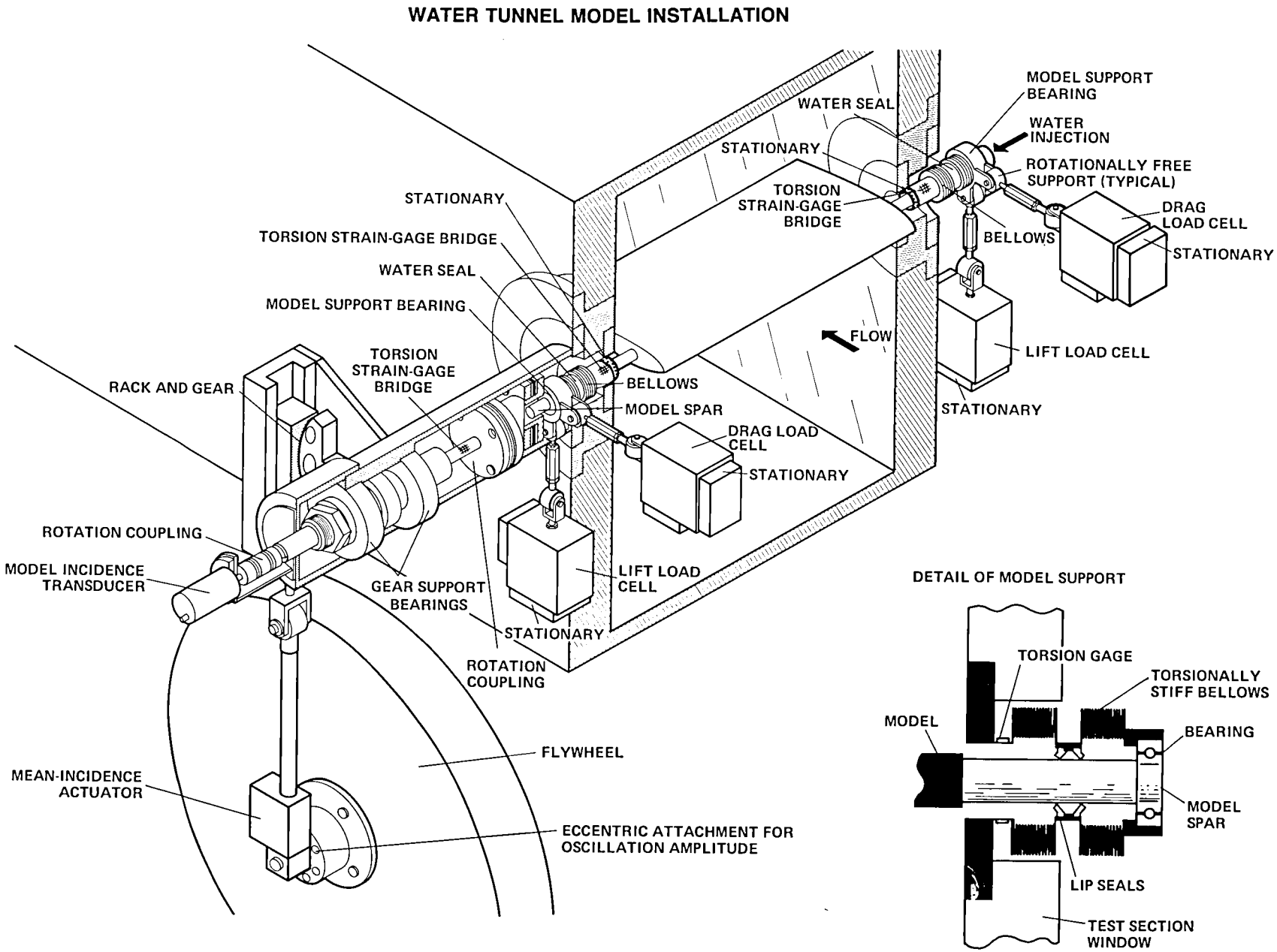

Figure 5.– Model installation and balance system for measuring lift, drag, and pitching moment.

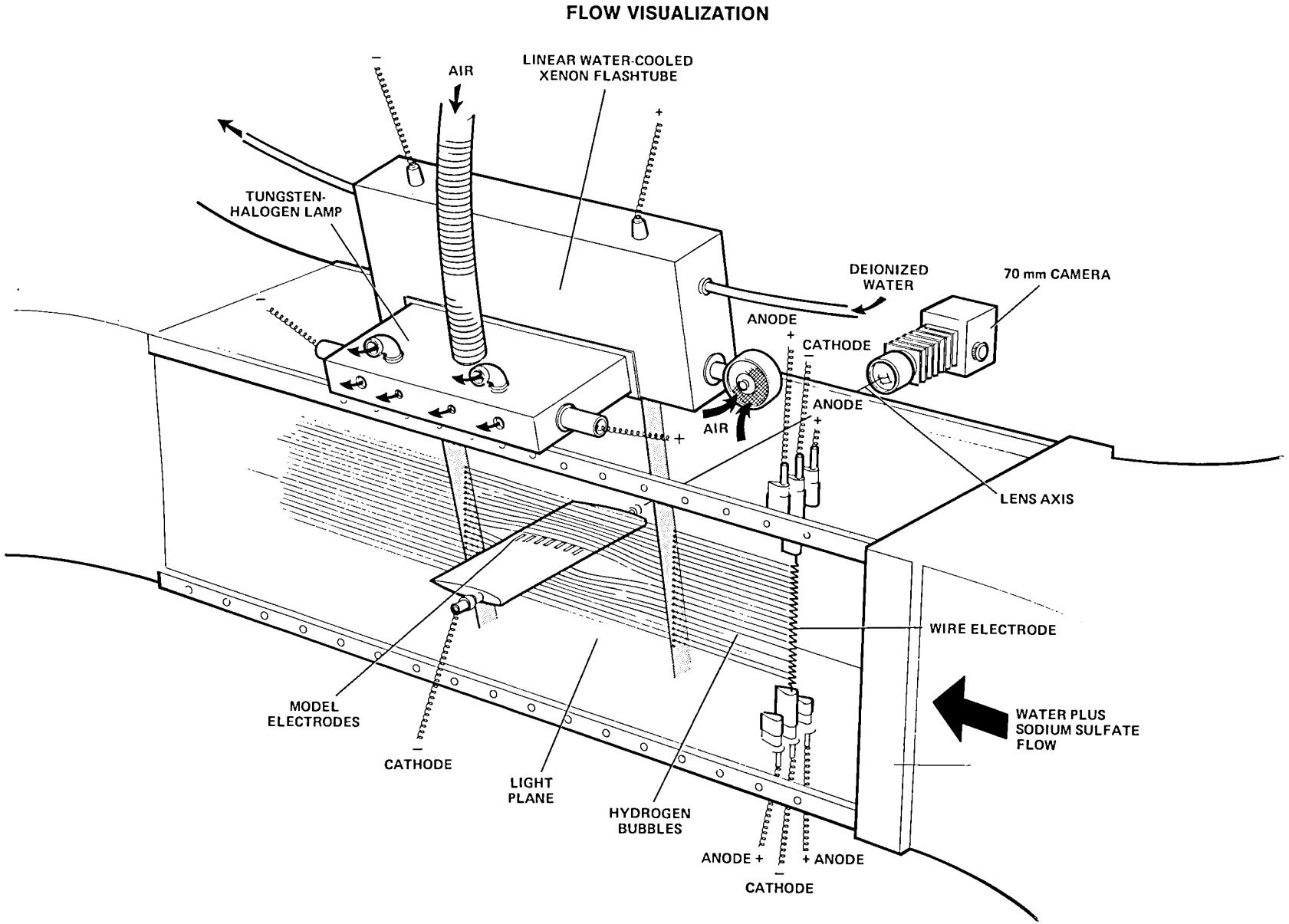

Figure 6.– Lighting system used to illuminate hydrogen bubbles.

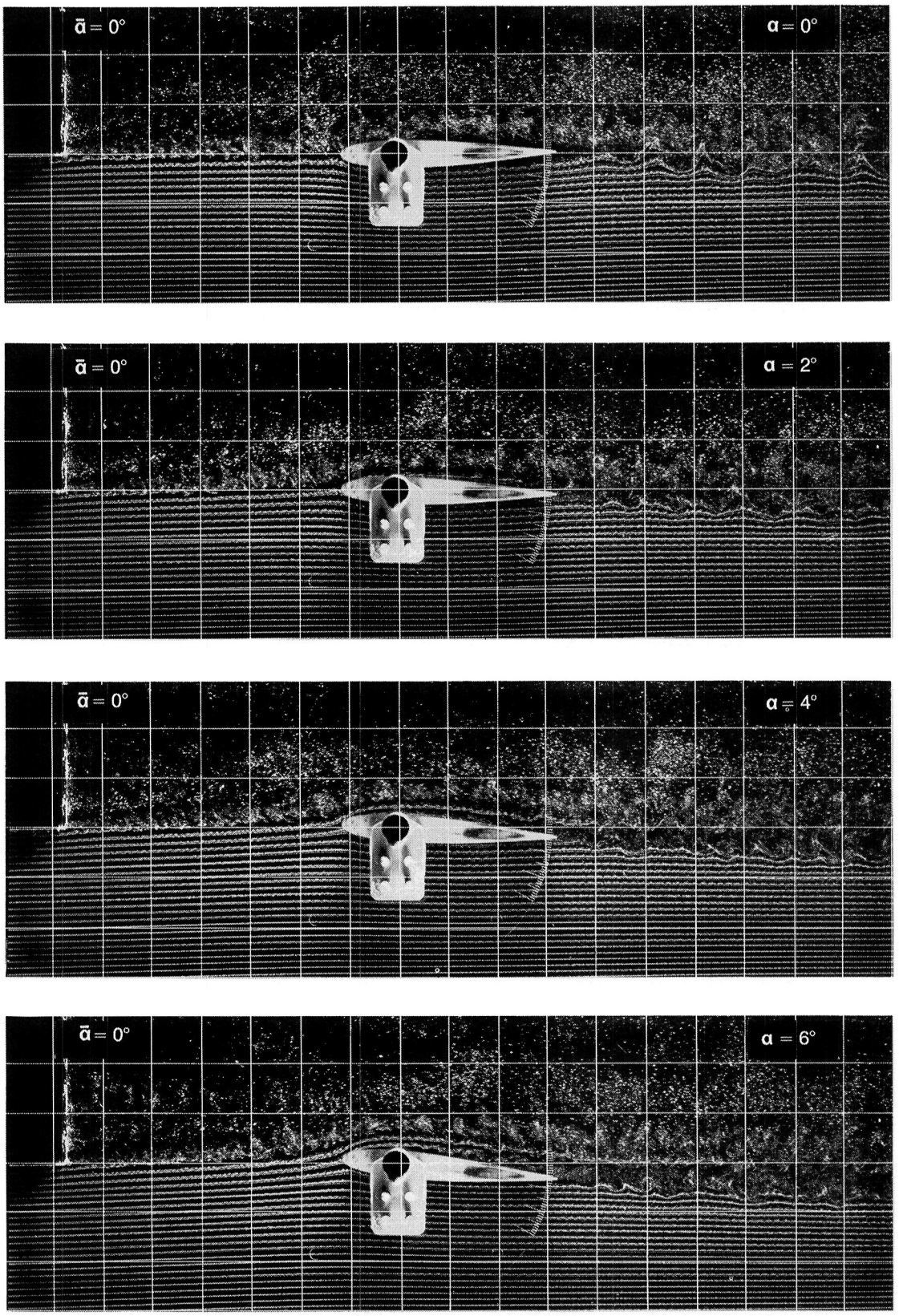

Figure 7.– Visualization of flow at Re = 60,000 with generator on centerline and set at $\tilde{\alpha} = 0°$ (no-vortex case).

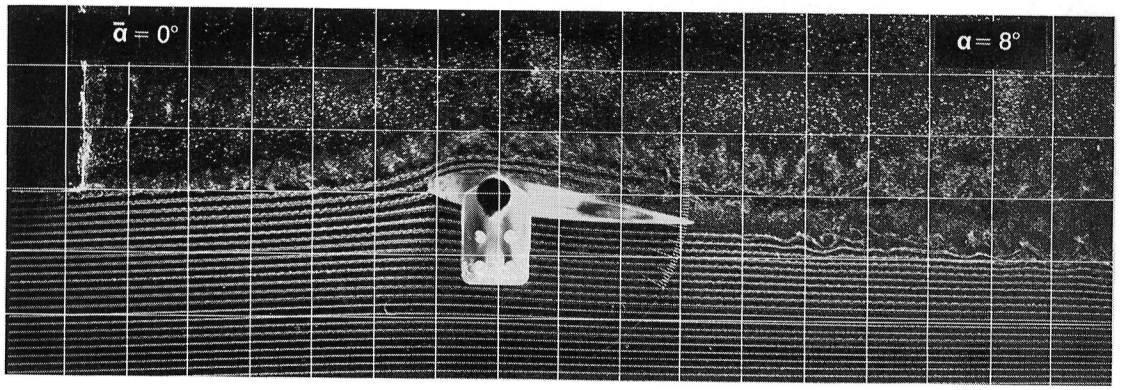

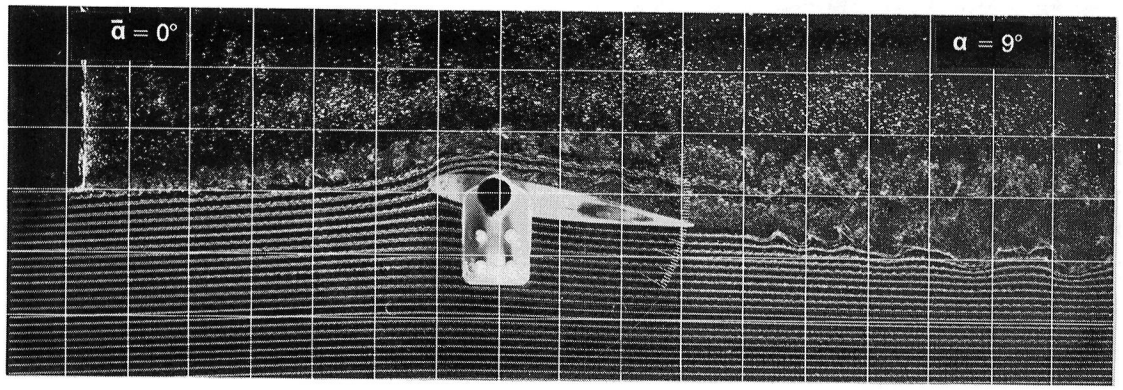

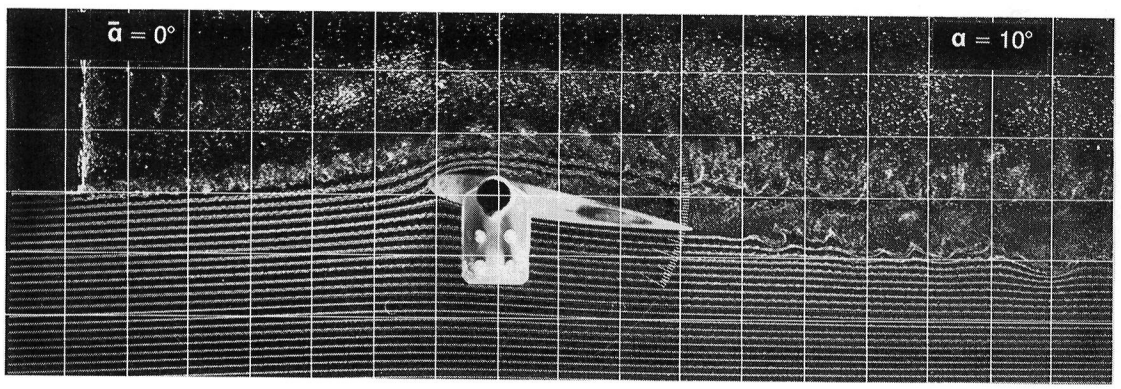

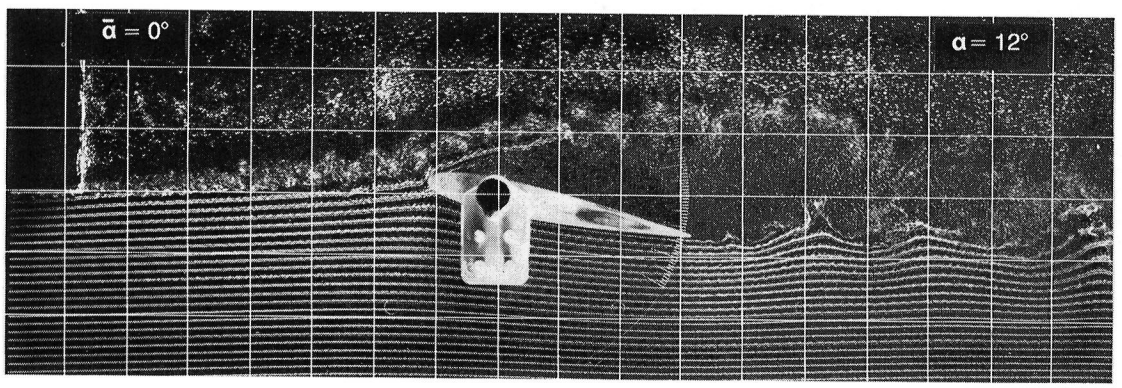

Figure 7.– Continued.

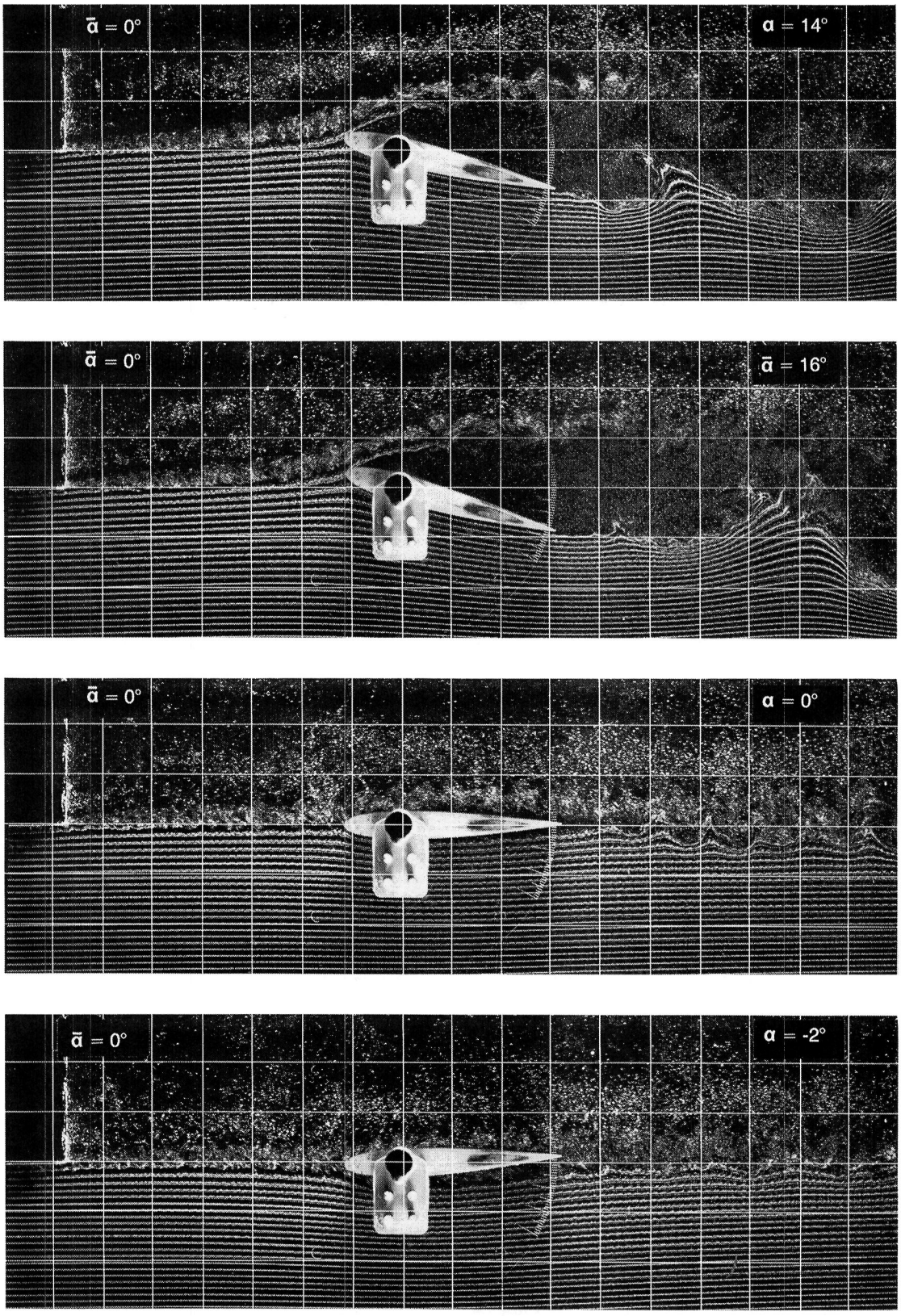

Figure 7.– Continued.

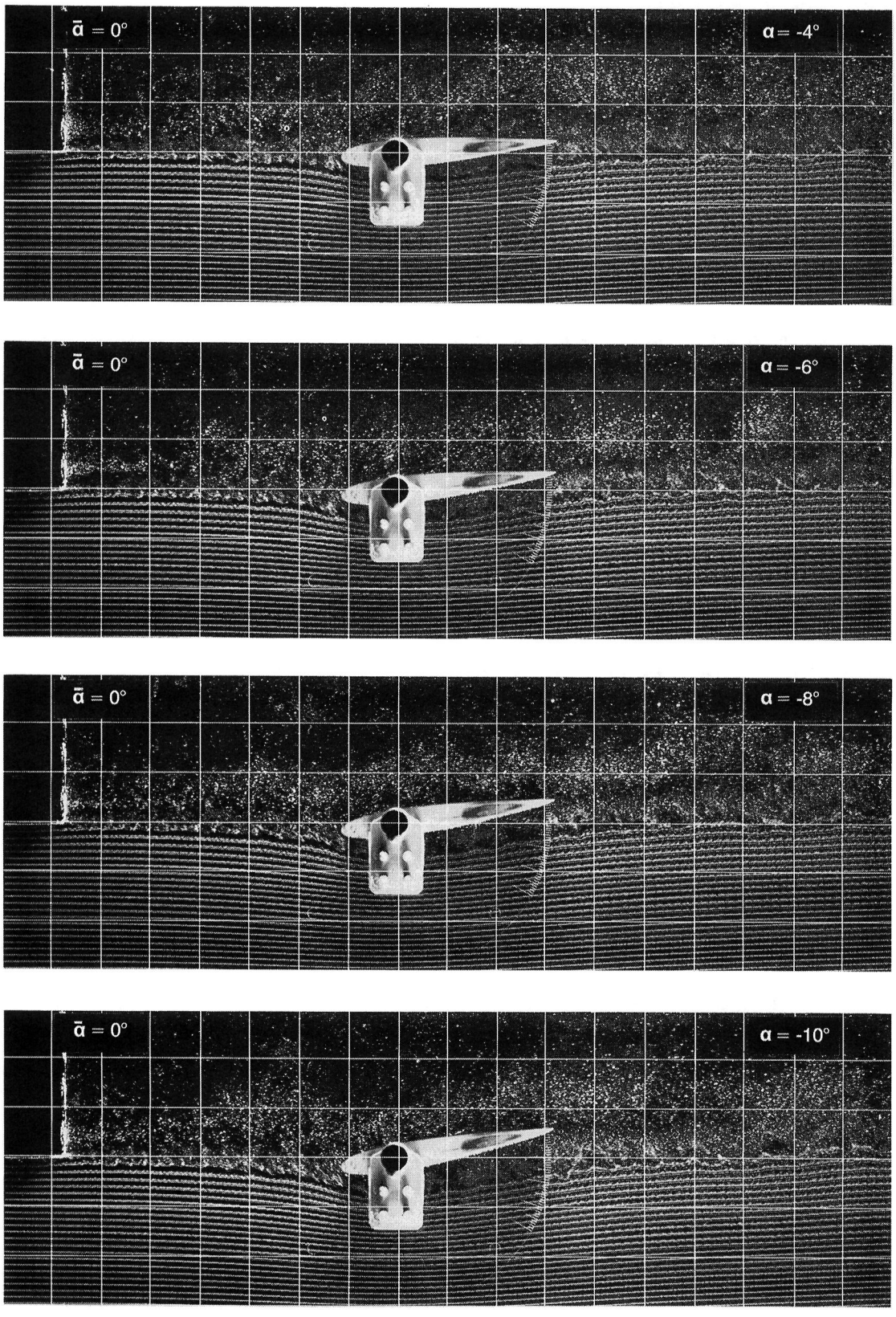

Figure 7.– Continued.

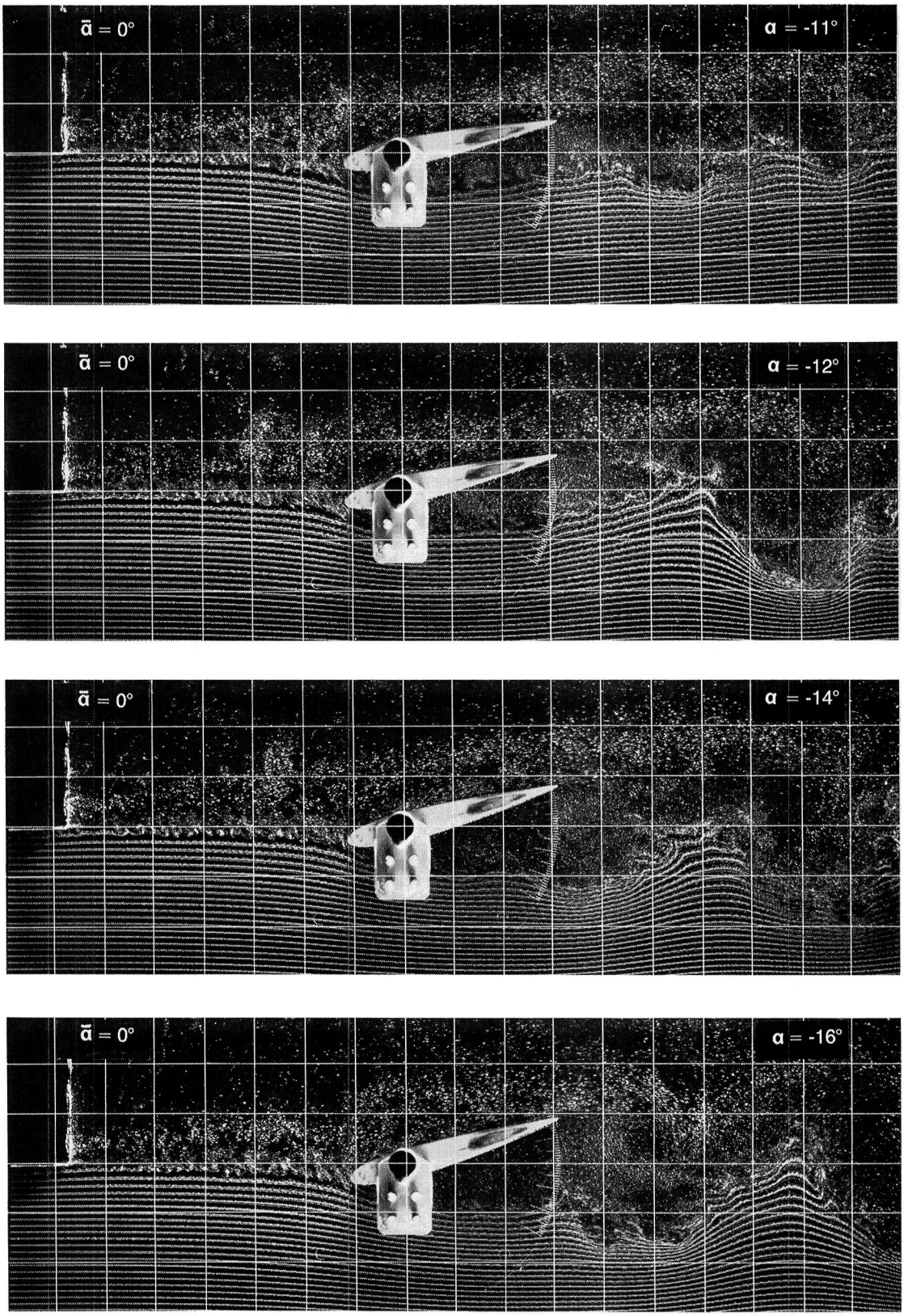

Figure 7.– Concluded.

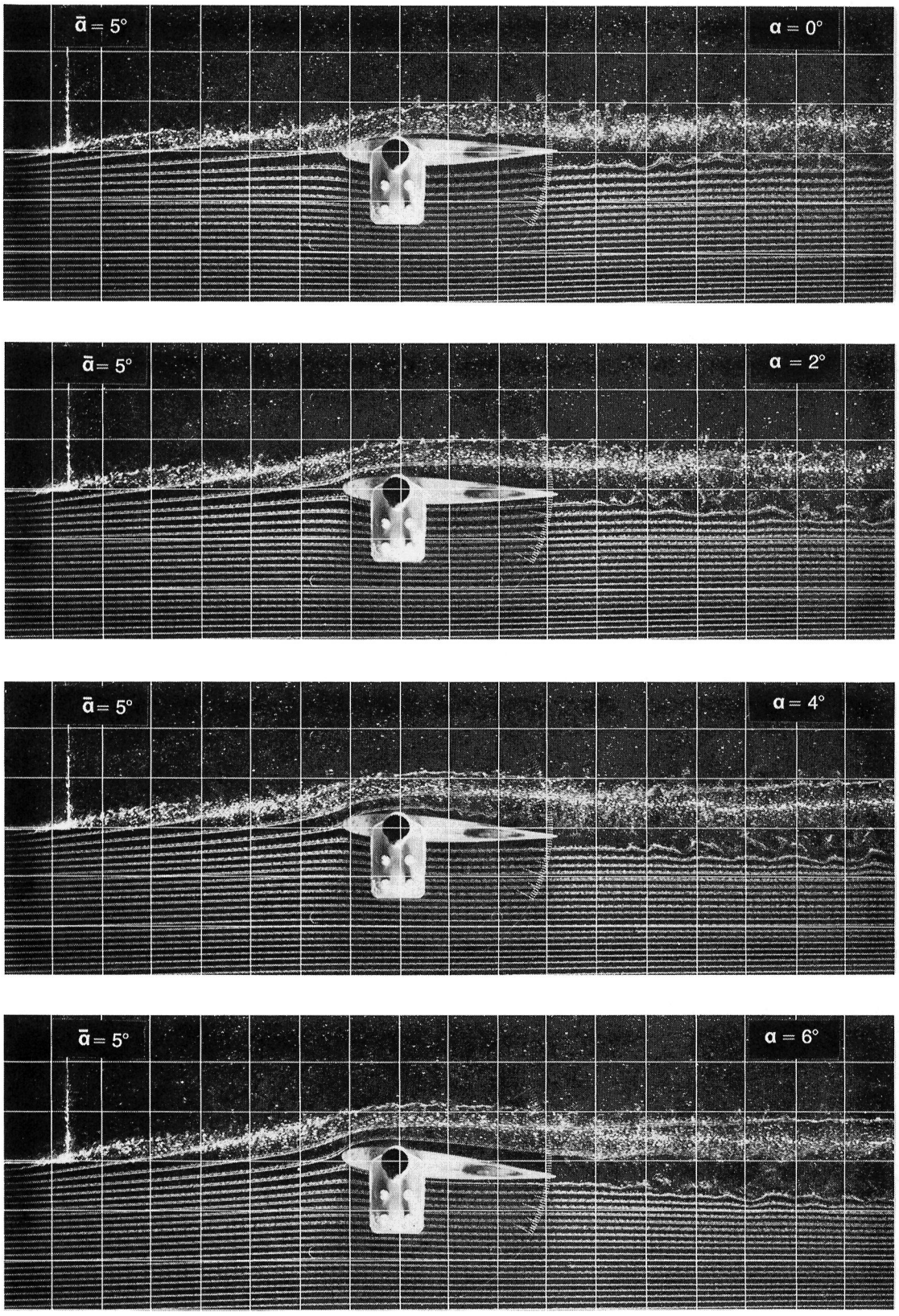

Figure 8.– Visualization of flow at Re = 60,000 with generator on centerline and set at $\tilde{\alpha} = 5°$ (weak-vortex case).

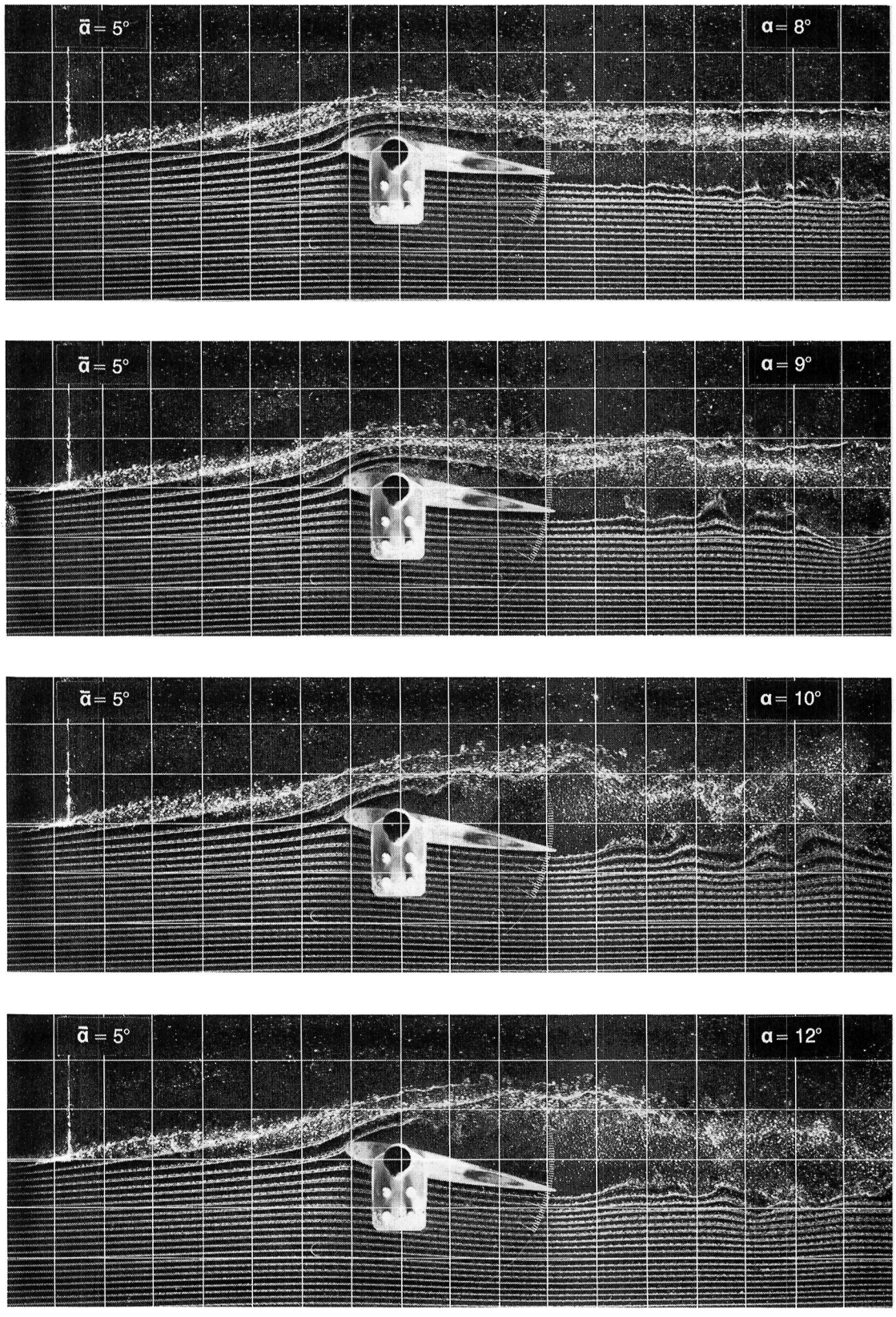

Figure 8.– Continued.

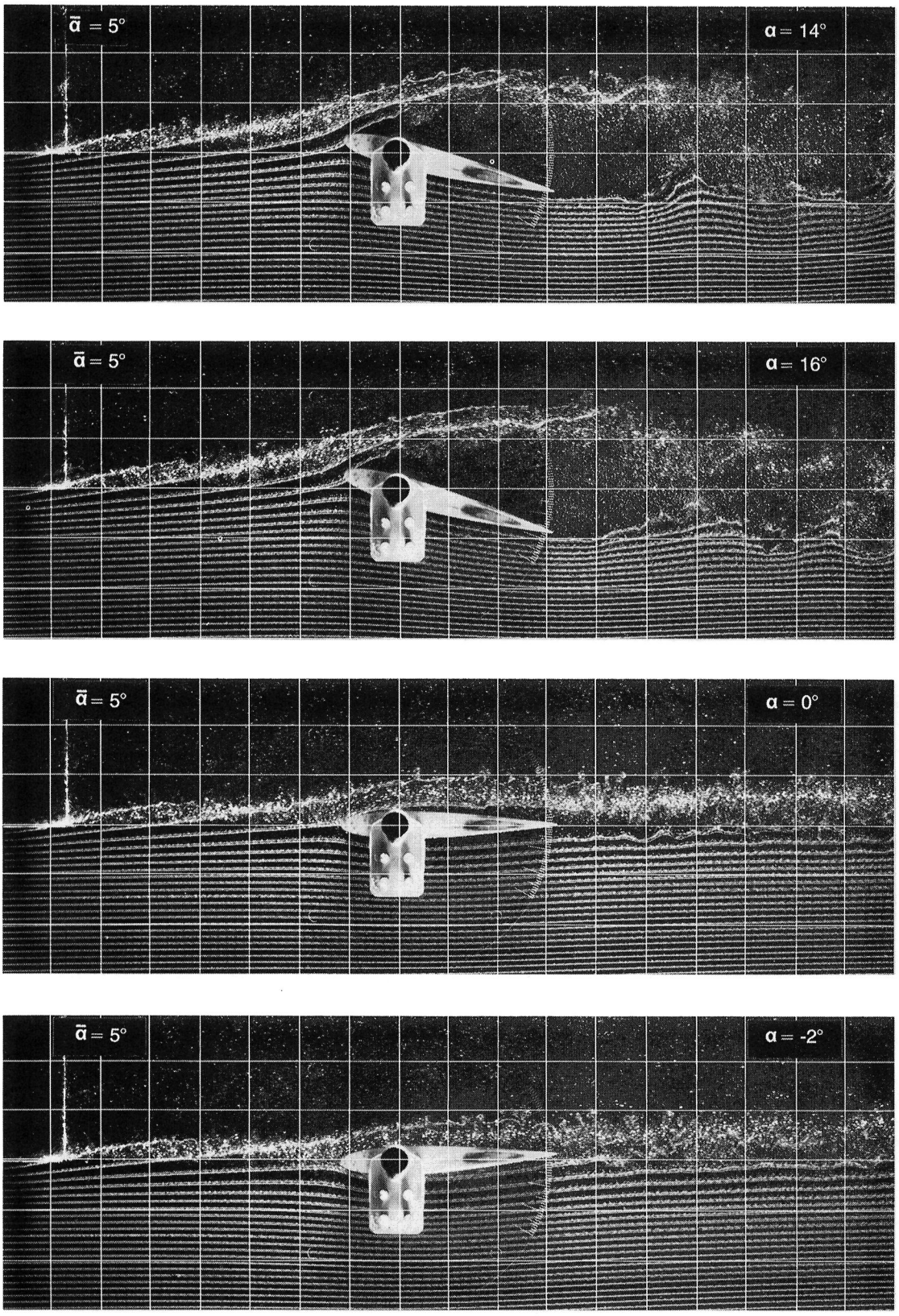

Figure 8.– Continued.

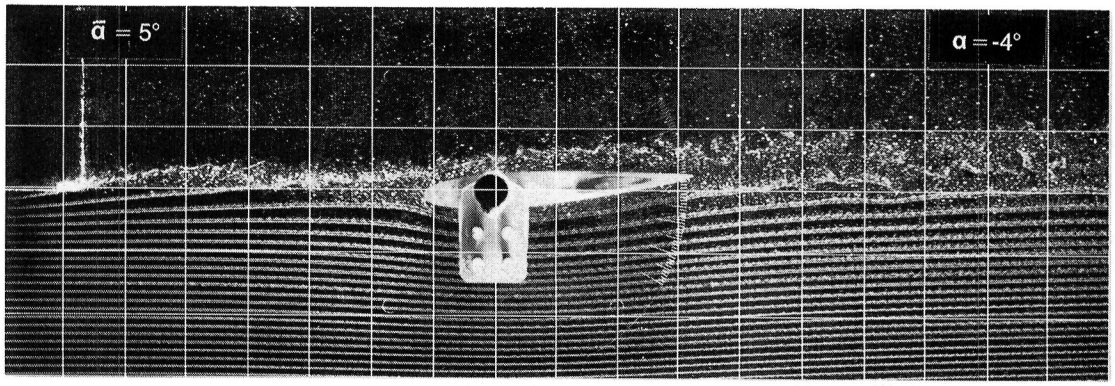

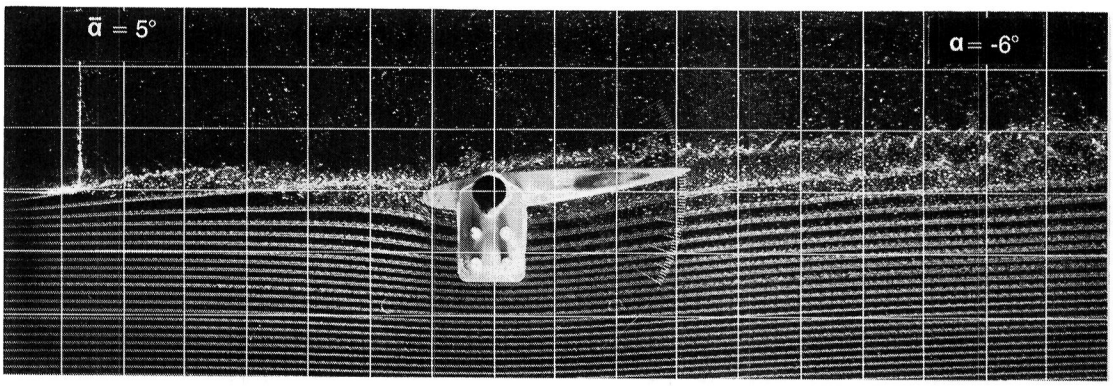

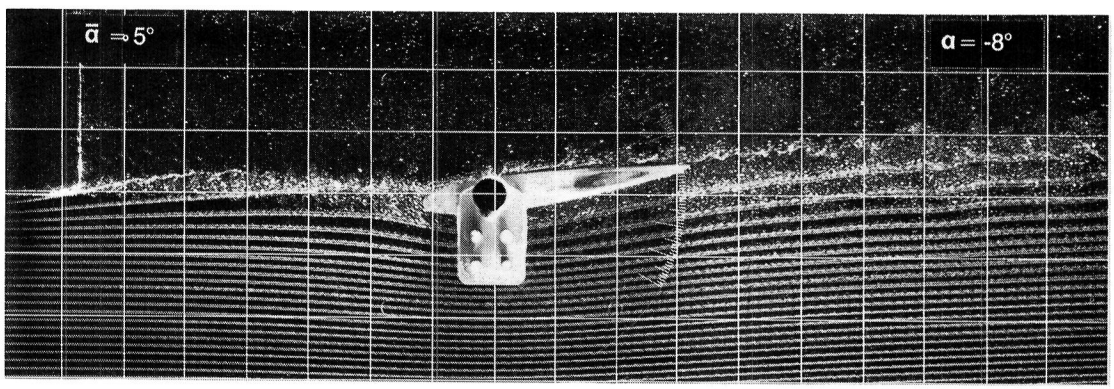

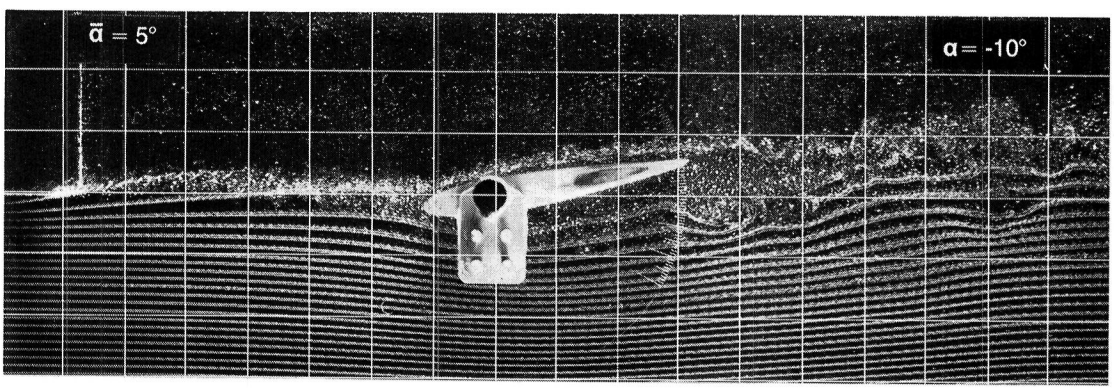

Figure 8.– Continued.

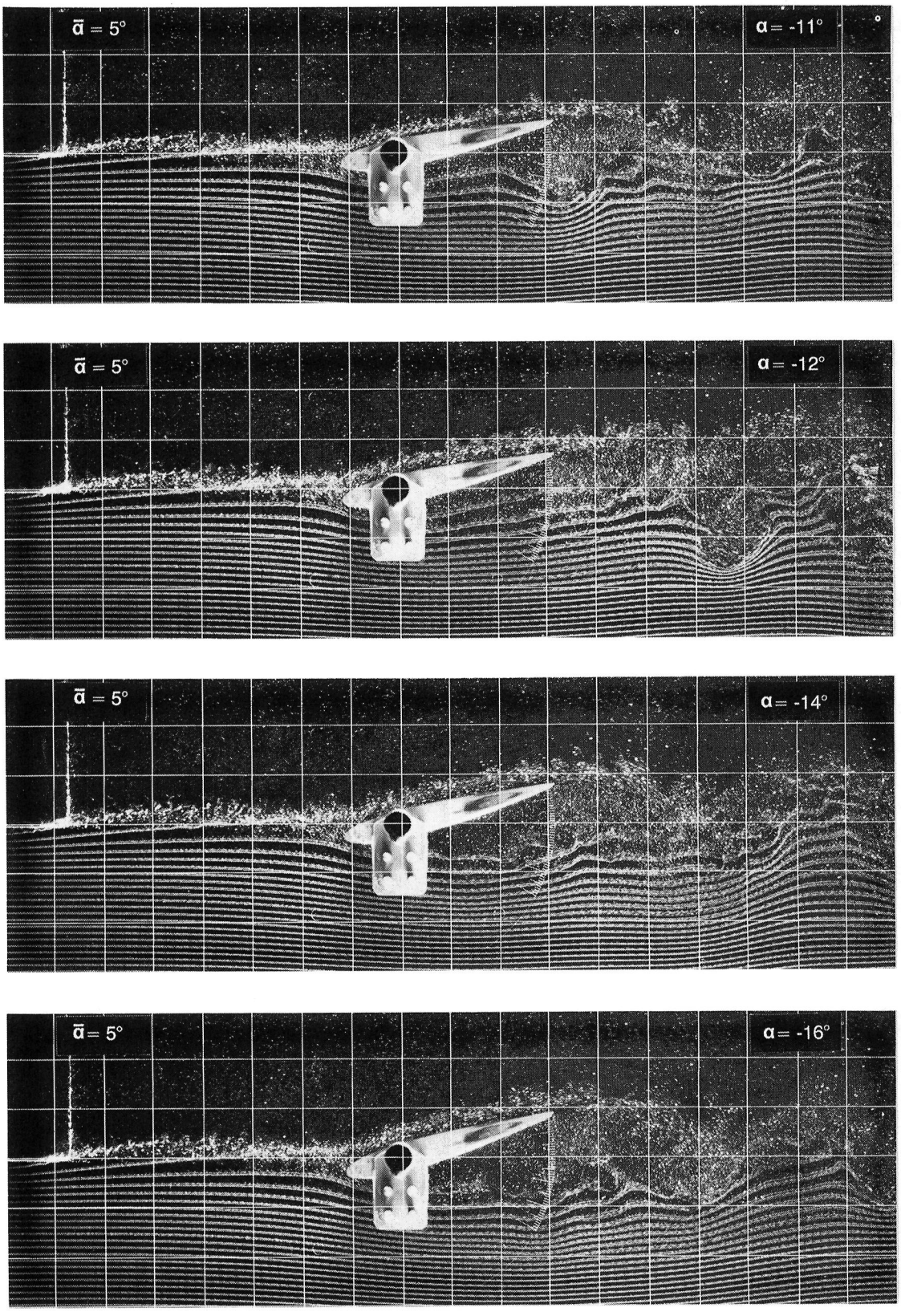

Figure 8.– Concluded.

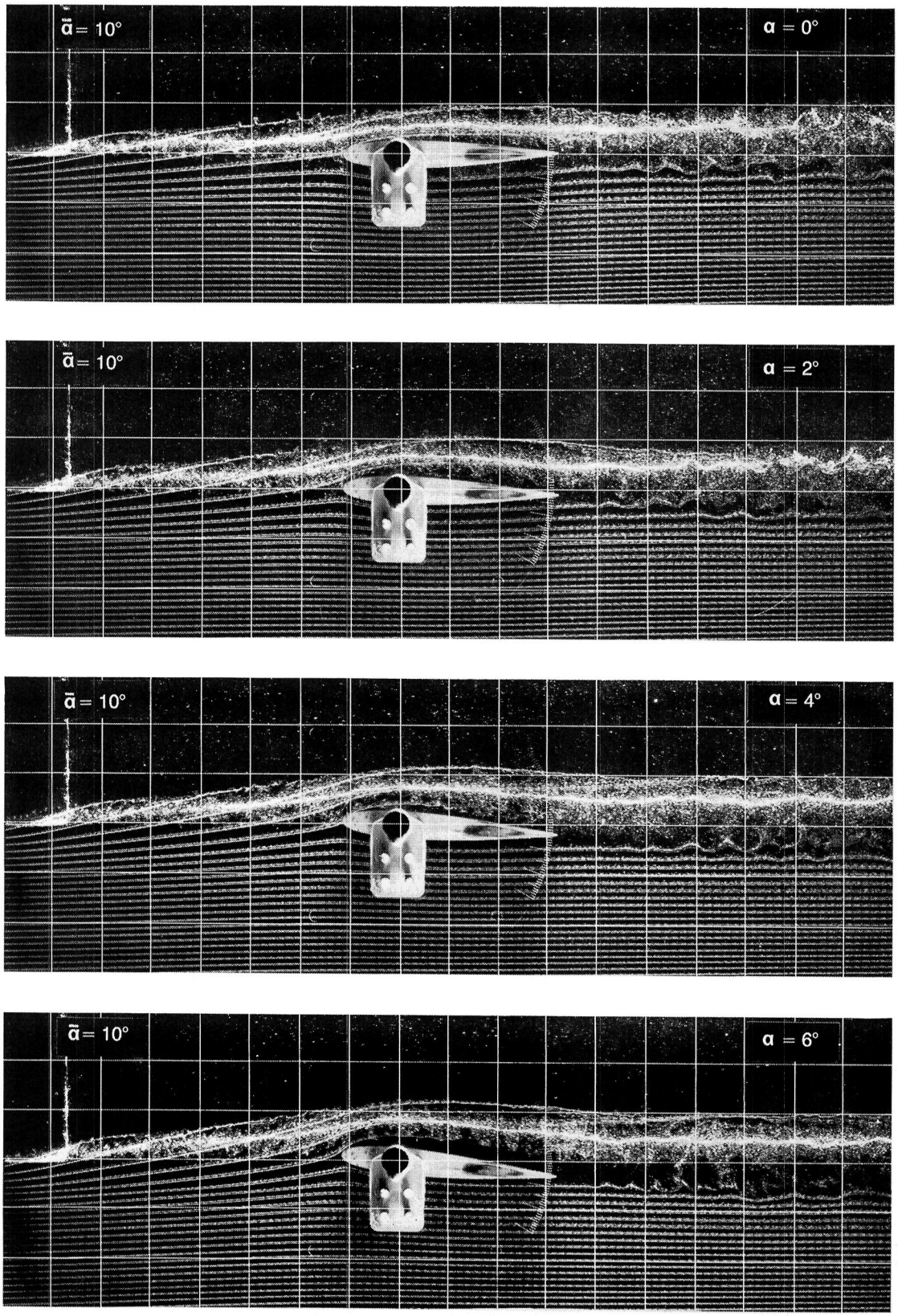

Figure 9.– Visualization of flow at Re = 60,000 with generator on centerline and set at $\tilde{\alpha} = 10°$ (strong–vortex case).

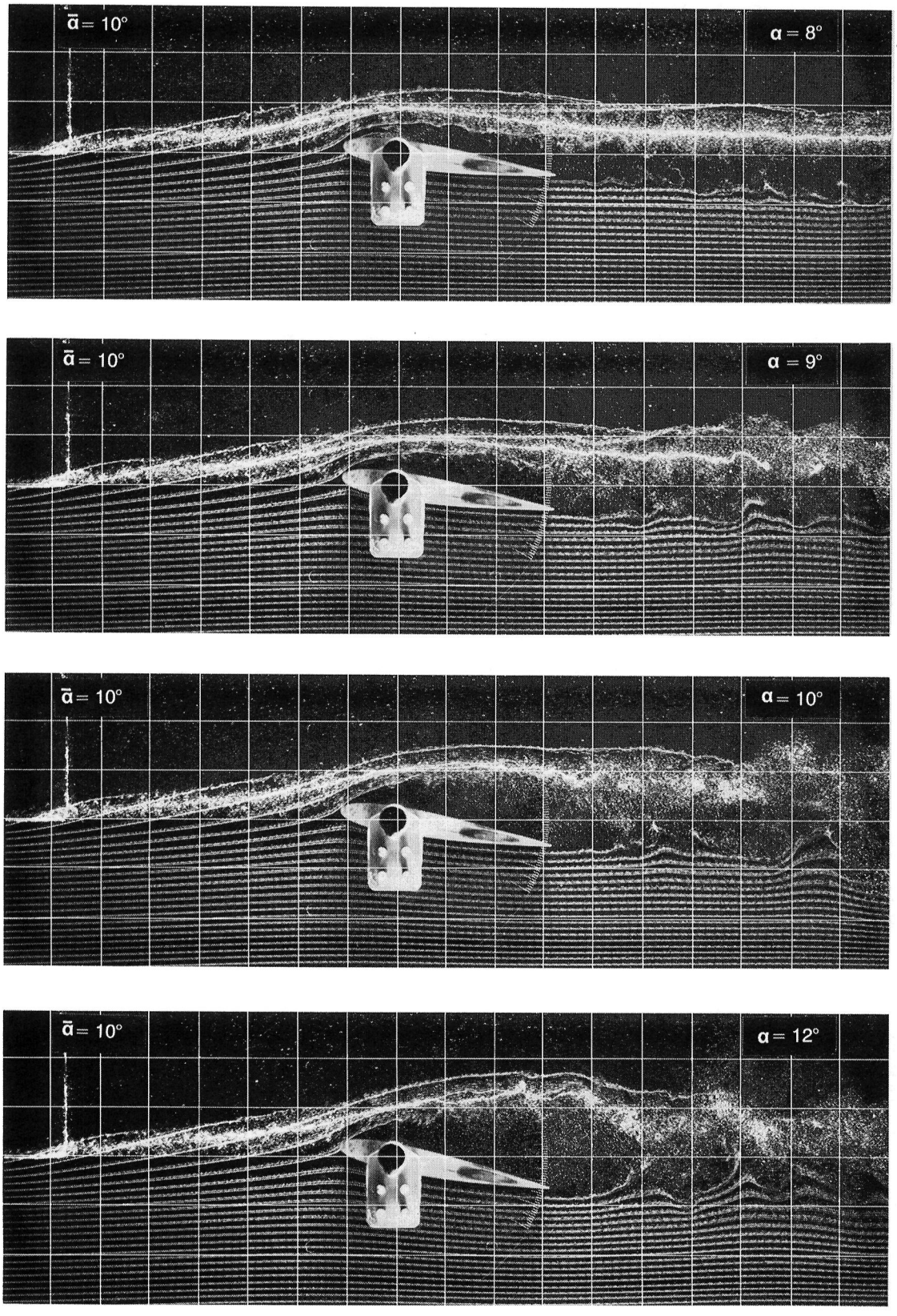

Figure 9.– Continued.

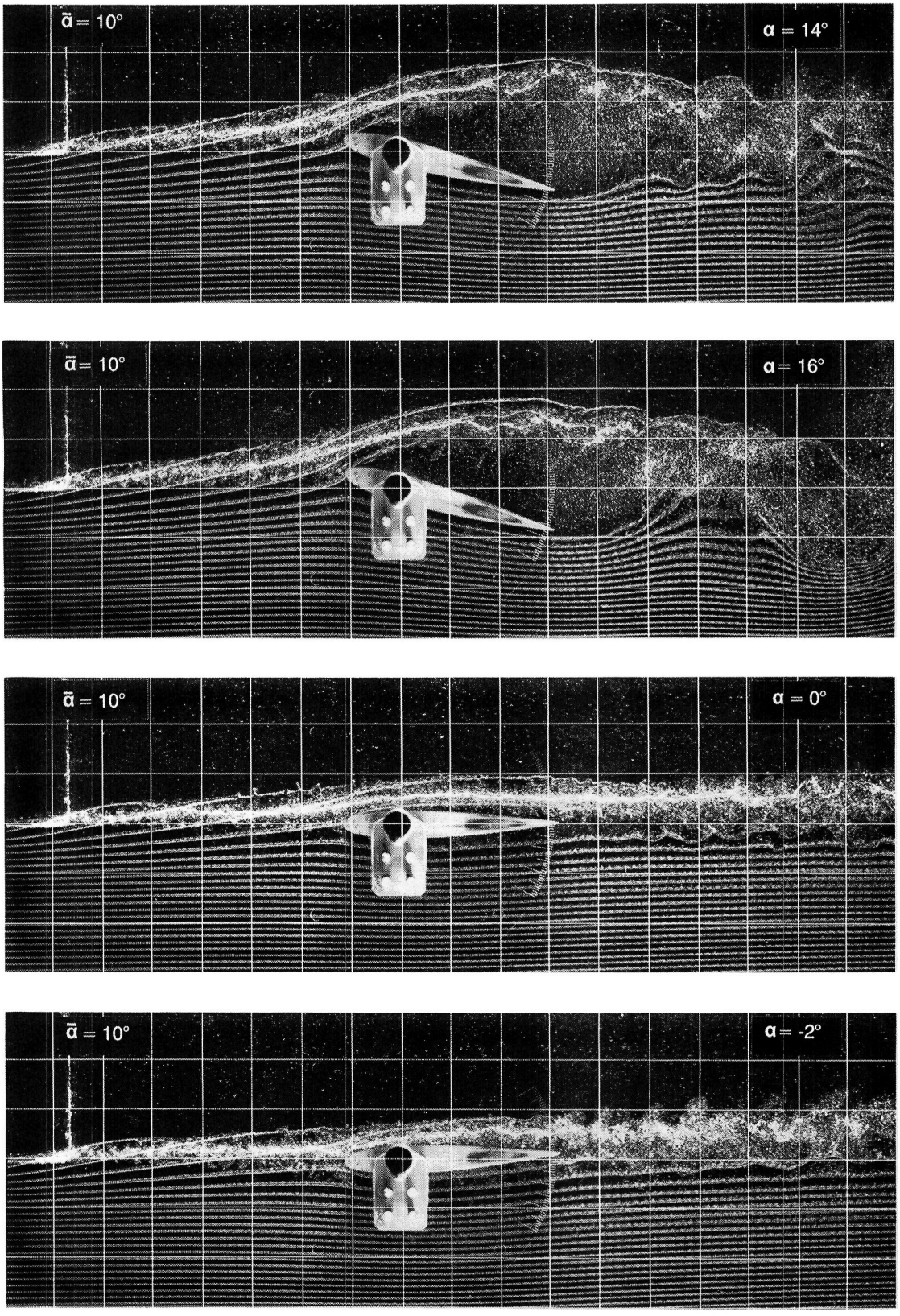

Figure 9.– Continued.

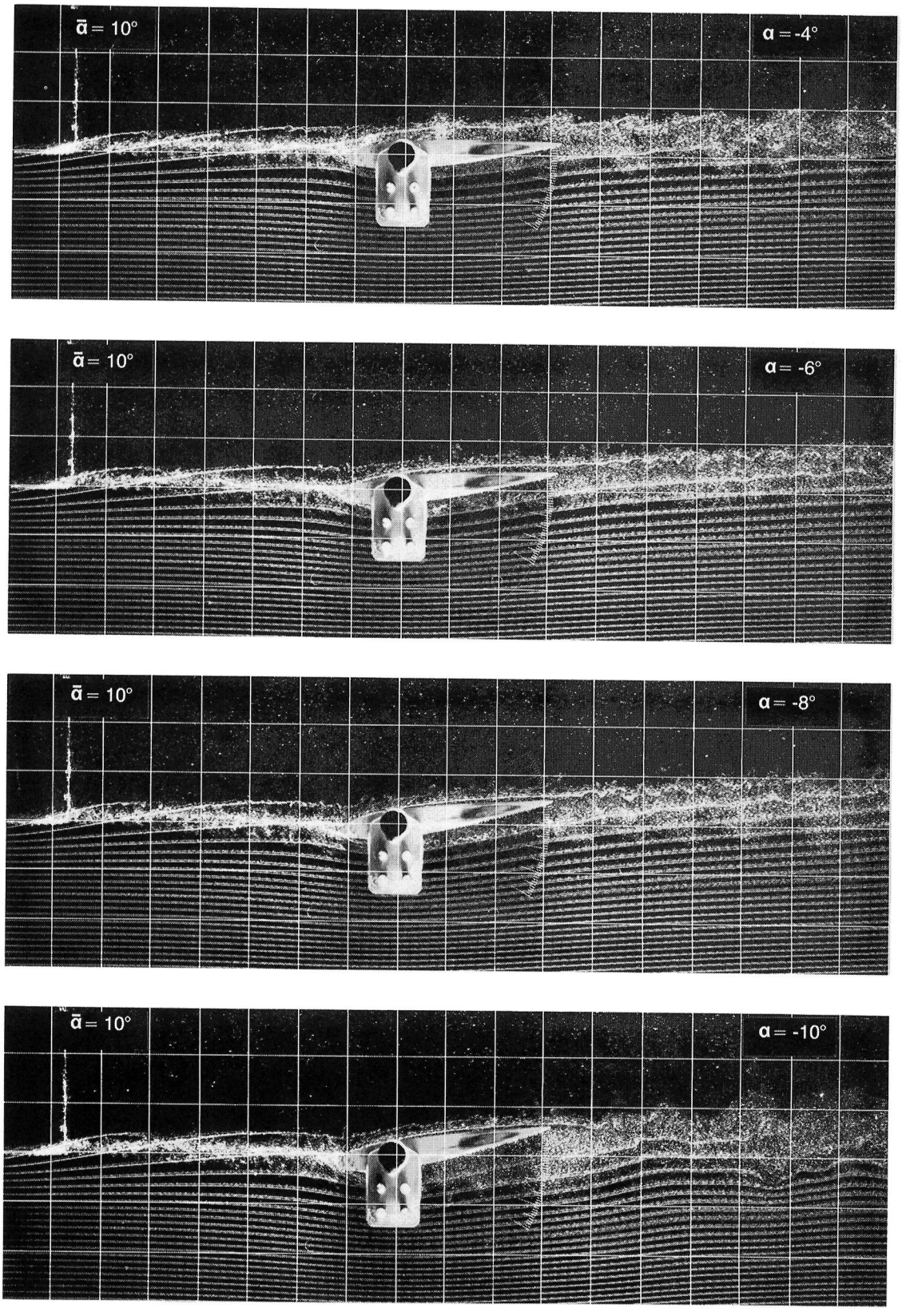

Figure 9.– Continued.

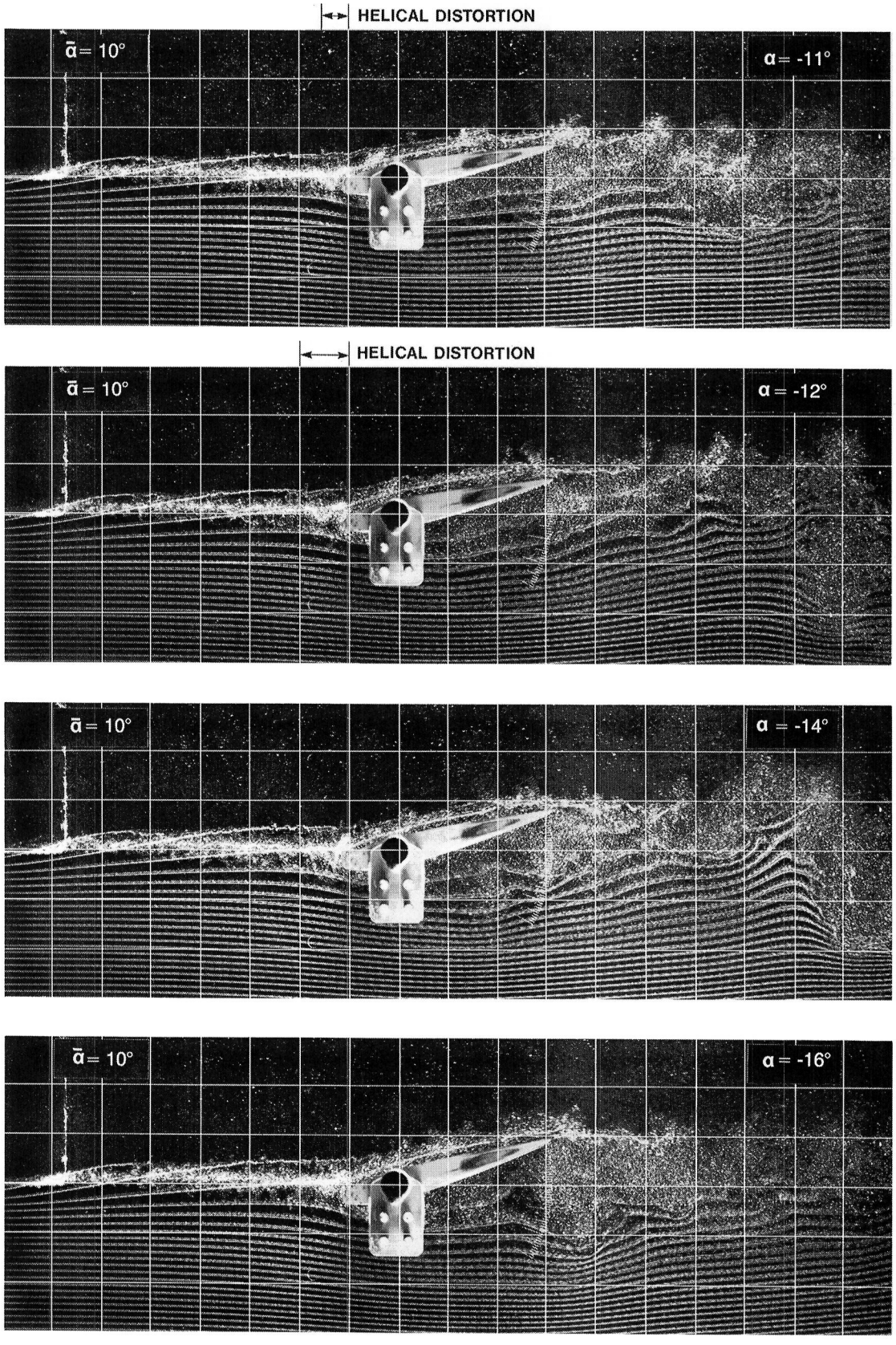

Figure 9.– Concluded.

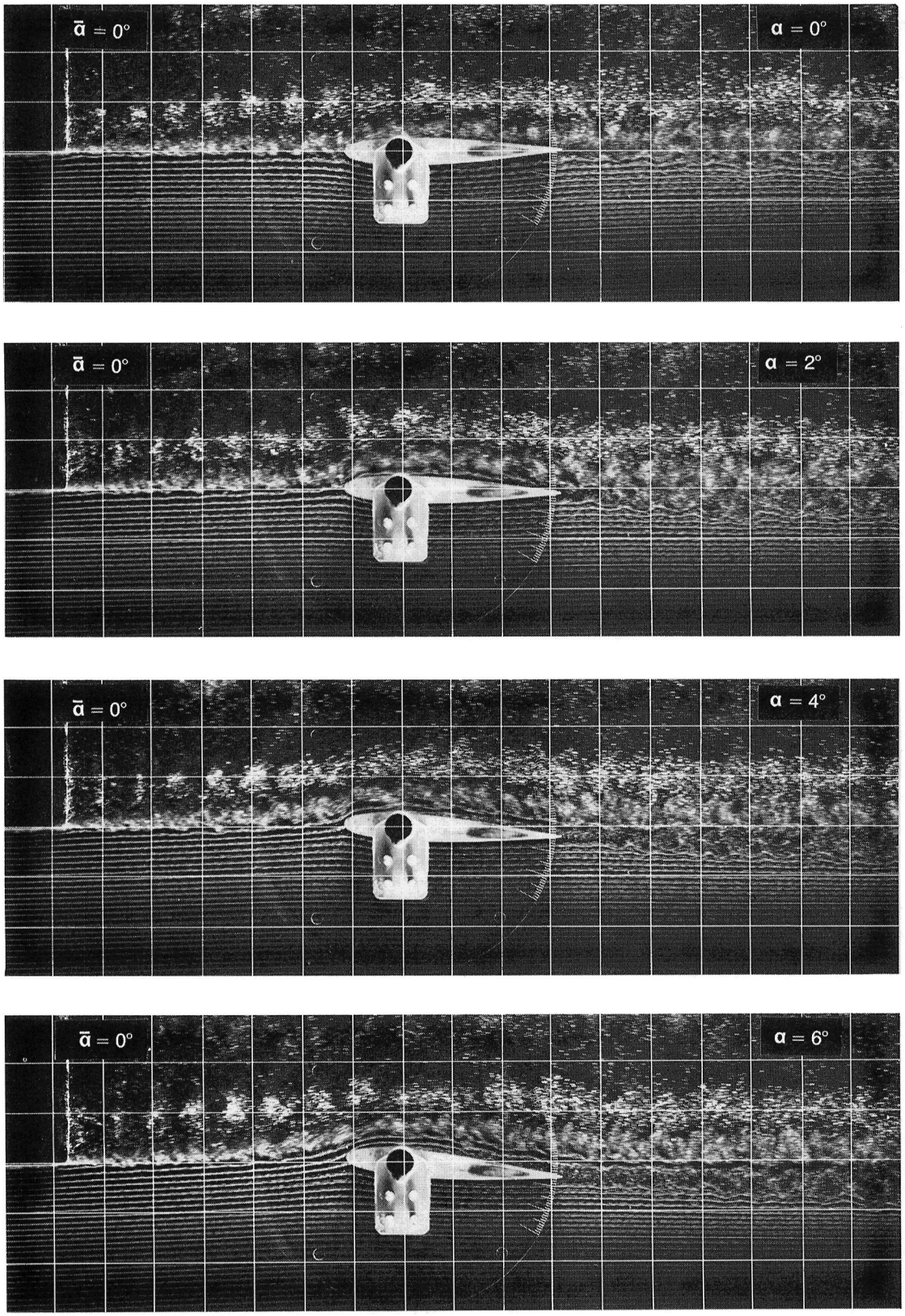

Figure 10.– Visualization of flow at Re = 120,000 with generator on centerline and set at $\tilde{\alpha} = 0°$ (no-vortex case).

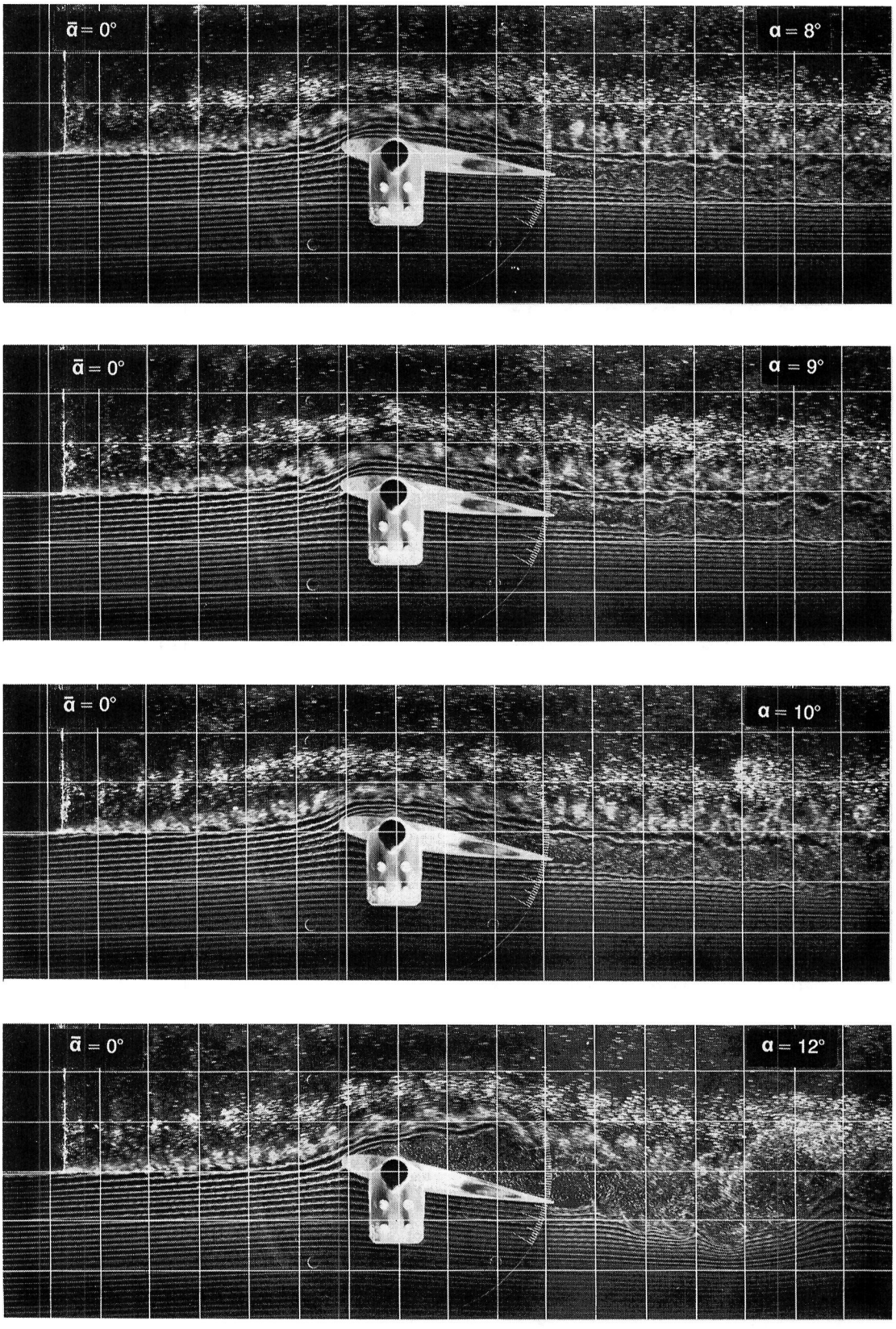

Figure 10.– Continued.

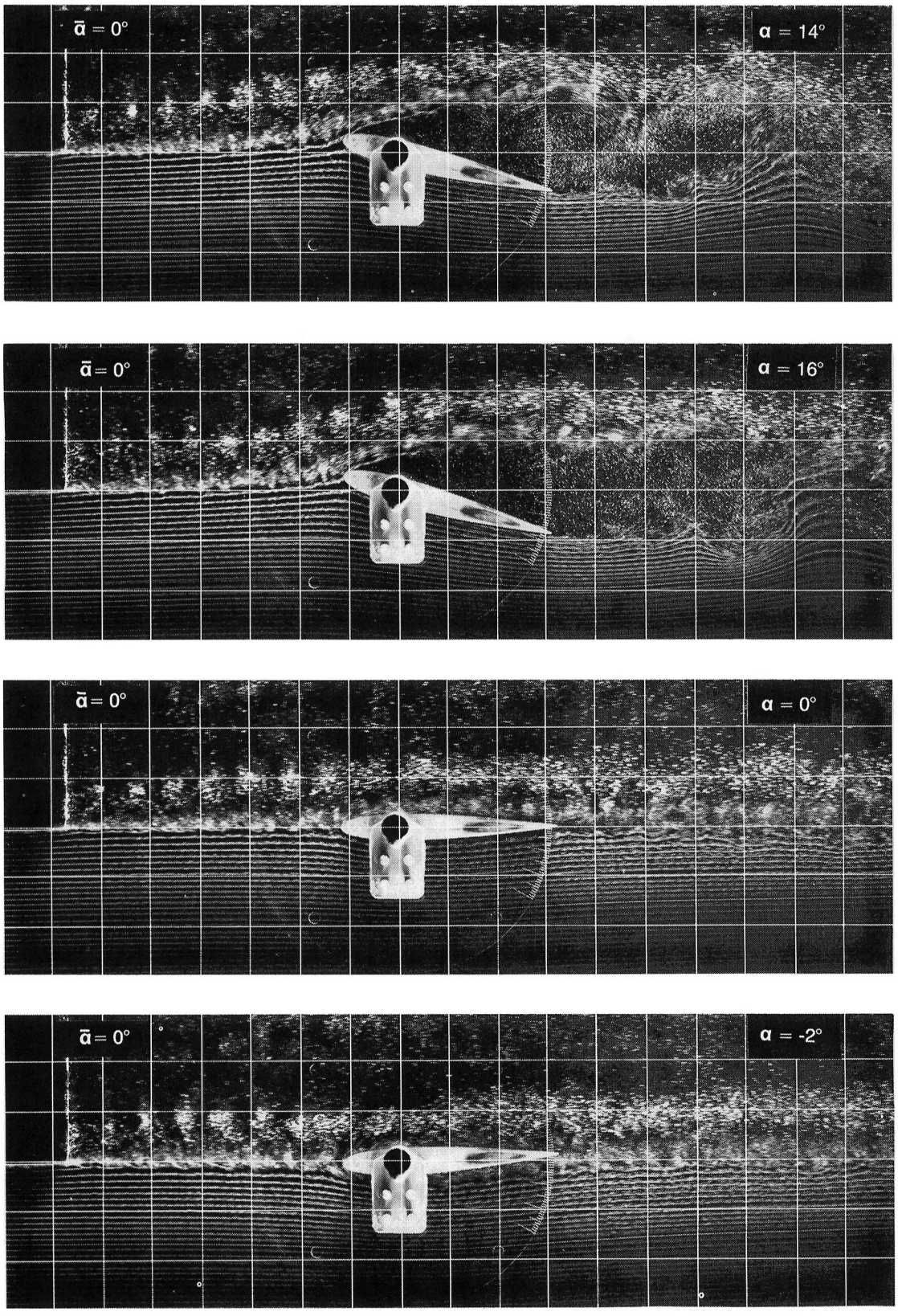

Figure 10.– Continued.

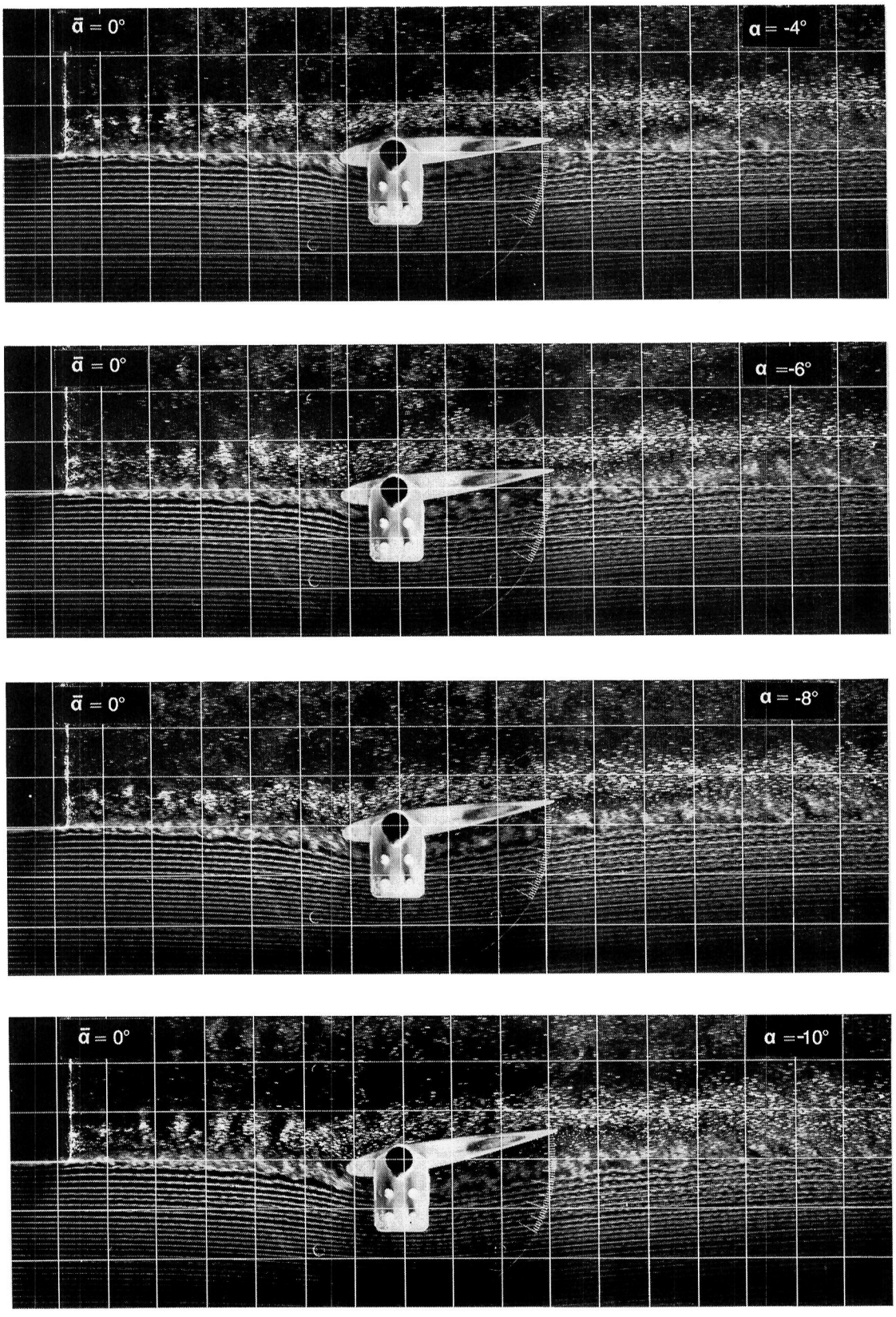

Figure 10.– Continued.

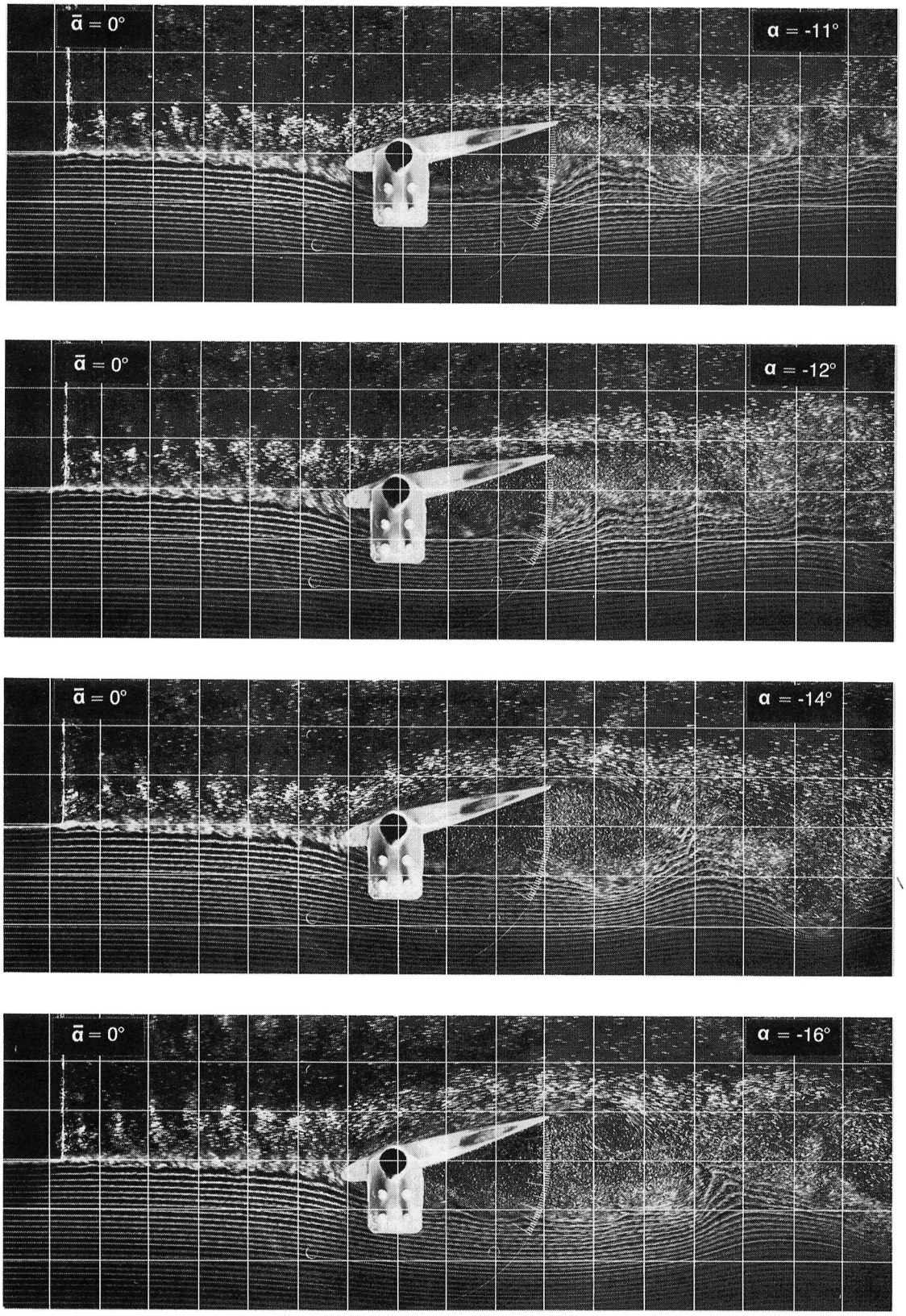

Figure 10.– Concluded.

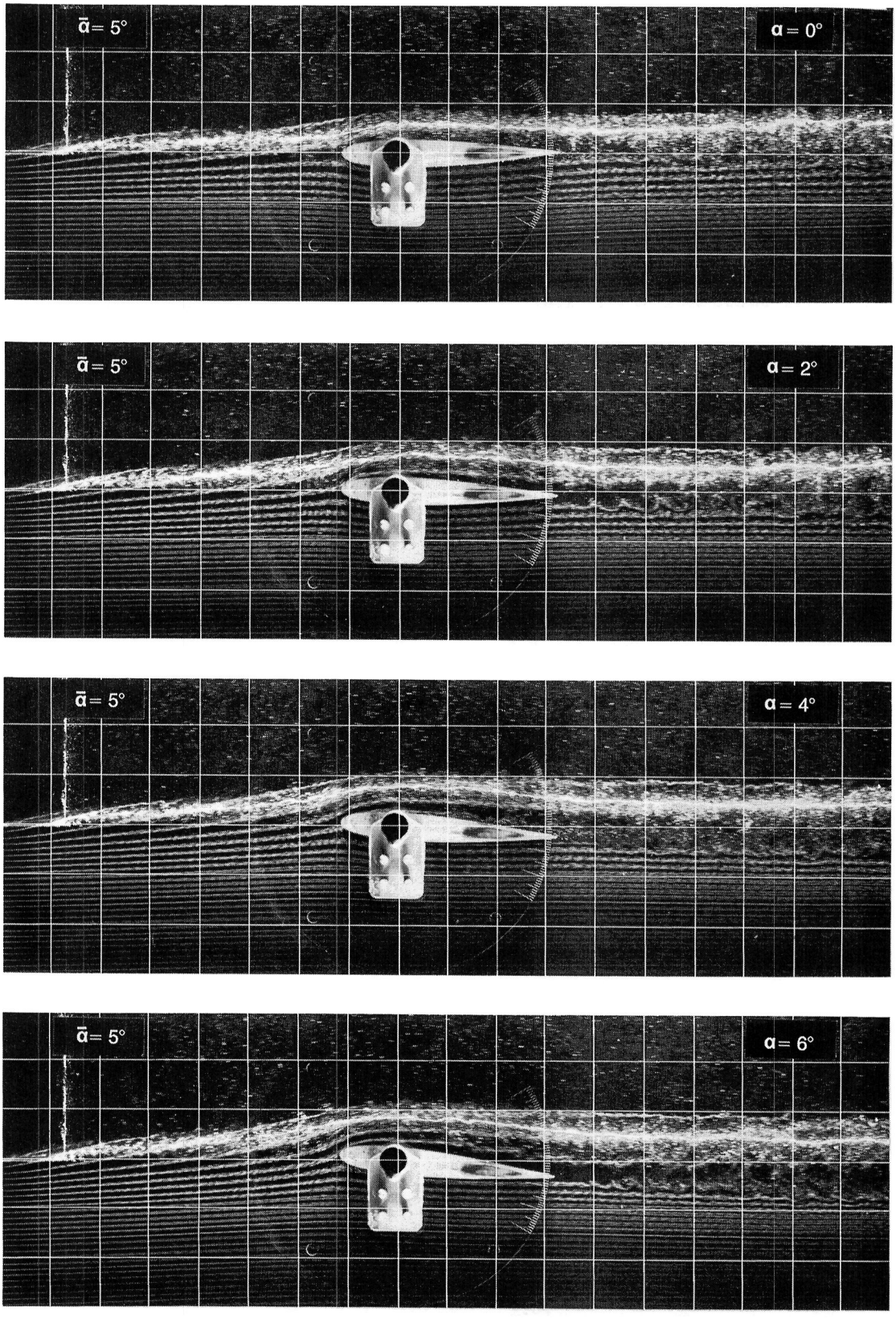

Figure 11.– Visualization of flow at Re = 120,000 with generator on centerline and set at $\tilde{\alpha} = 5°$ (weak-vortex case).

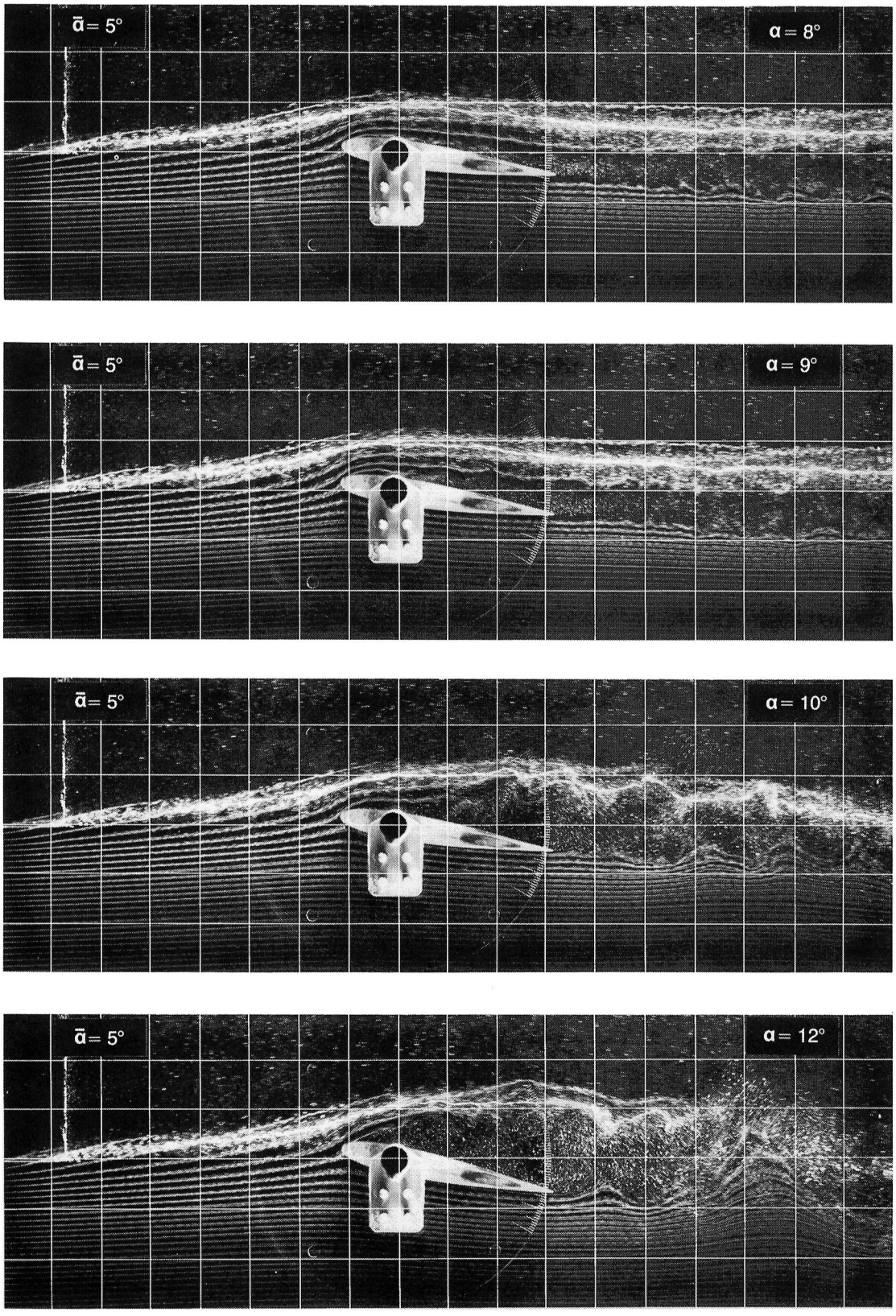

Figure 11.– Continued.

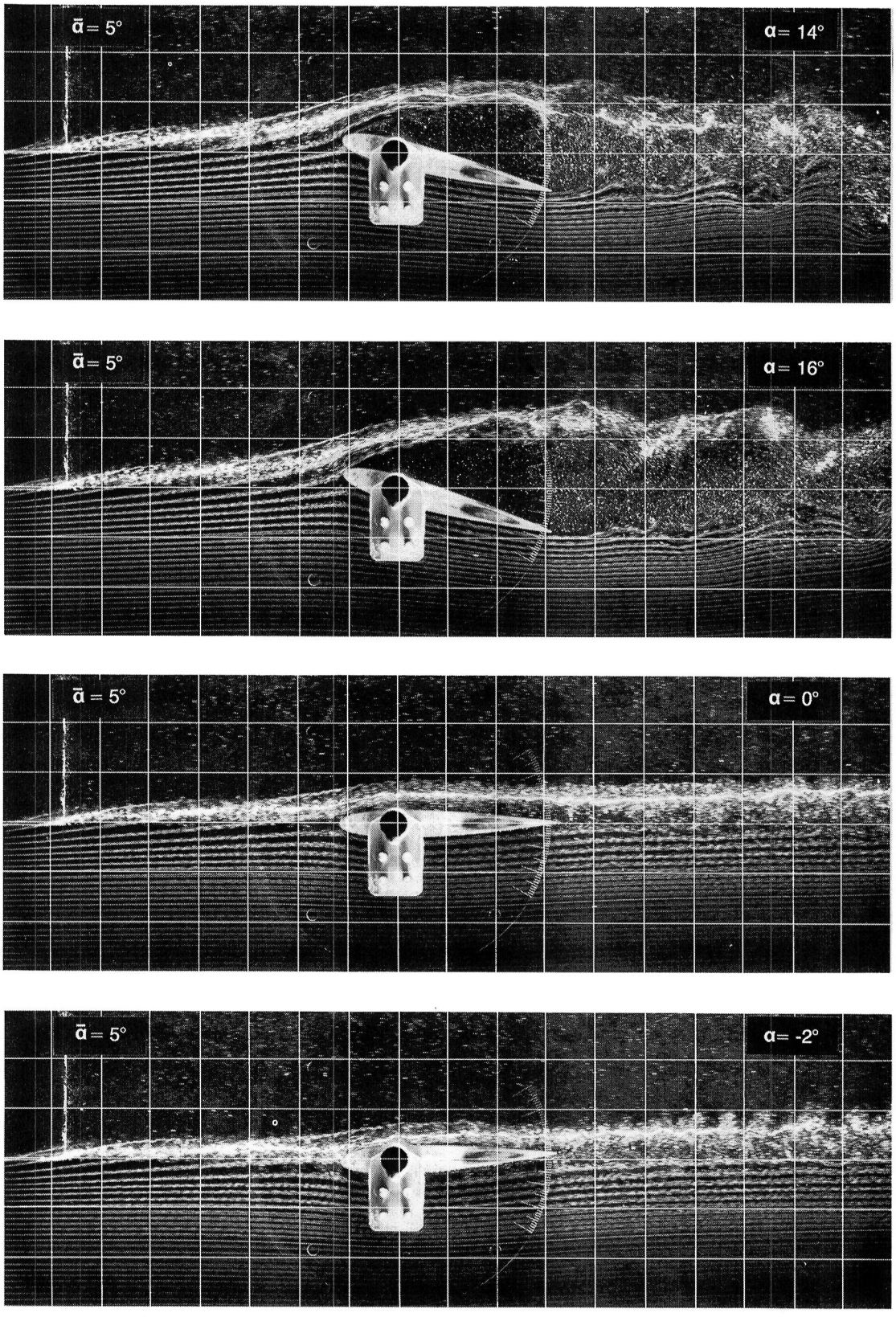

Figure 11.– Continued.

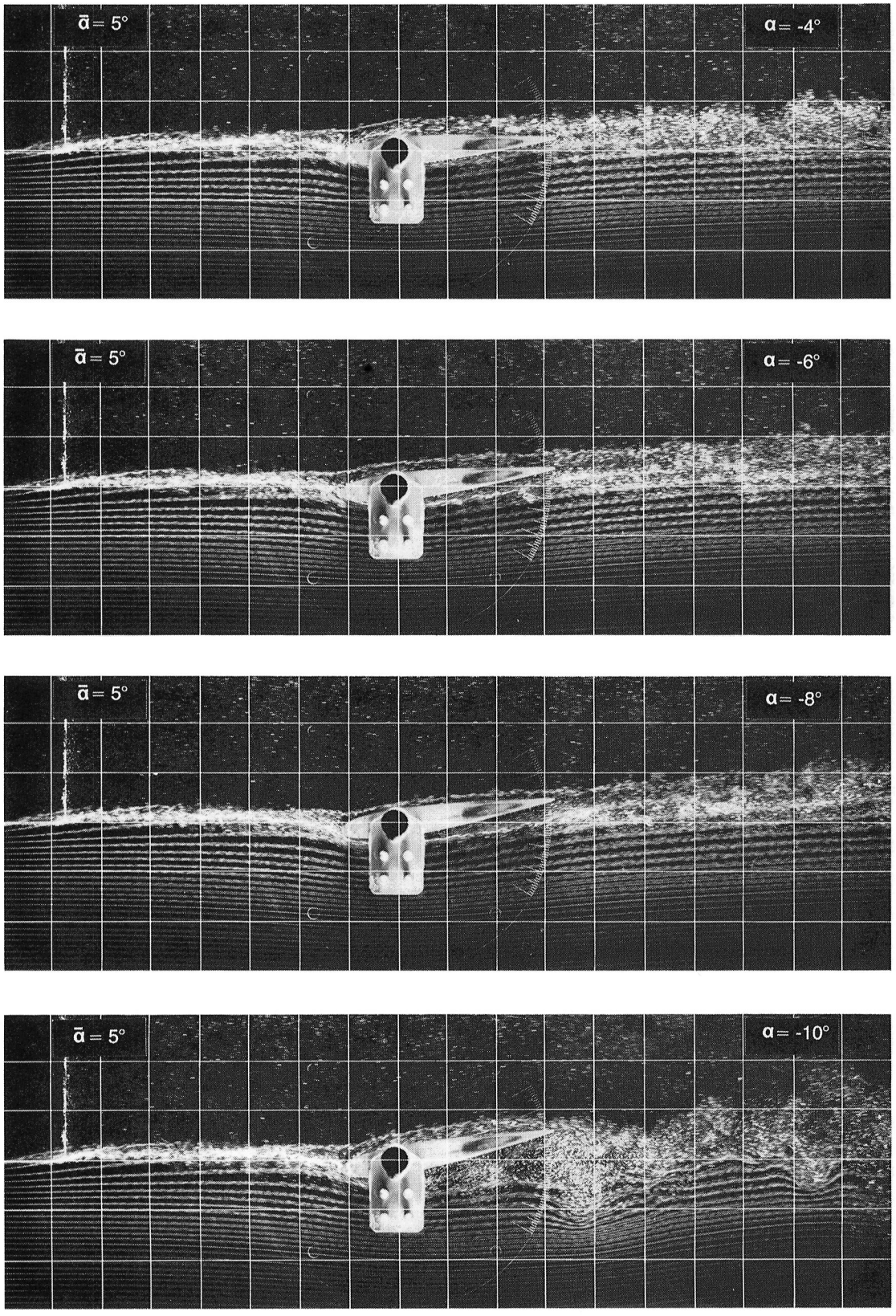

Figure 11.– Continued.

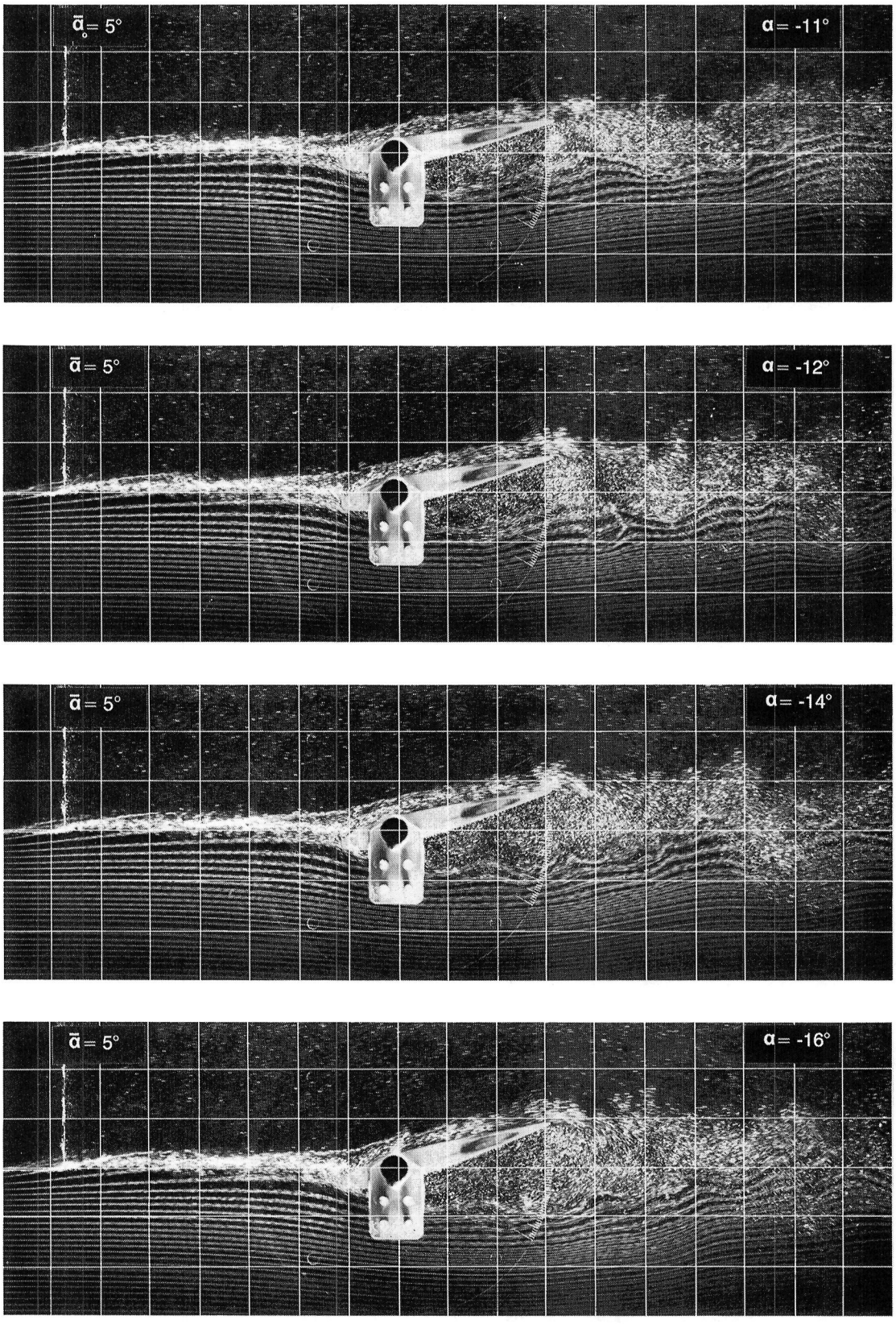

Figure 11.– Concluded.

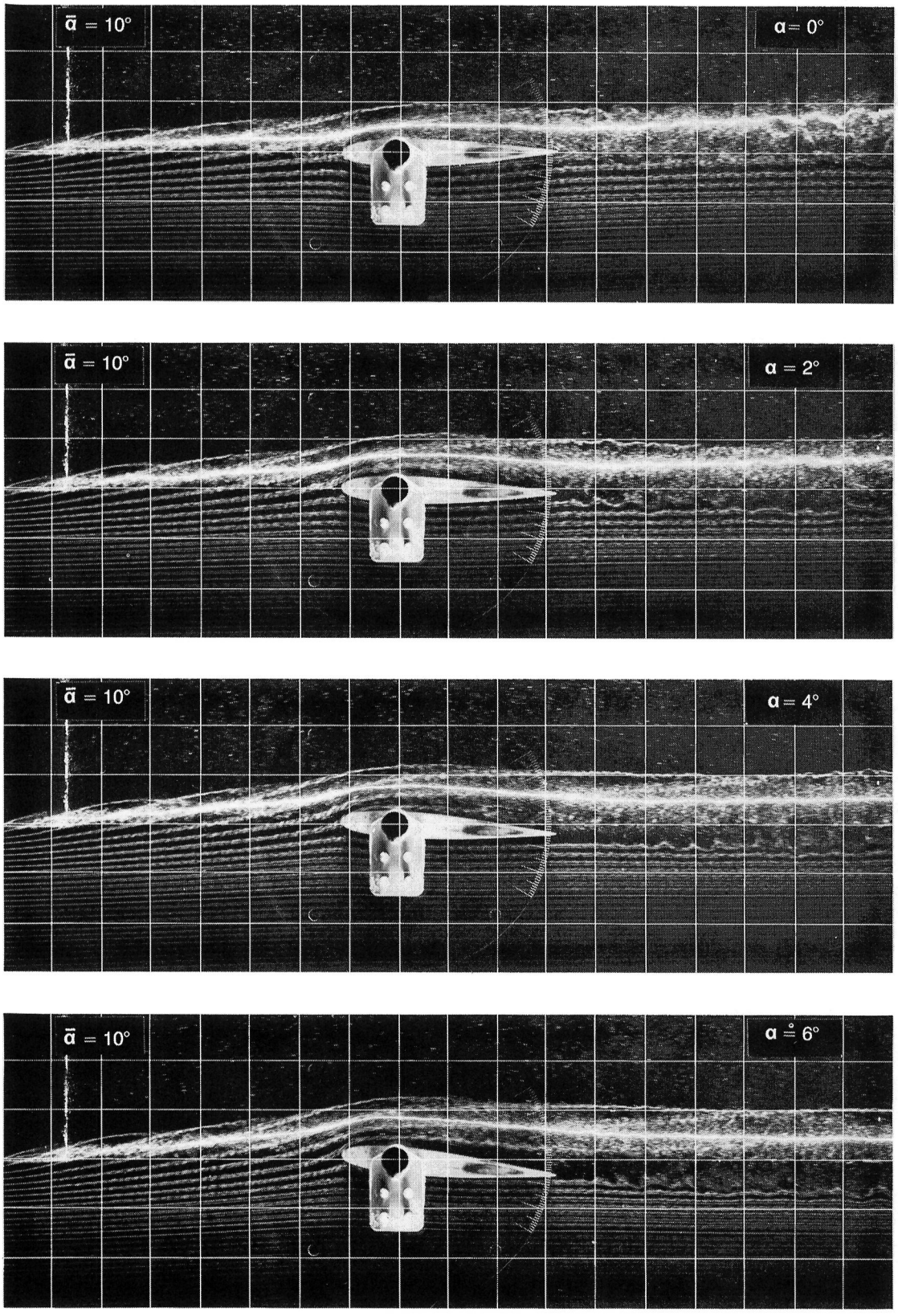

Figure 12.– Visualization of flow at Re = 120,000 with generator on centerline and set at $\tilde{\alpha} = 10^{\circ}$ (strong-vortex case).

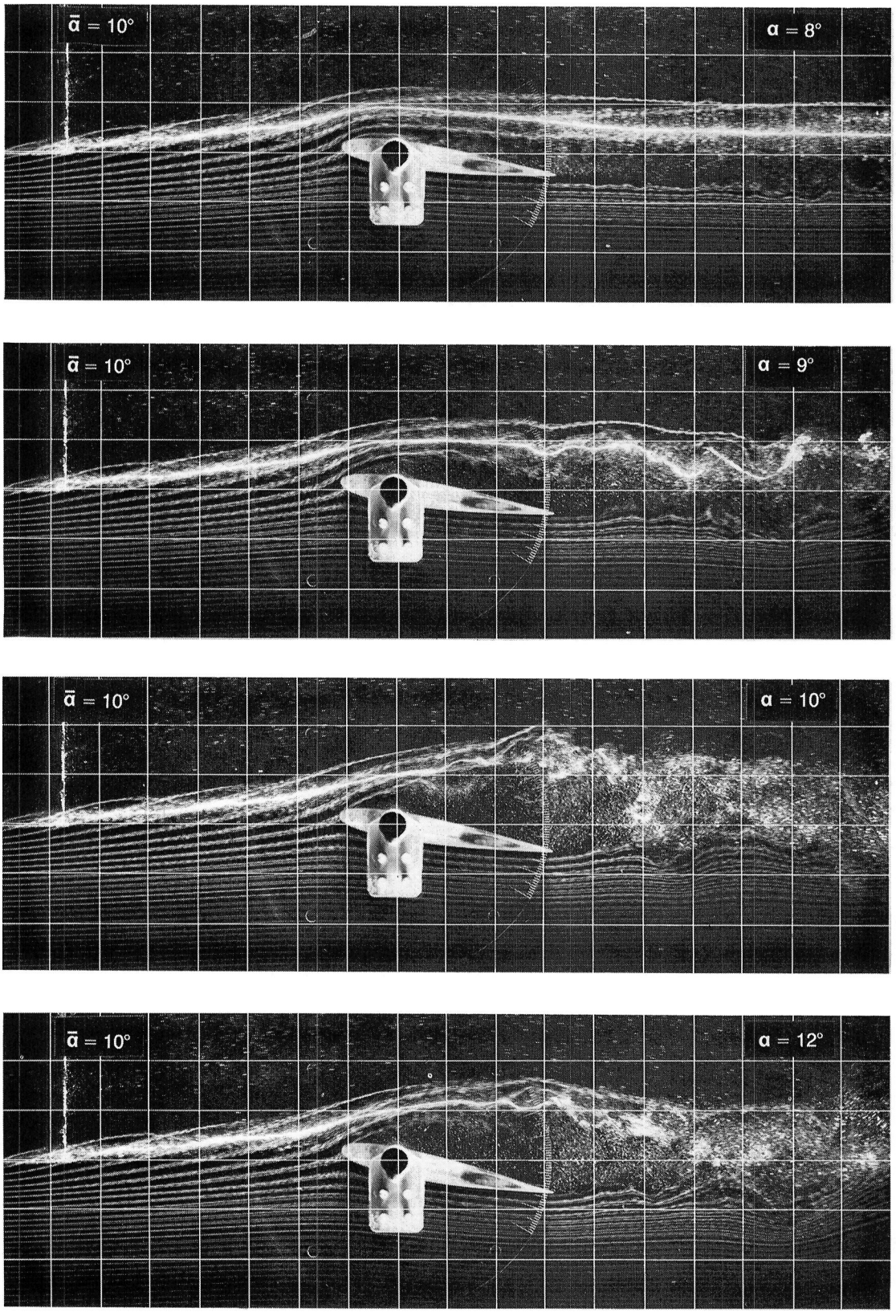

Figure 12.– Continued.

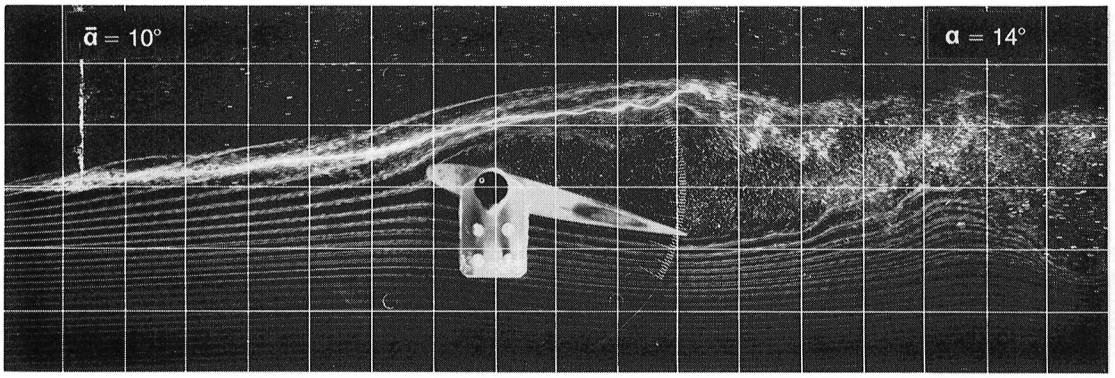

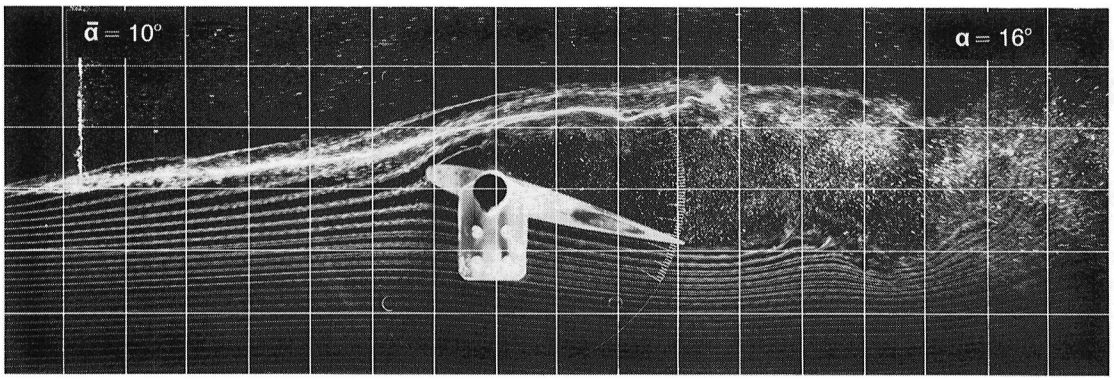

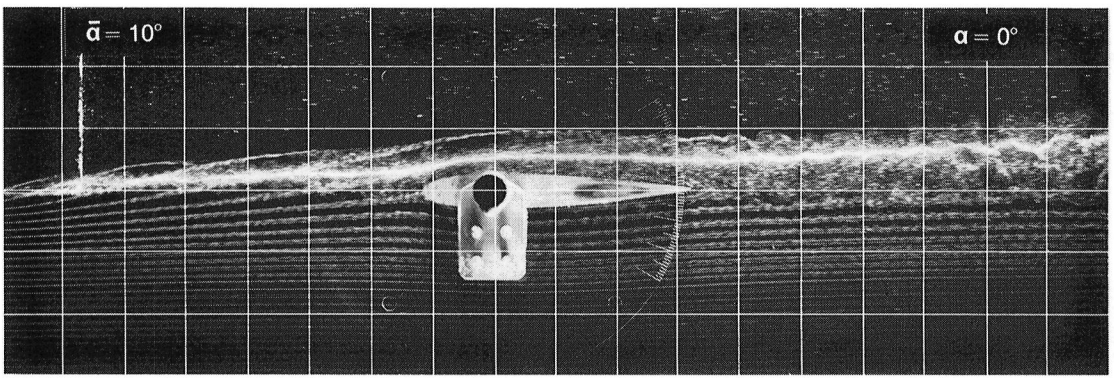

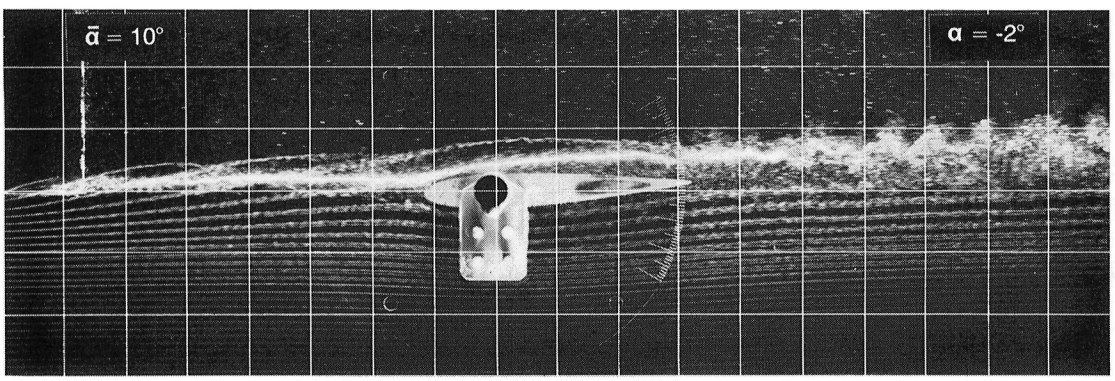

Figure 12.– Continued.

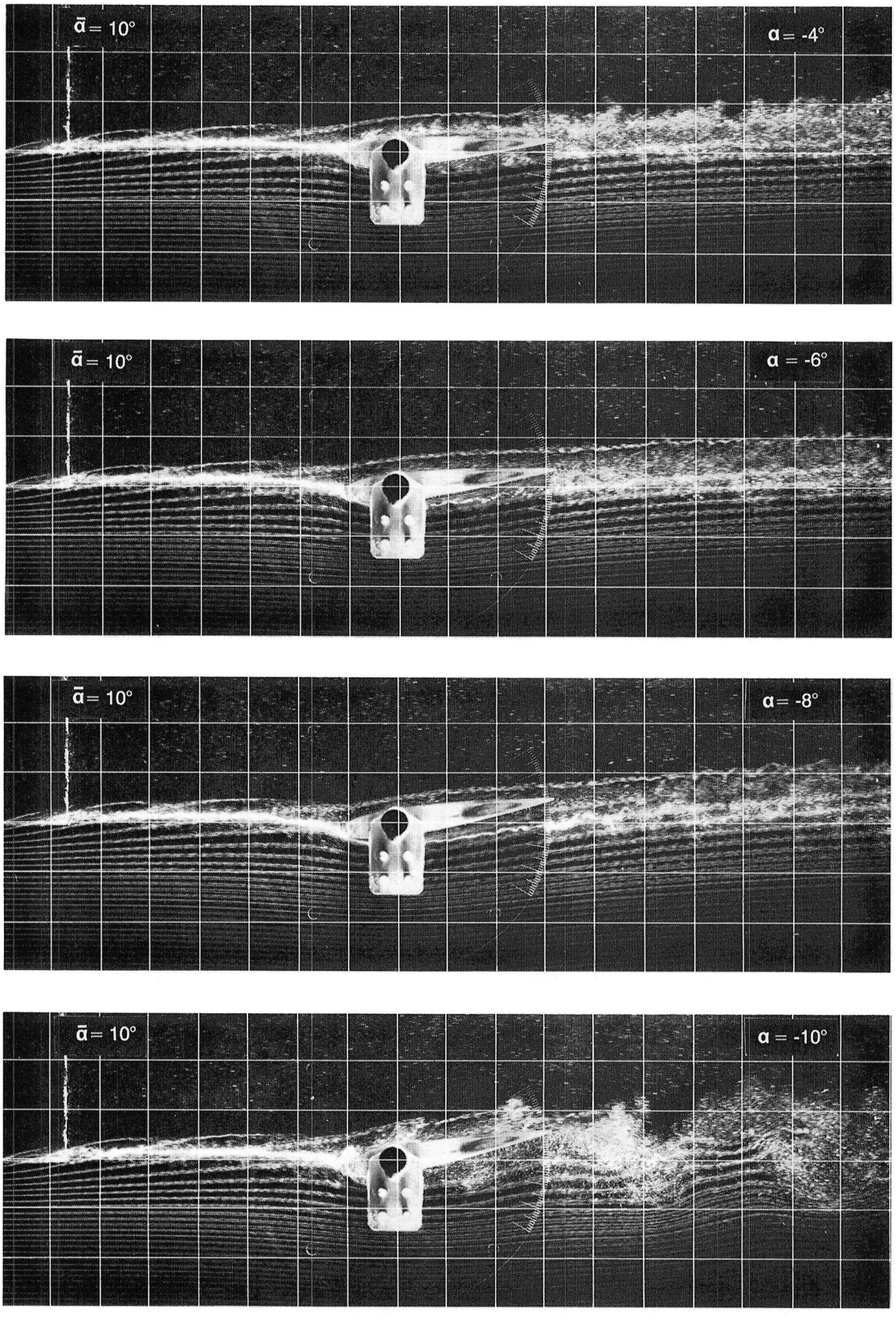

Figure 12.– Continued.

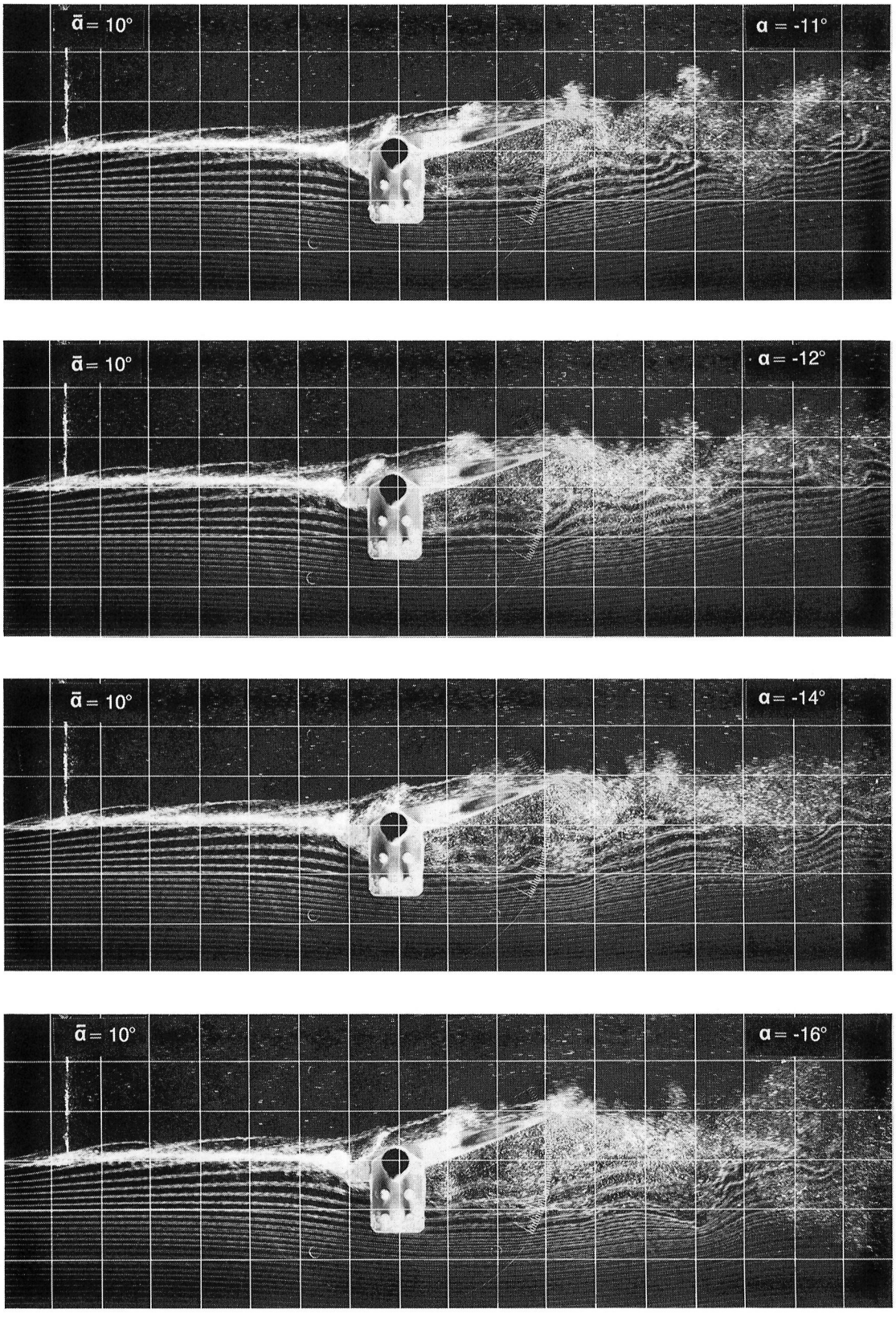

Figure 12.– Concluded.

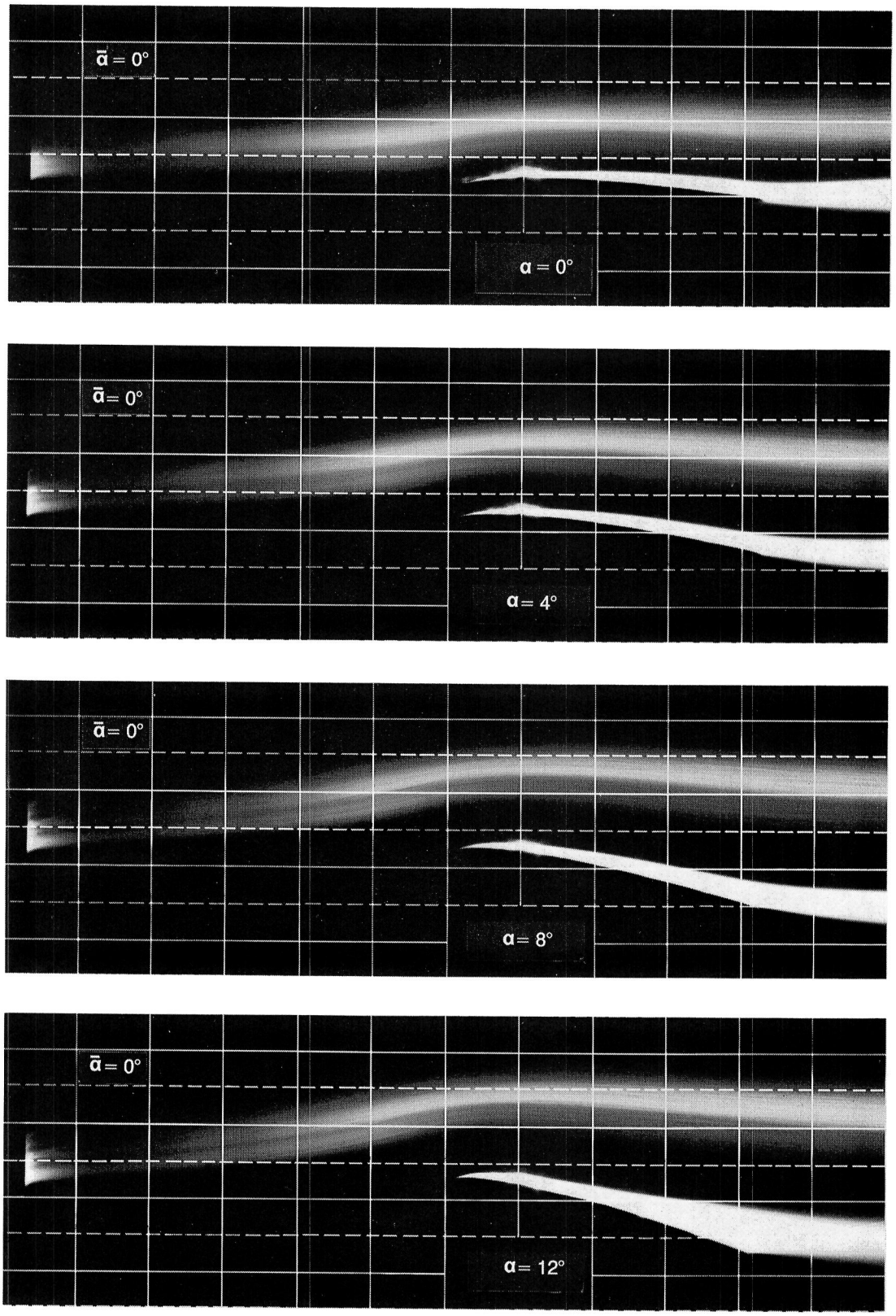

Figure 13.– Long-exposure visualization of flow at Re = 120,000 with generator on centerline and set at $\tilde{\alpha} = 0°$ (no-vortex case).

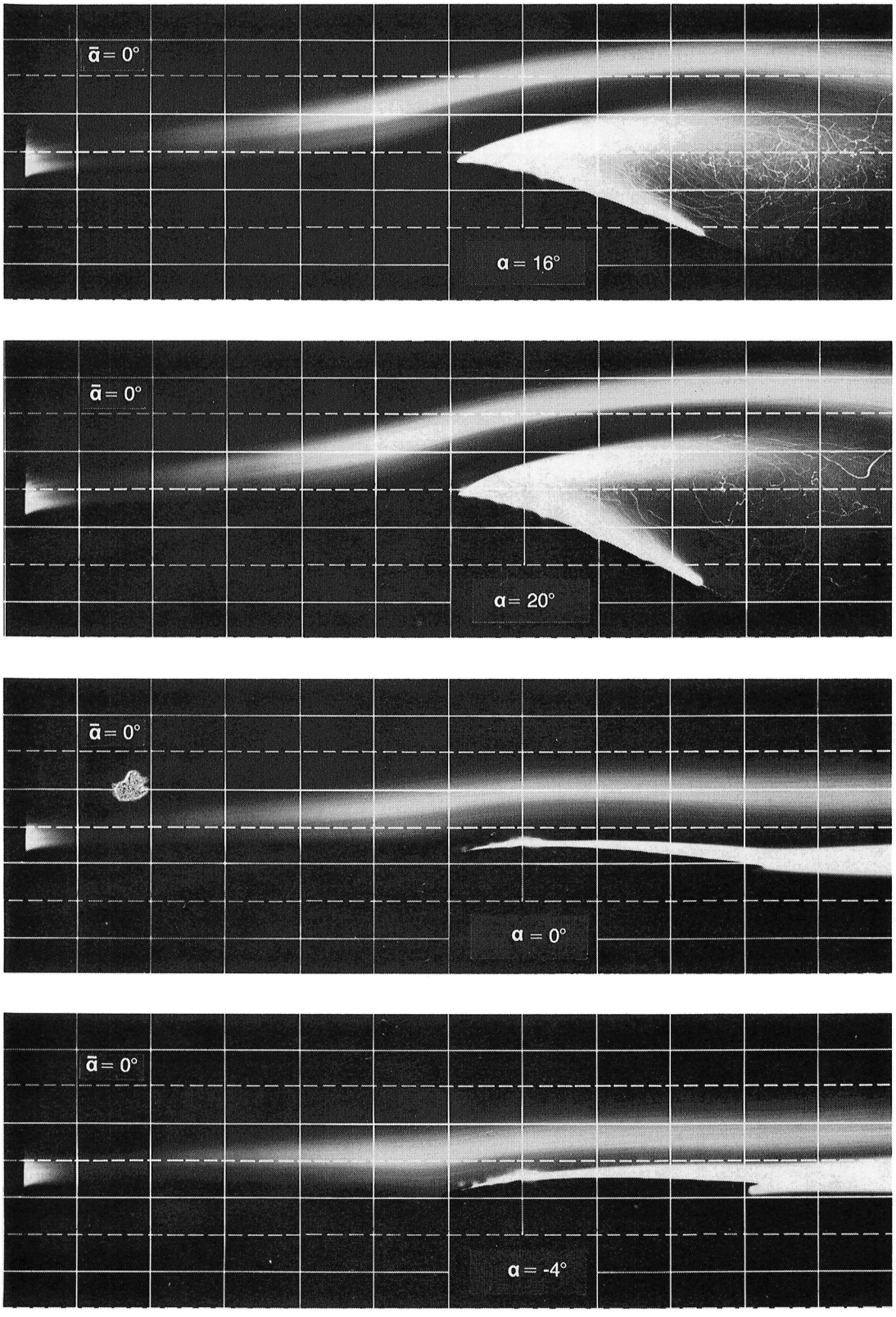

Figure 13.– Continued.

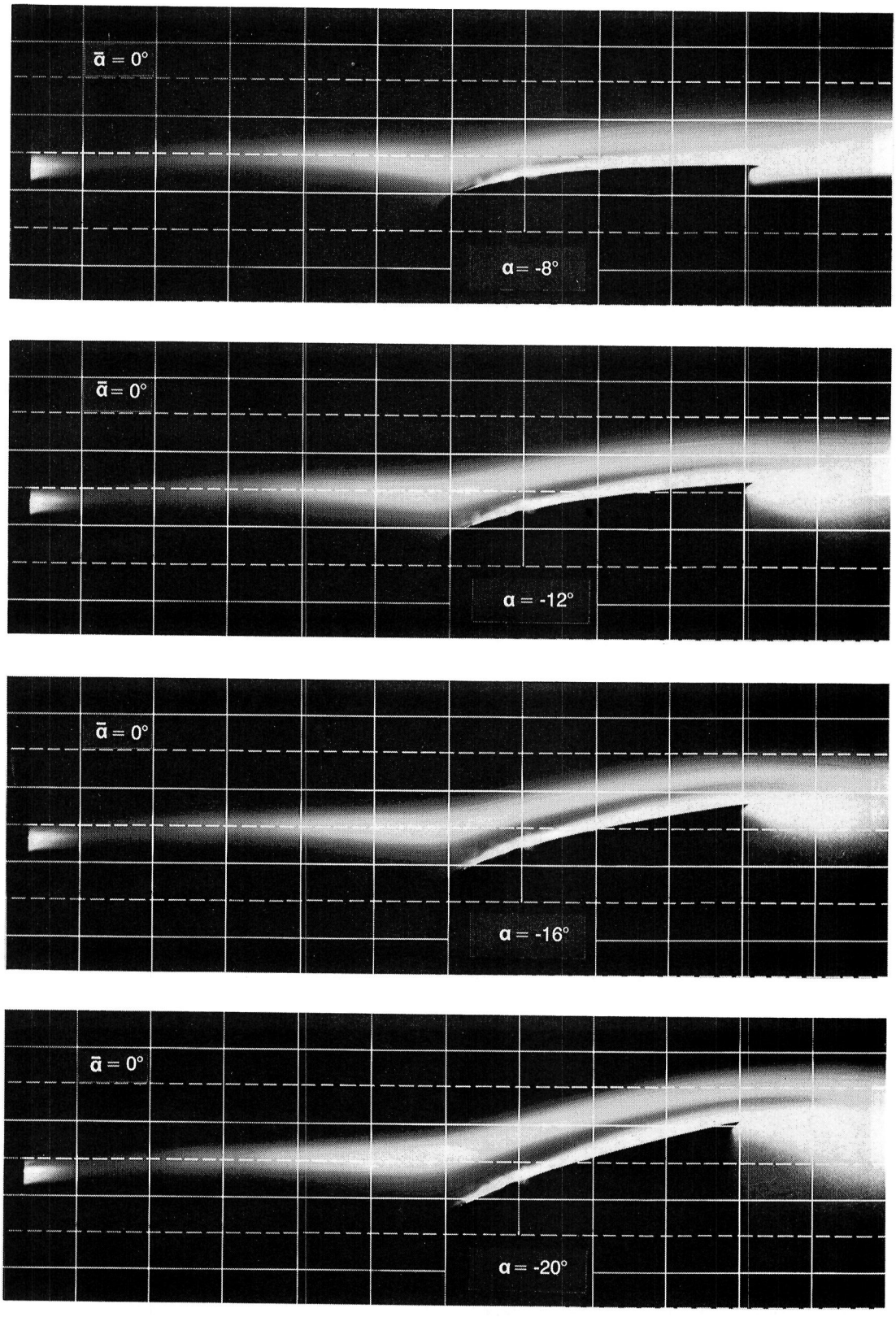

Figure 13.– Concluded.

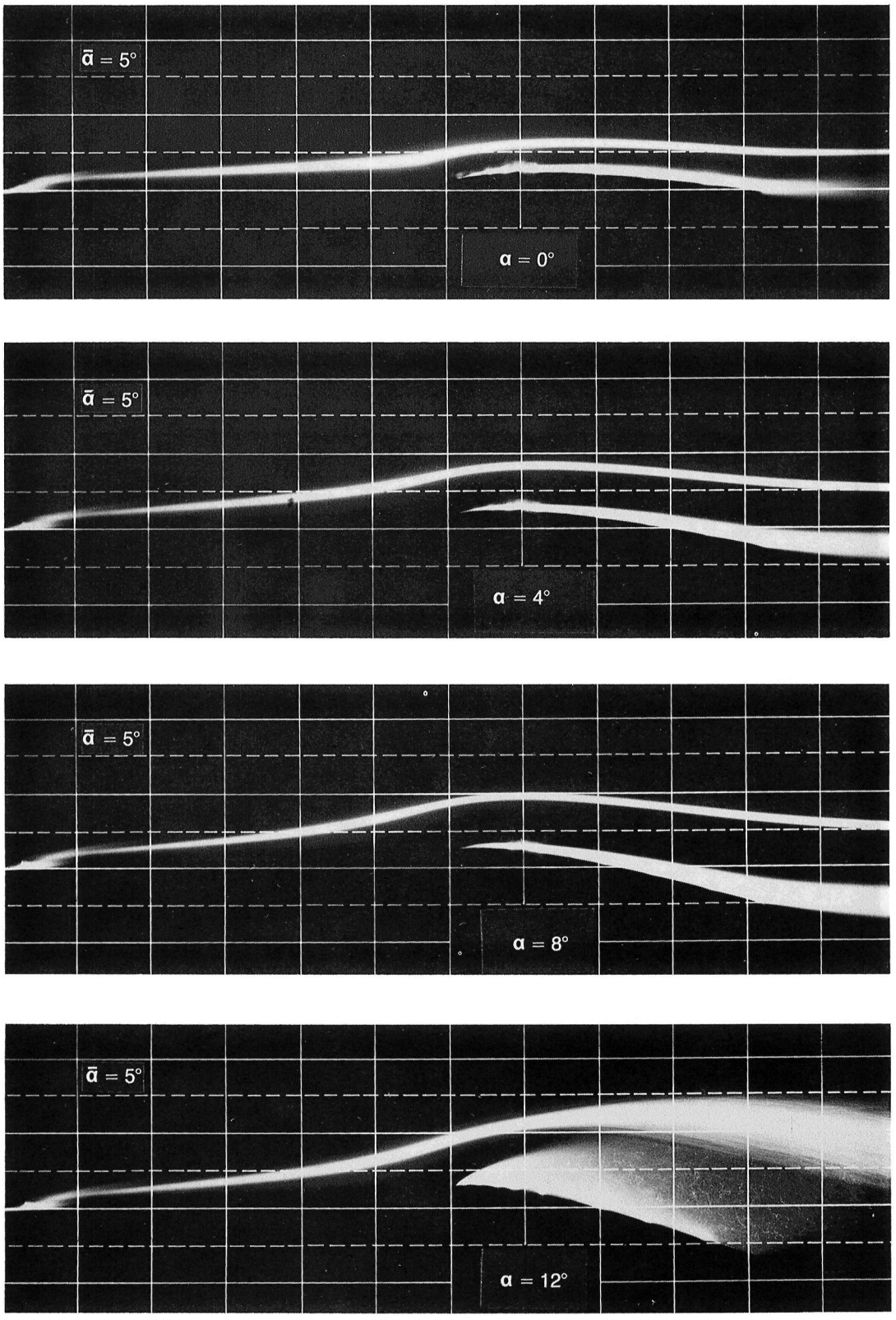

Figure 14.– Long-exposure visualization of flow at Re = 120,000 with generator on centerline and set at $\tilde{\alpha} = 5°$ (weak-vortex case).

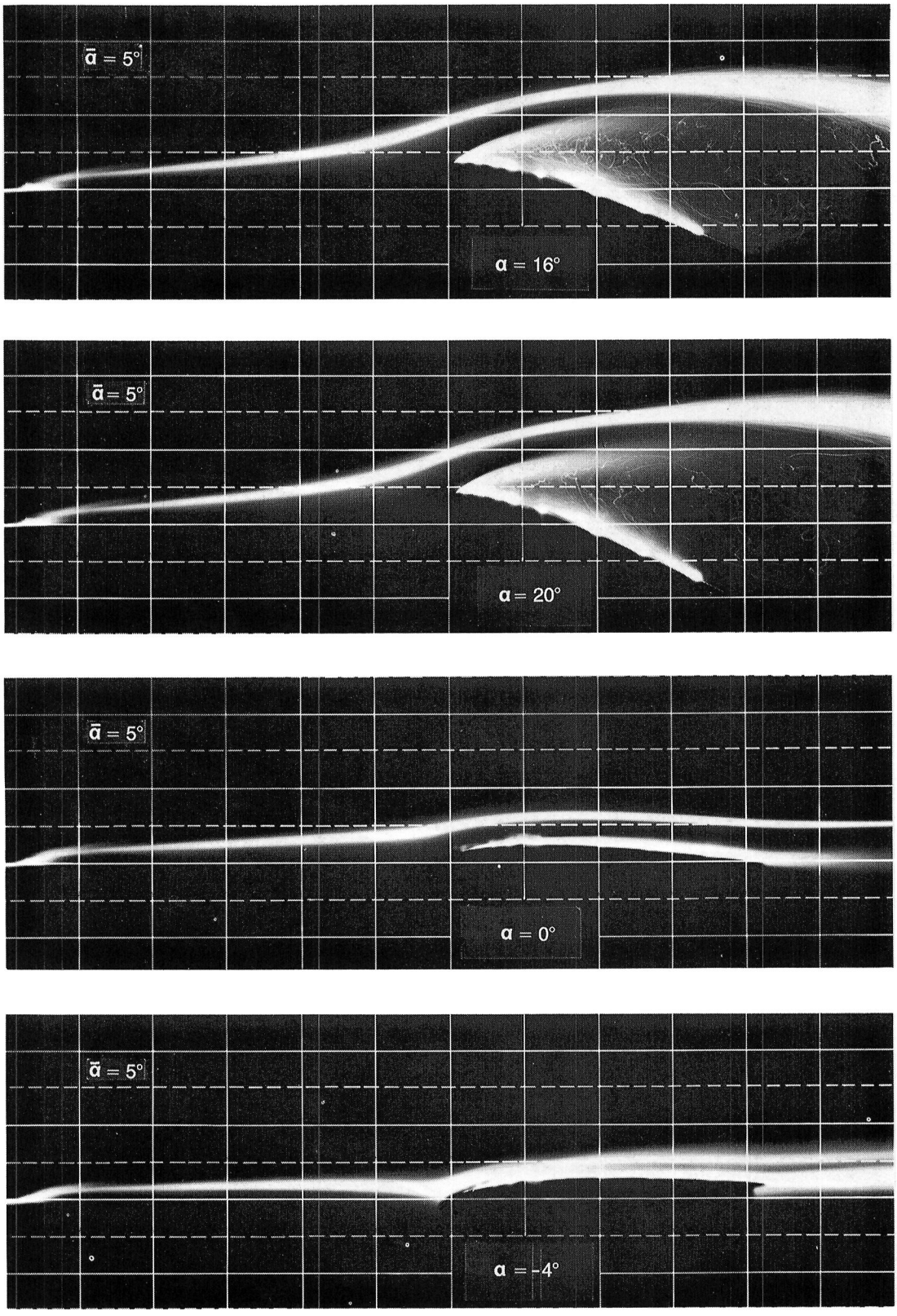

Figure 14.– Continued.

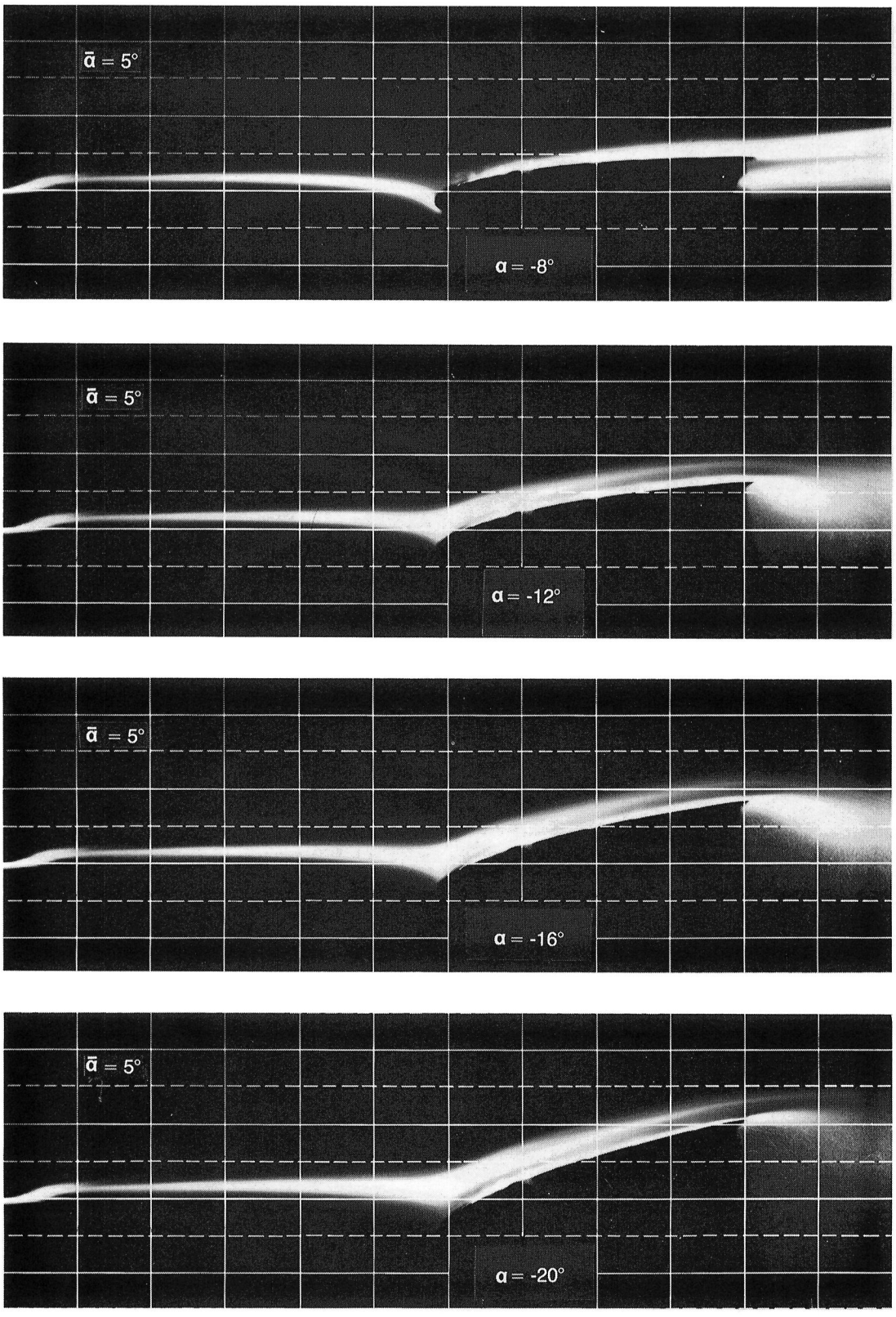

Figure 14.– Concluded.

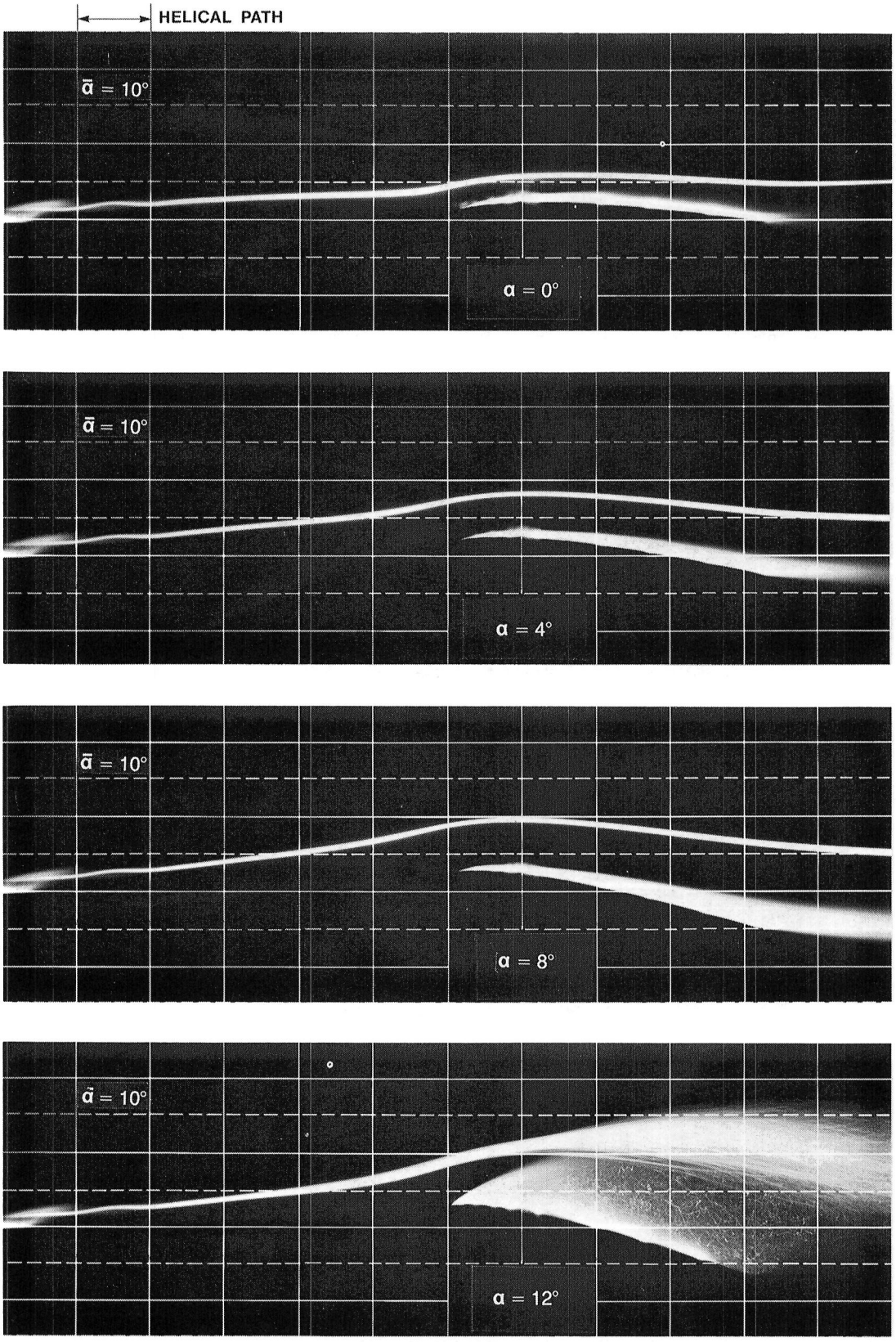

Figure 15.– Long-exposure visualization of flow at Re = 120,000 with generator on centerline and set at $\tilde{\alpha} = 10^{\circ}$ (strong-vortex case).

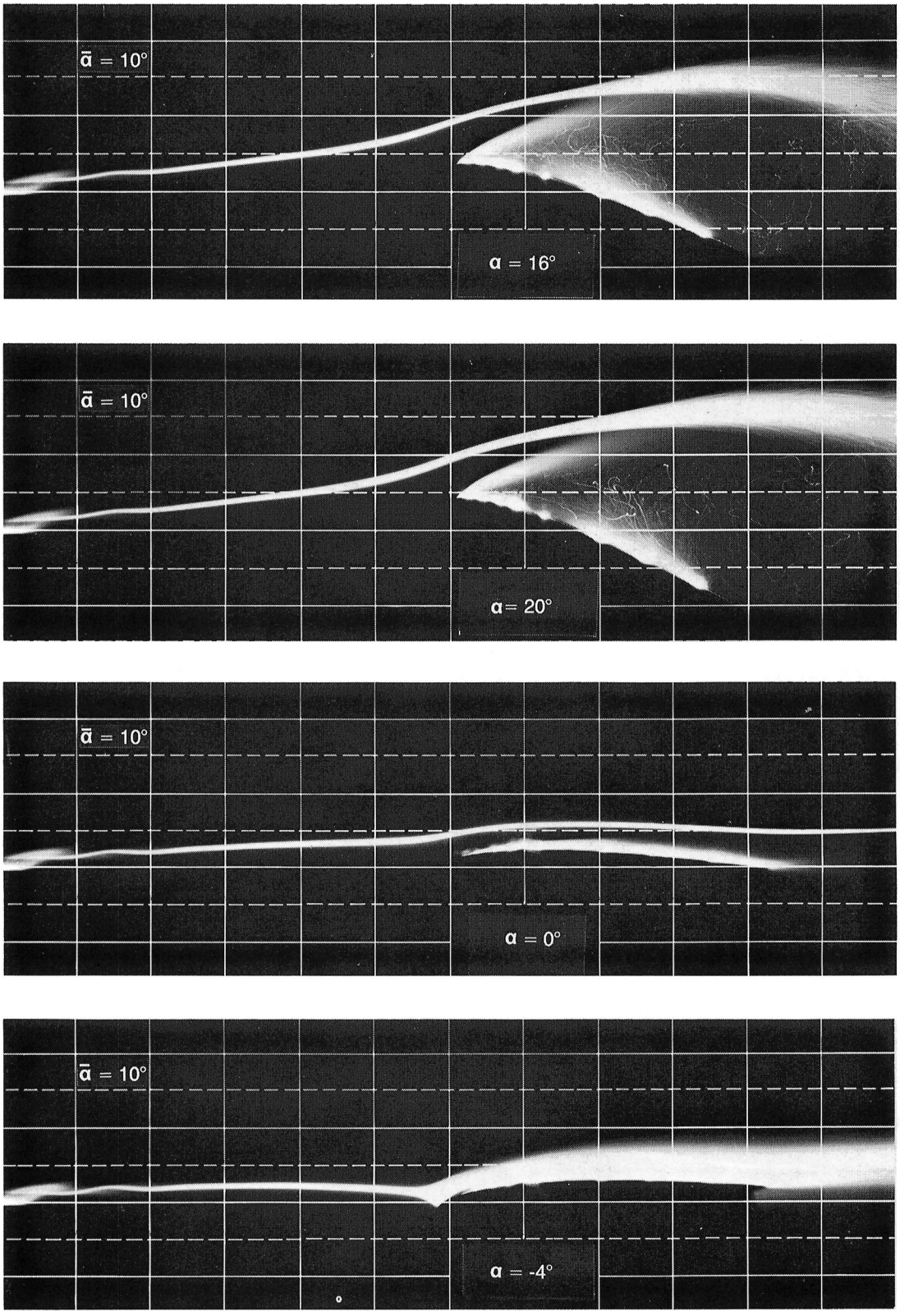

Figure 15.– Continued.

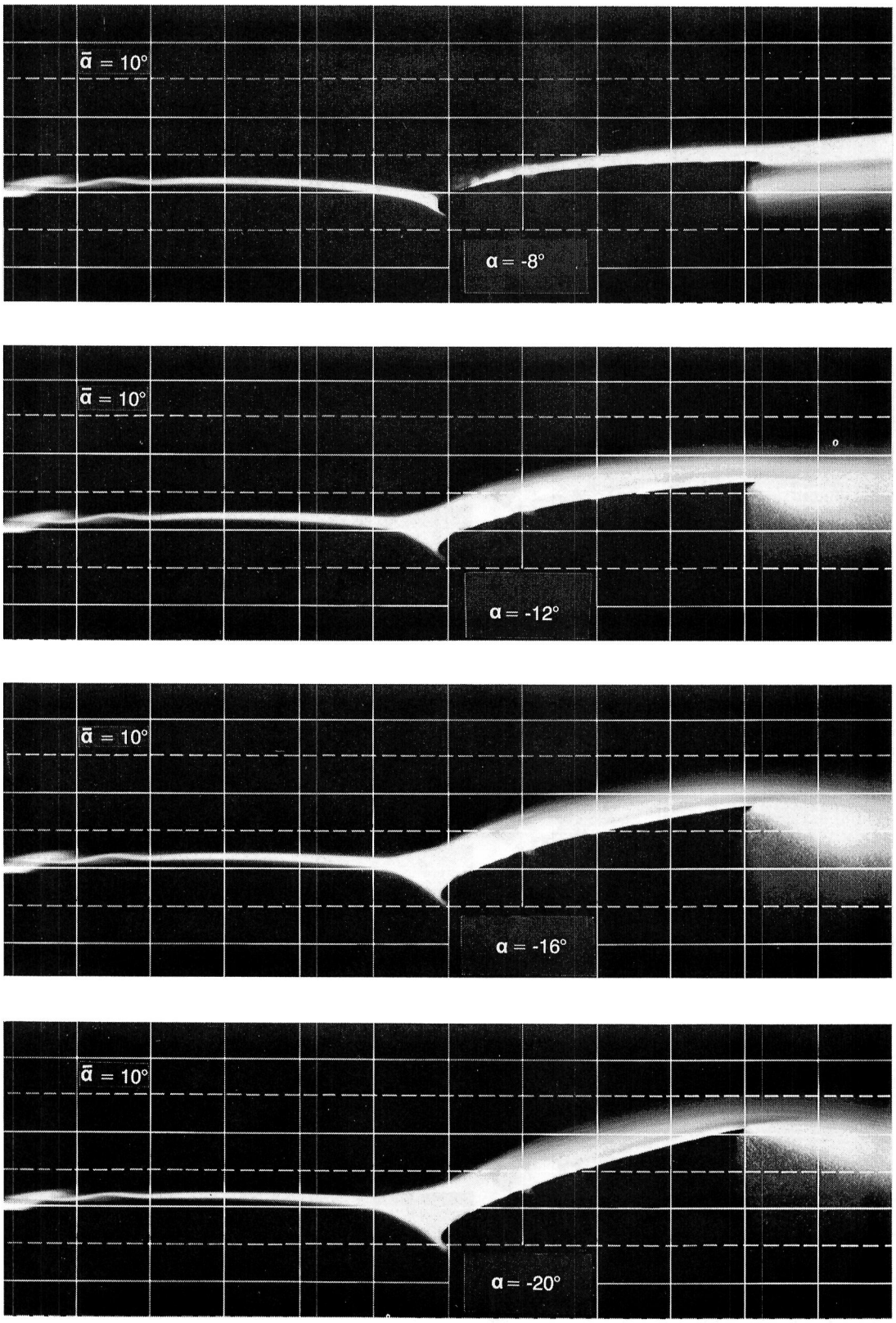

Figure 15.– Concluded.

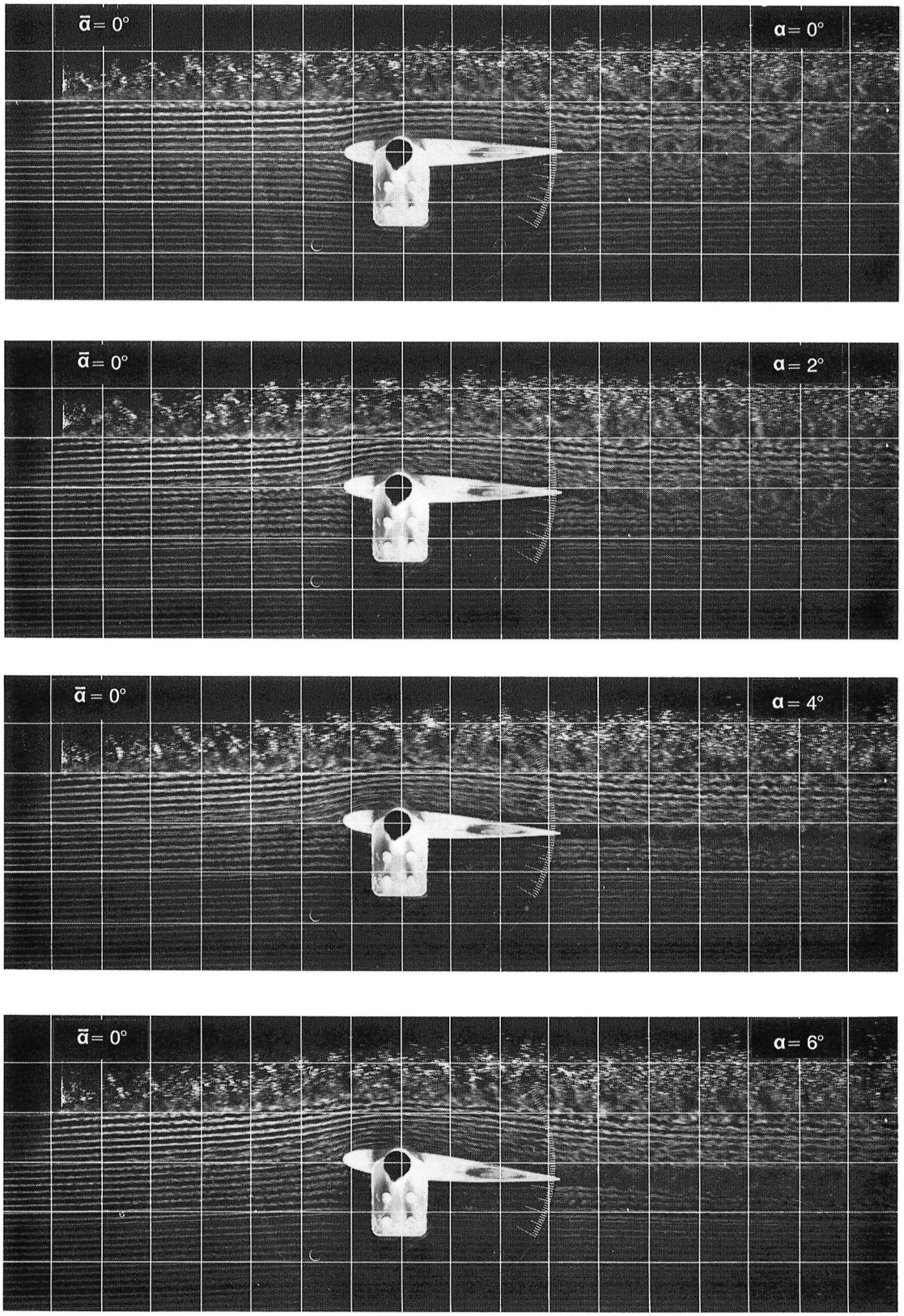

Figure 16.– Visualization of flow at Re = 120,000 with generator off centerline and set at $\tilde{\alpha} = 0°$ (no-vortex case).

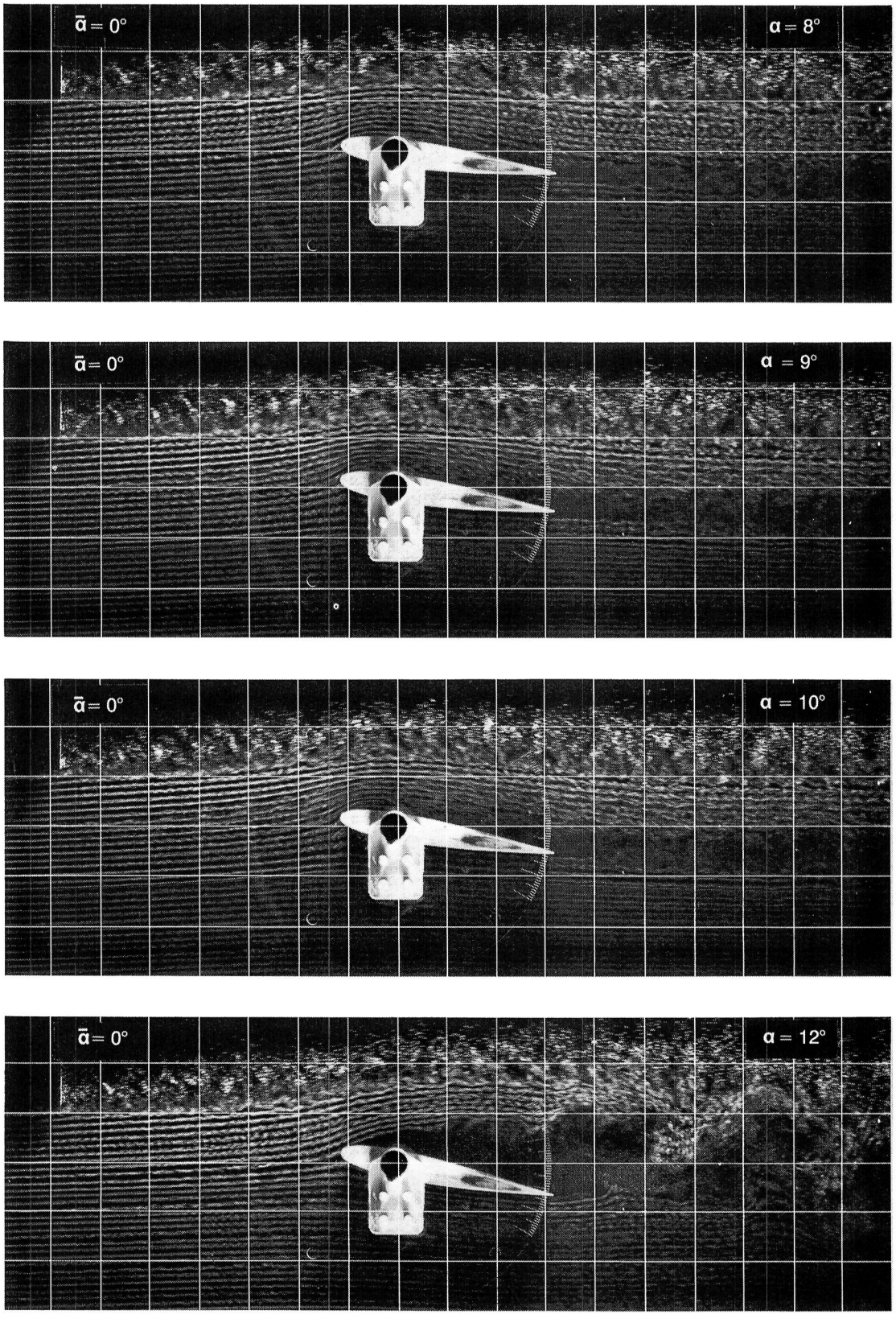

Figure 16.– Continued.

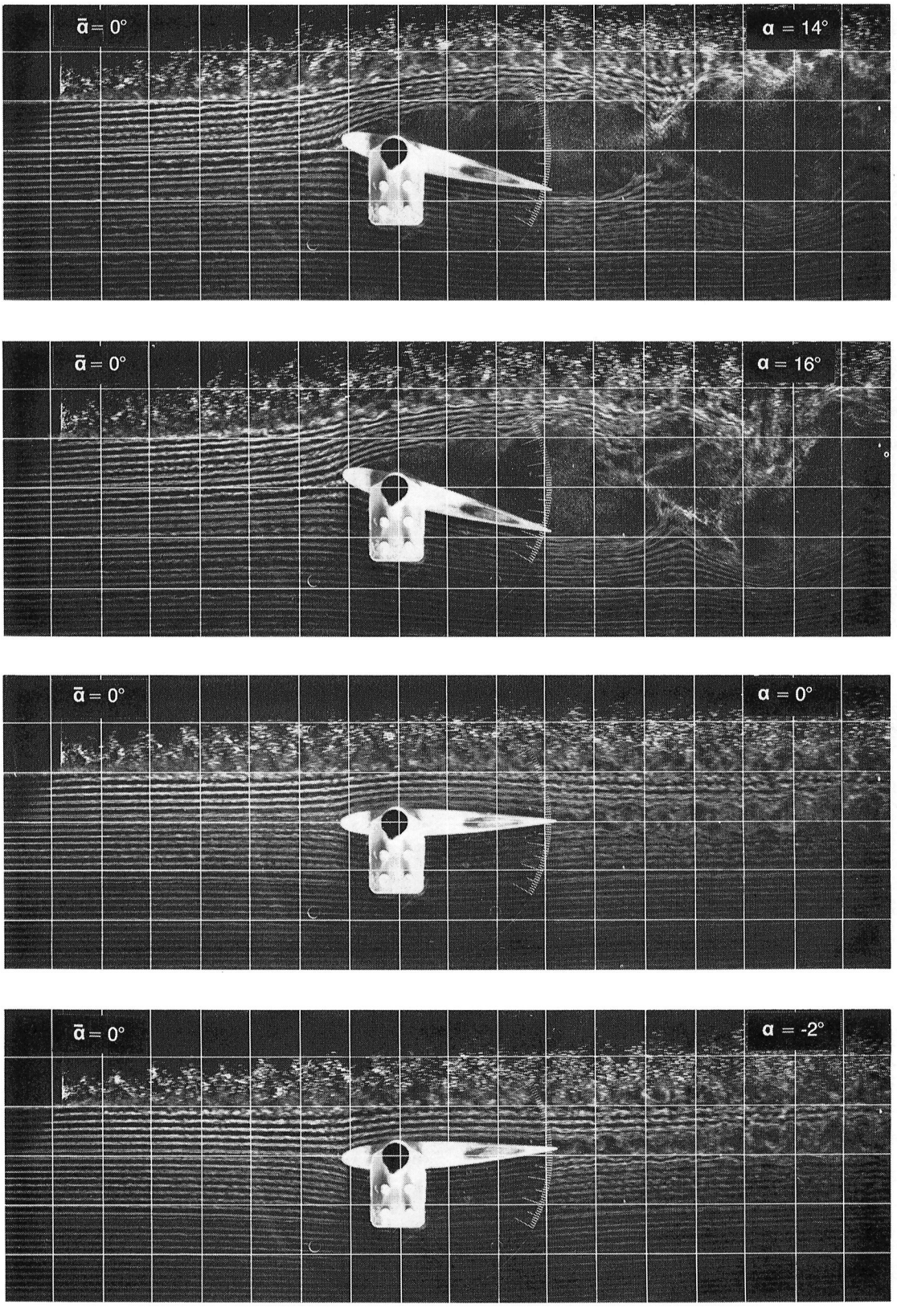

Figure 16.– Continued.

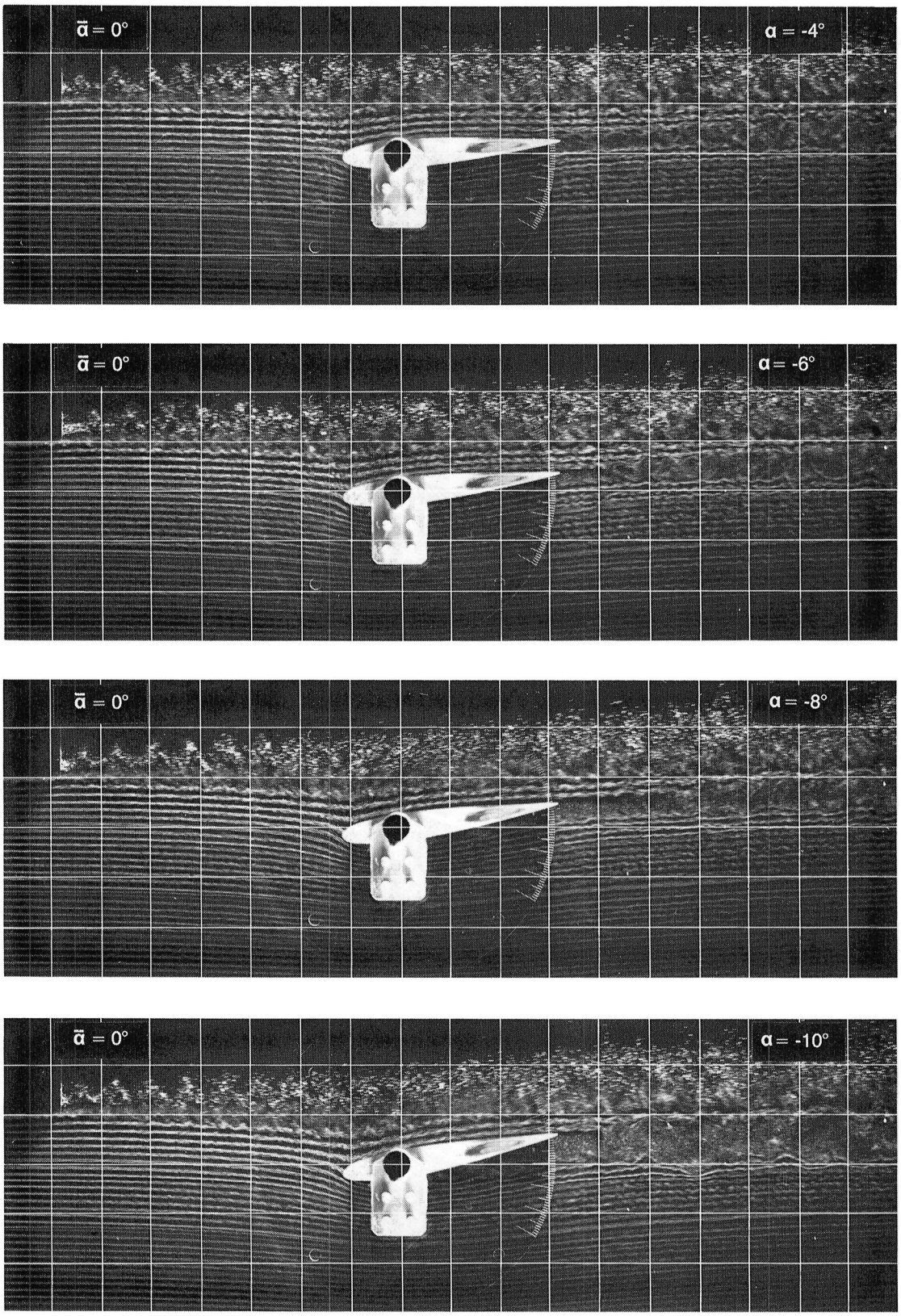

Figure 16.– Continued.

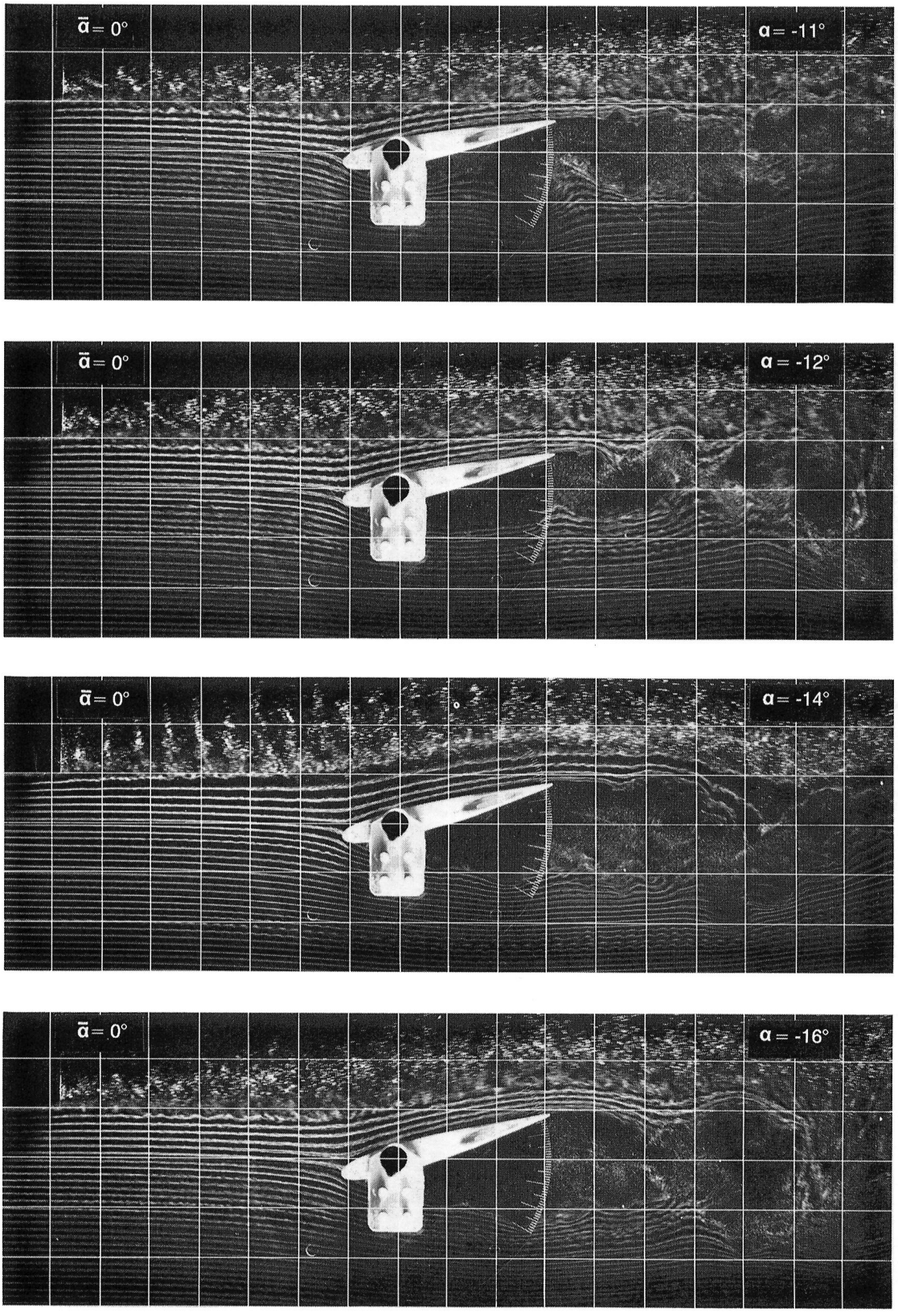

Figure 16.– Concluded.

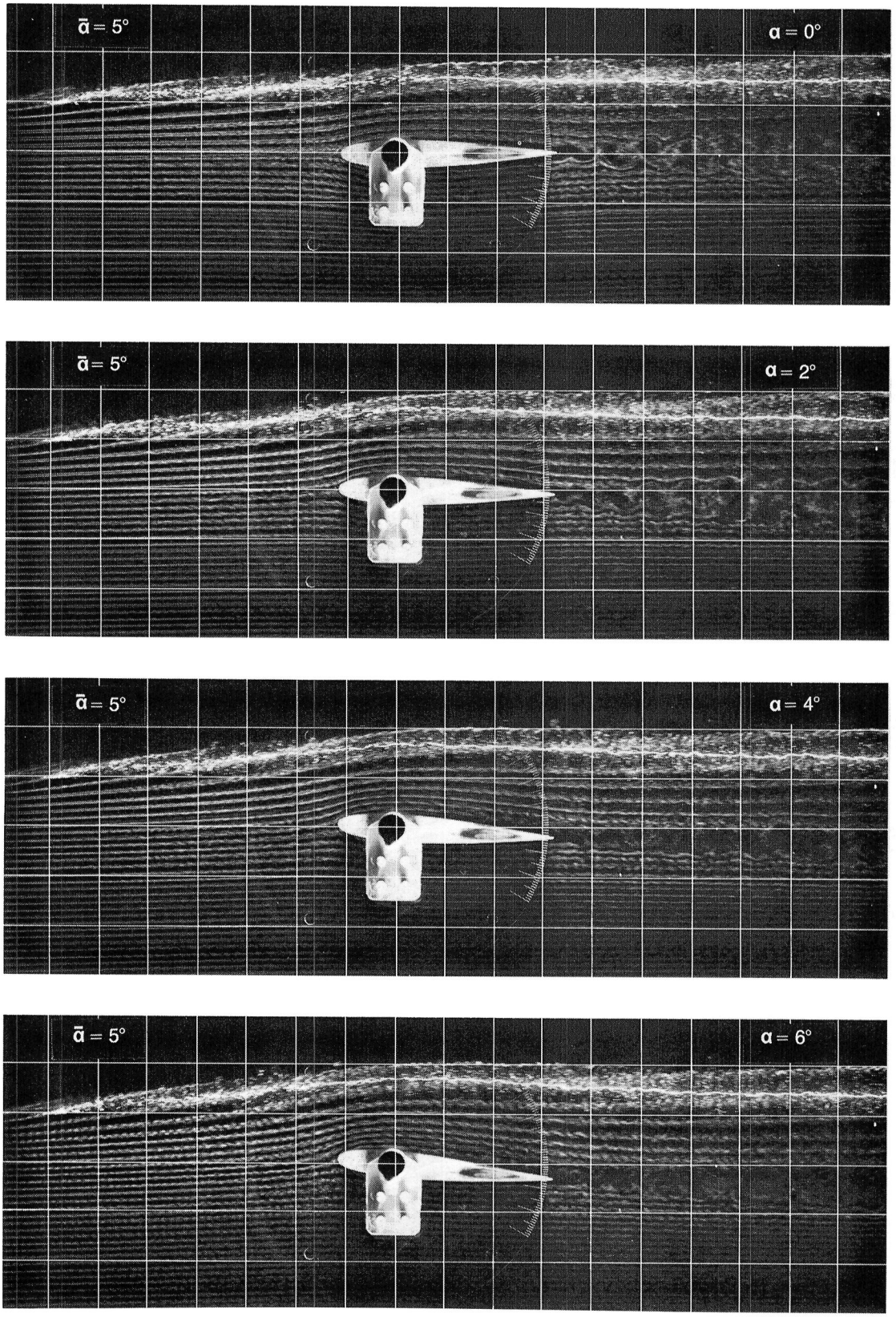

Figure 17.– Visualization of flow at Re = 120,000 with generator off centerline and set at $\tilde{\alpha} = 5°$ (weak-vortex case).

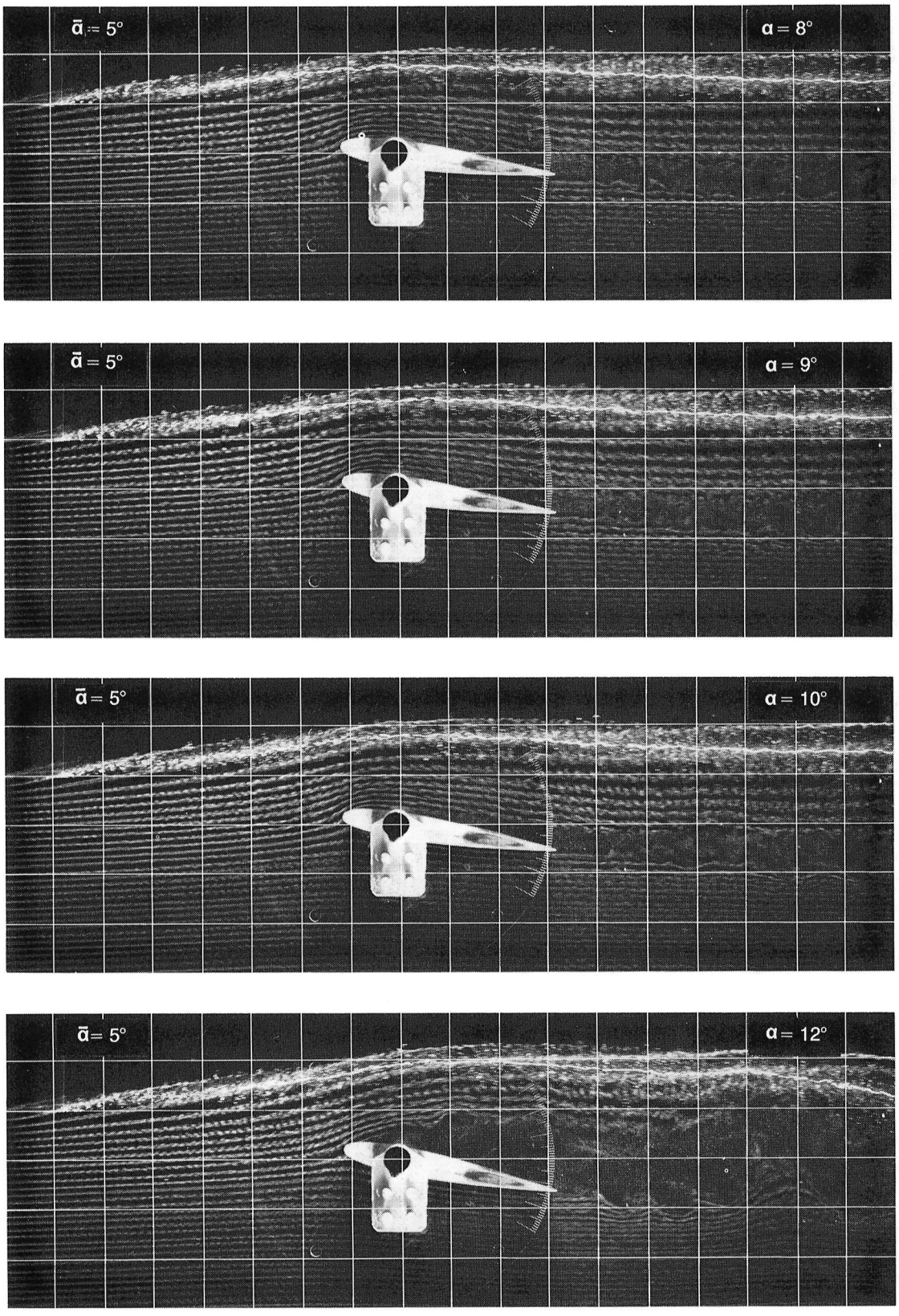

Figure 17.– Continued.

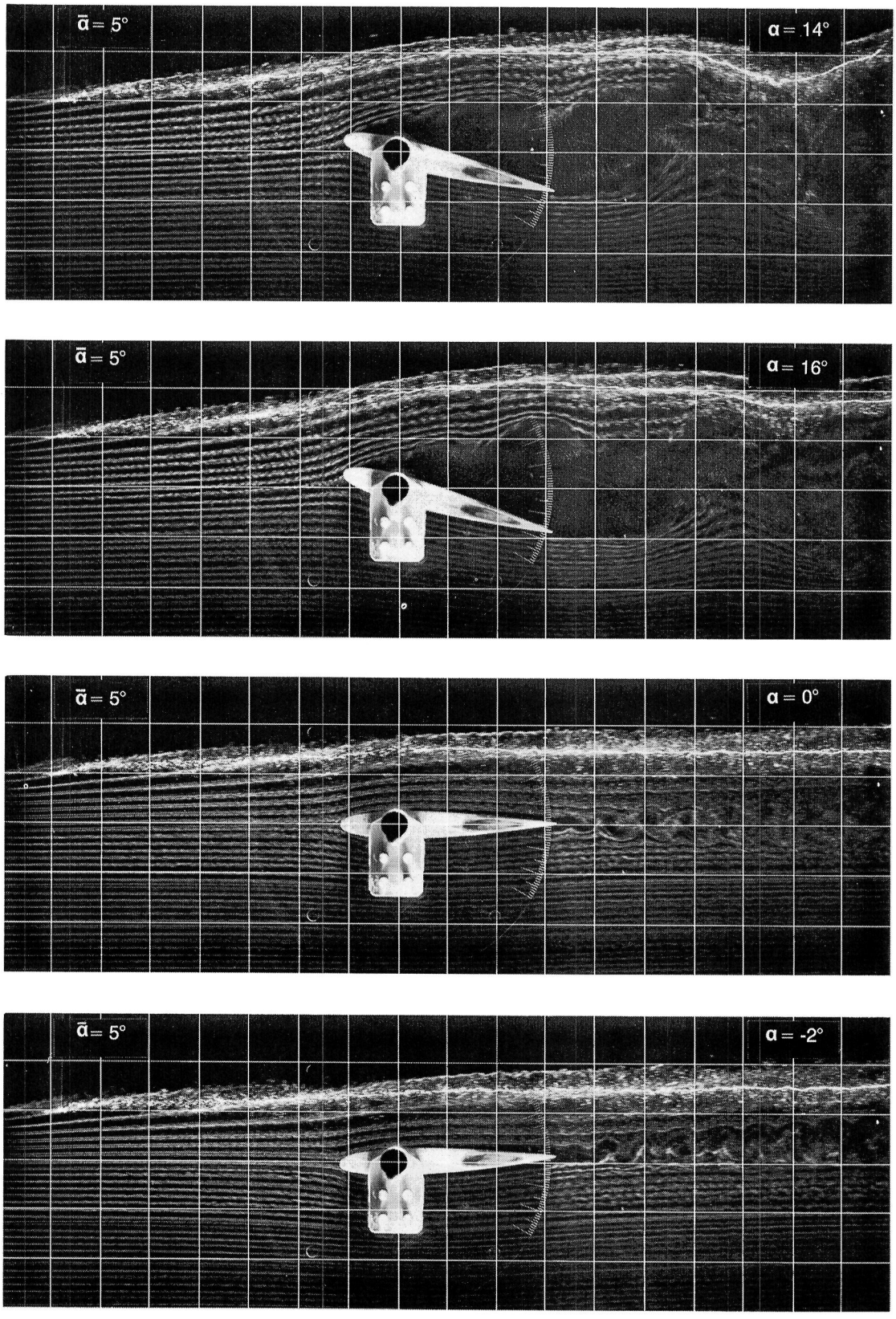

Figure 17.– Continued.

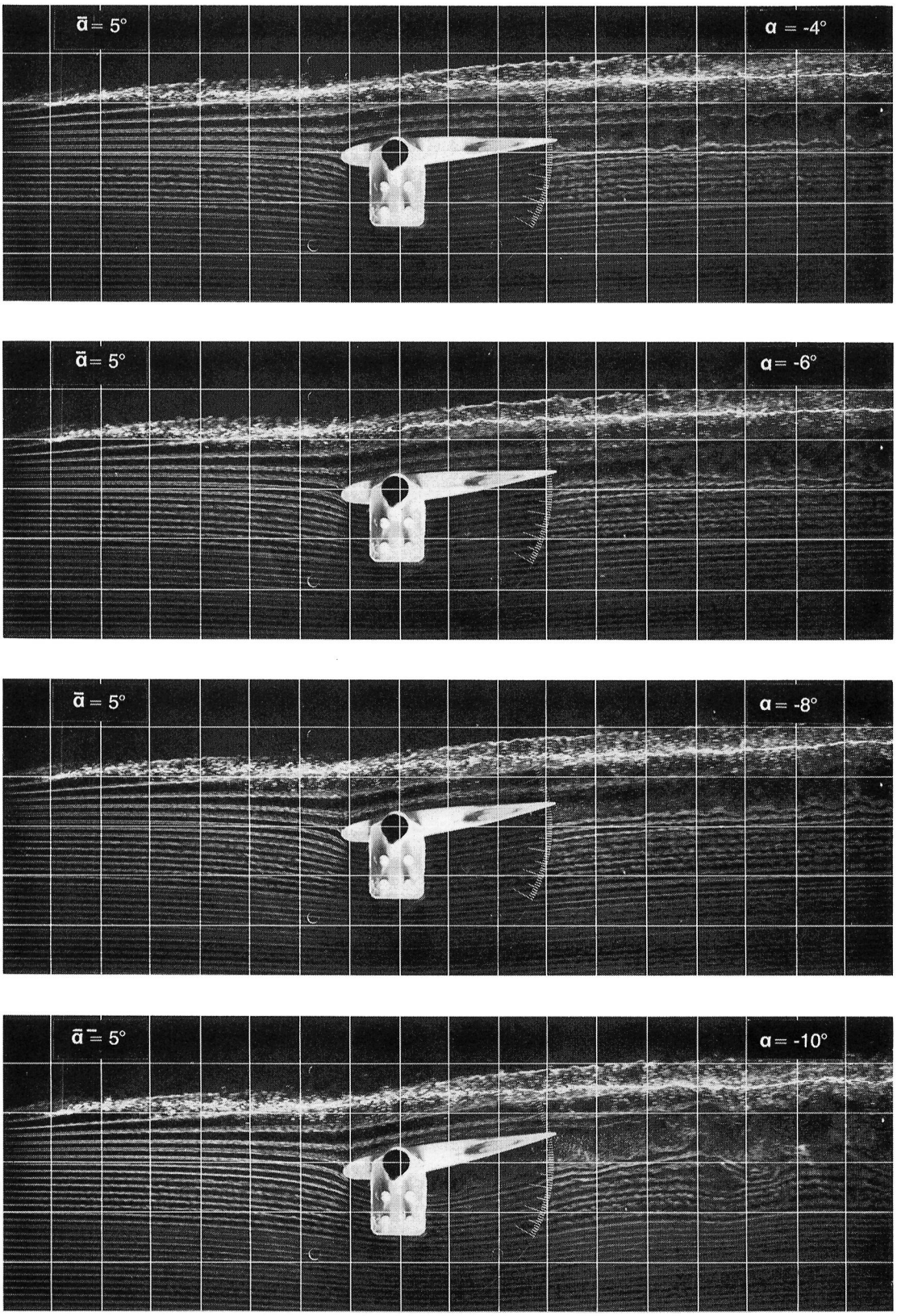

Figure 17.– Continued.

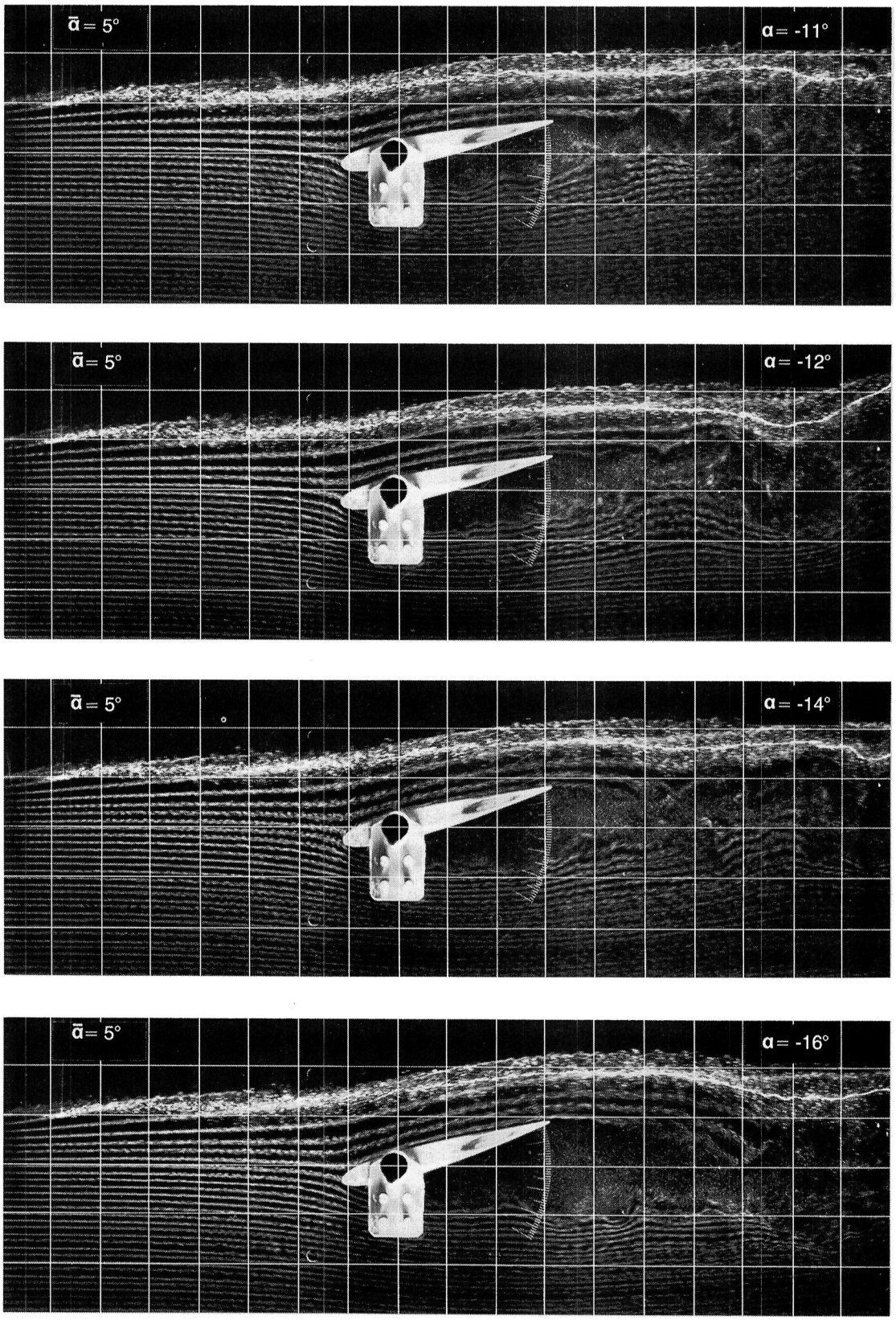

Figure 17.– Concluded.

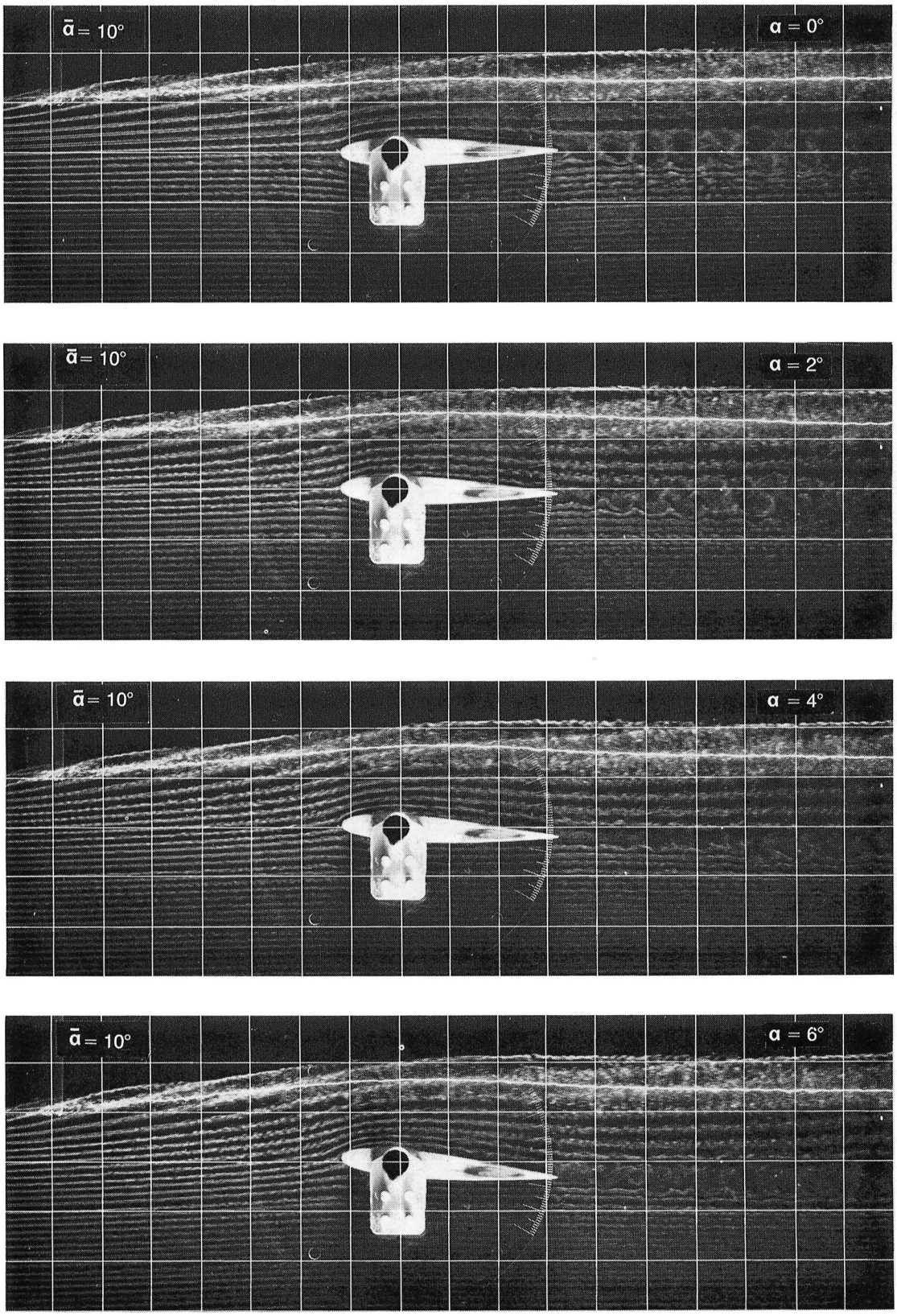

Figure 18.– Visualization of flow at Re = 120,000 with generator off centerline and set at $\tilde{\alpha} = 10^{\circ}$ (strong-vortex case).

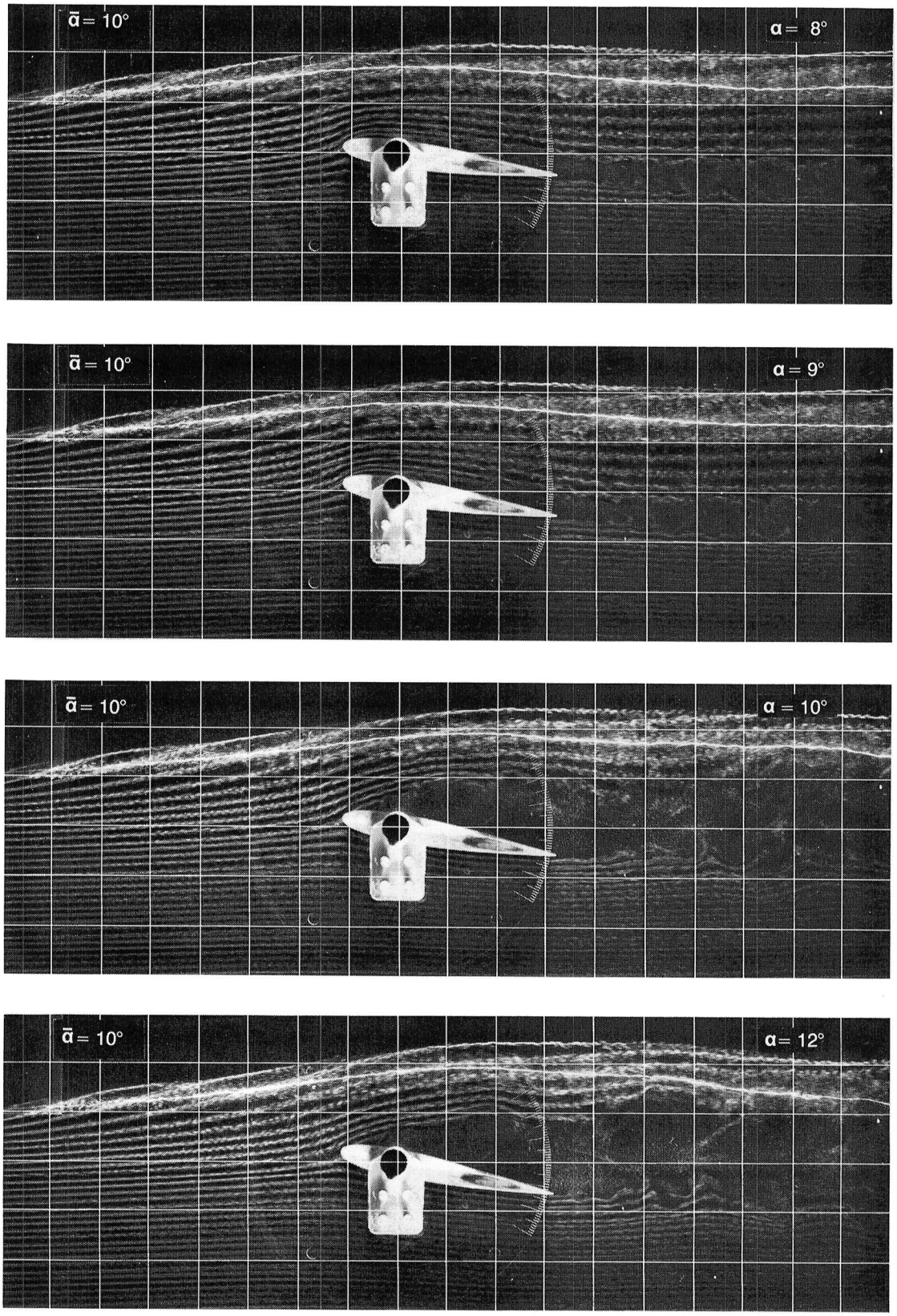

Figure 18.– Continued.

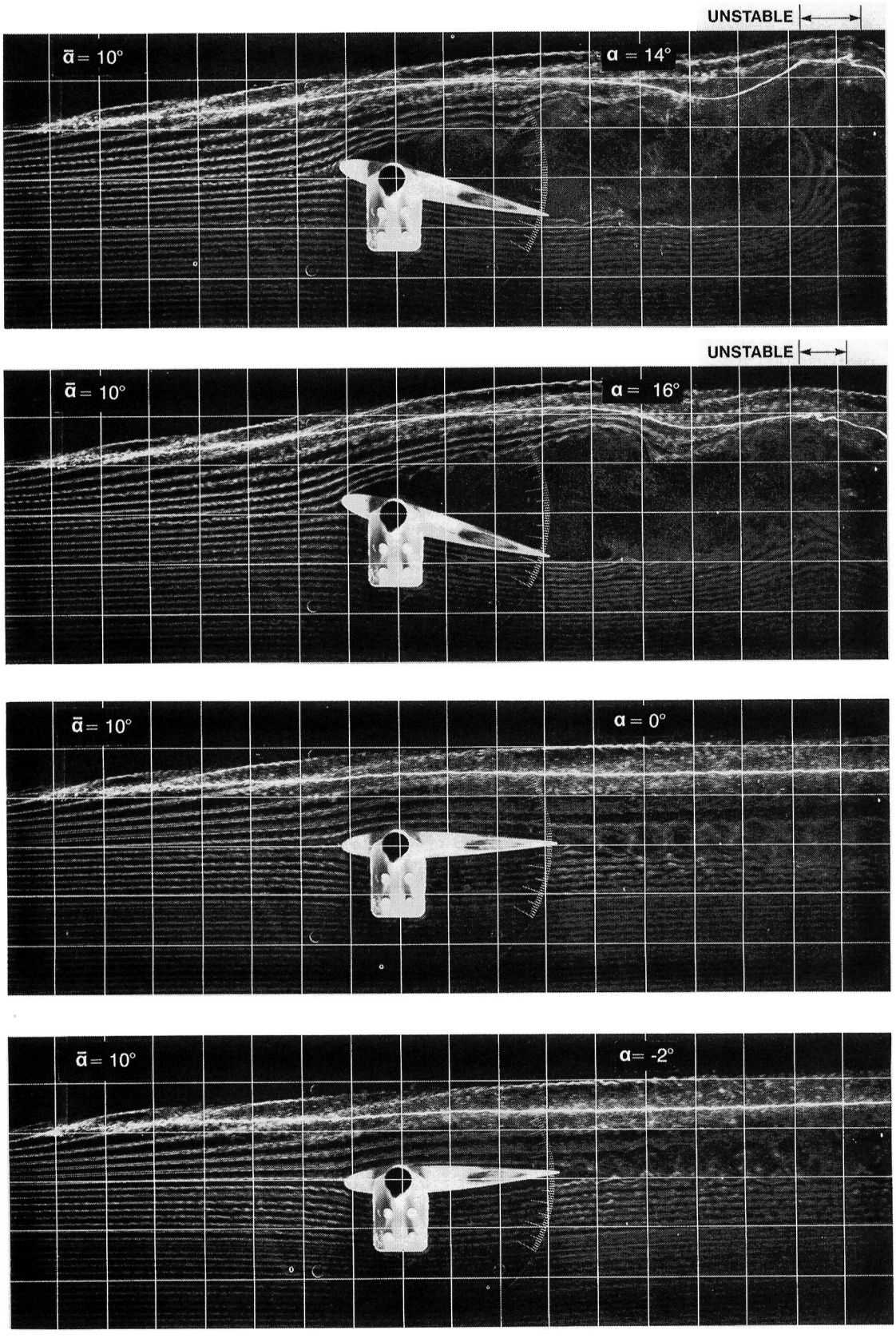

Figure 18.– Continued.

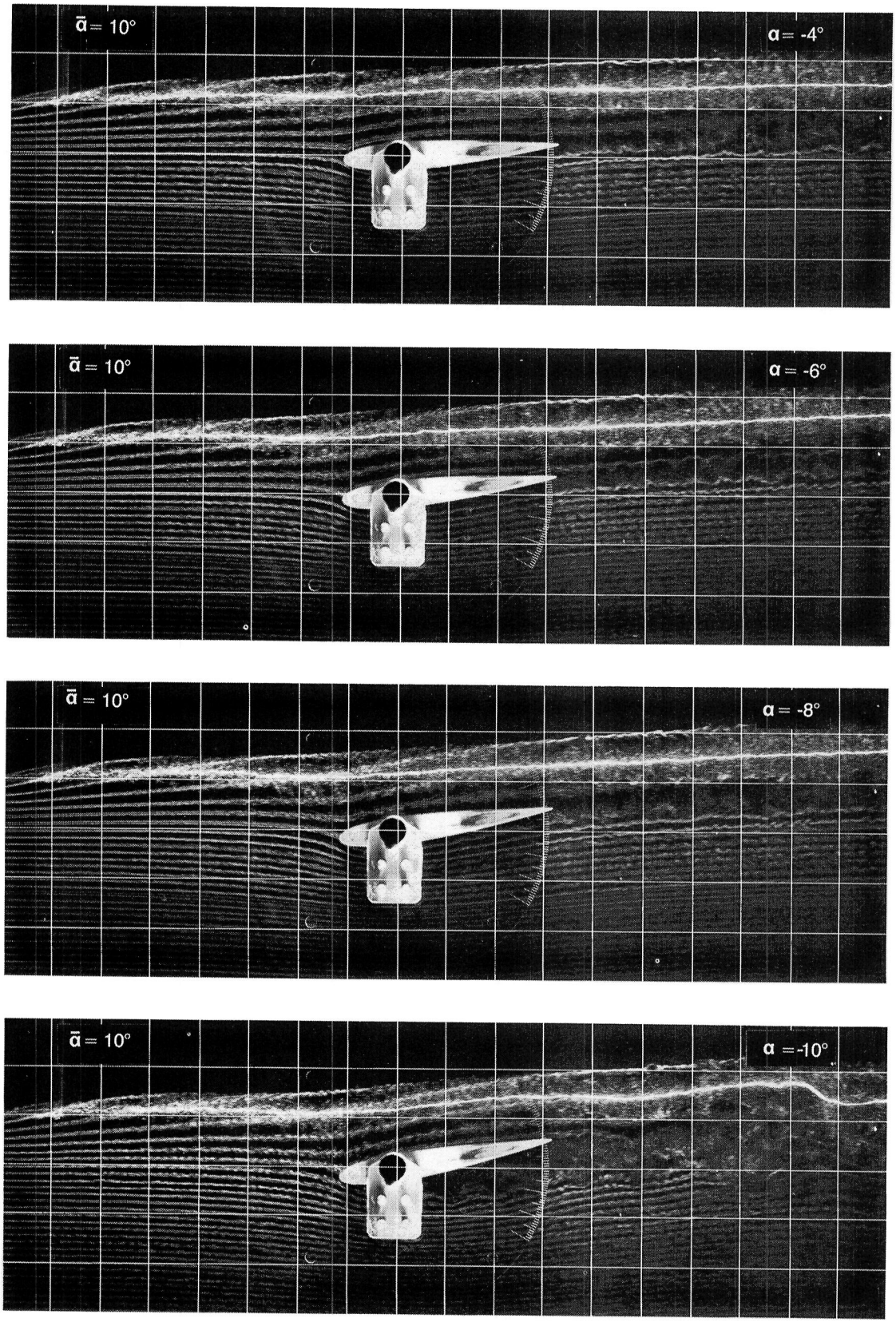

Figure 18.– Continued.

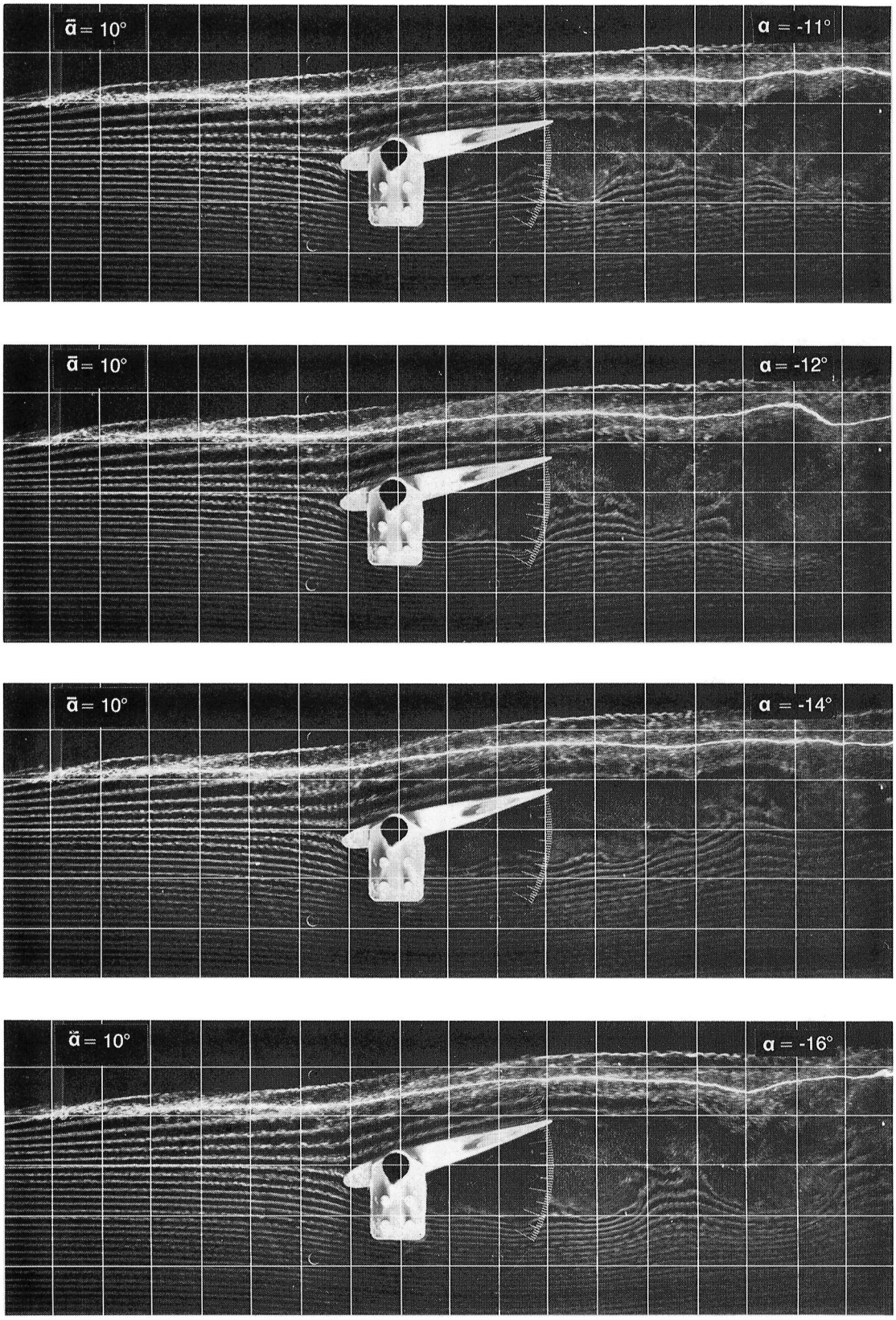

Figure 18.– Concluded.

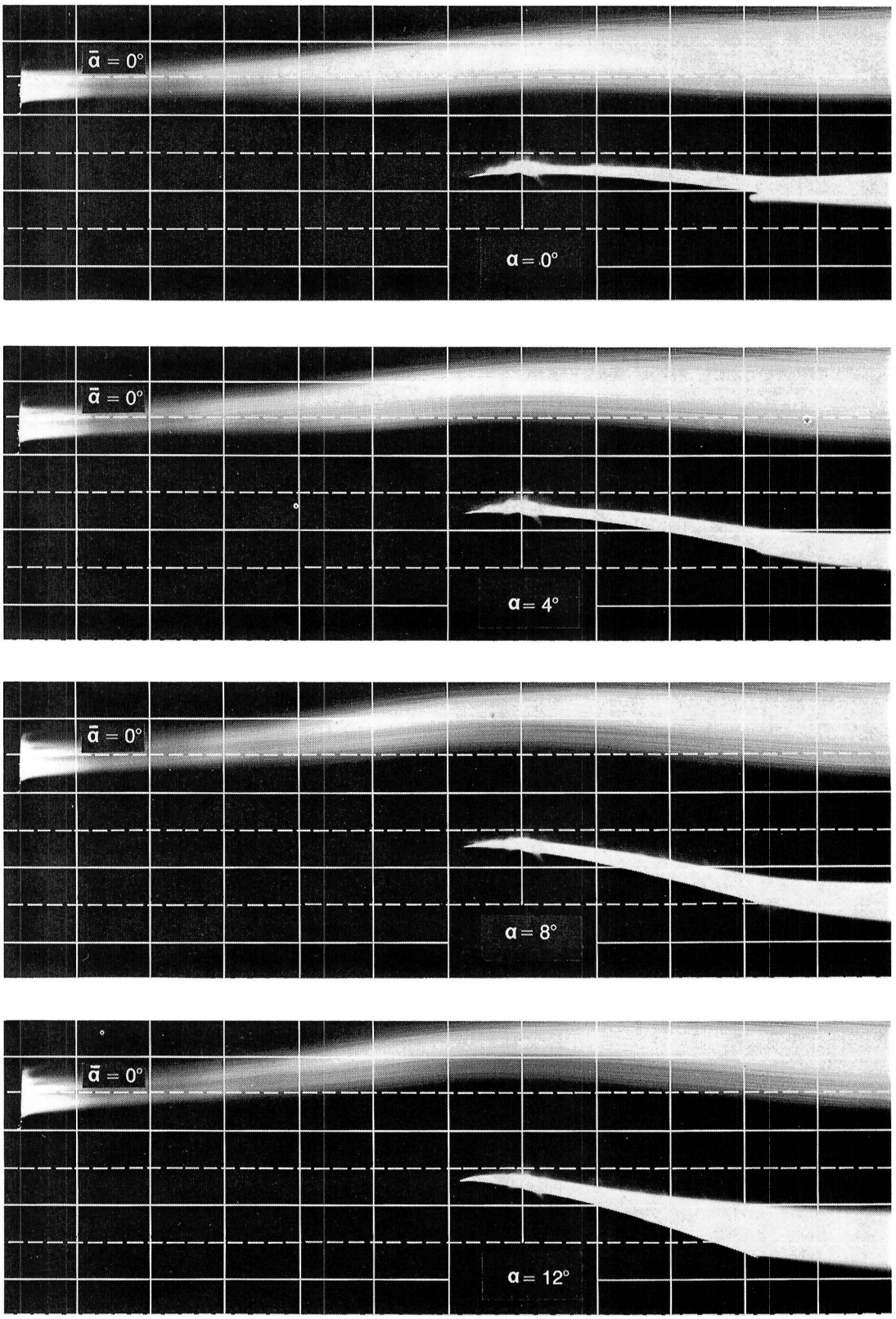

Figure 19.– Long-exposure visualization of flow at Re = 120,000 with generator off centerline and set at $\tilde{\alpha} = 0°$ (no-vortex case).

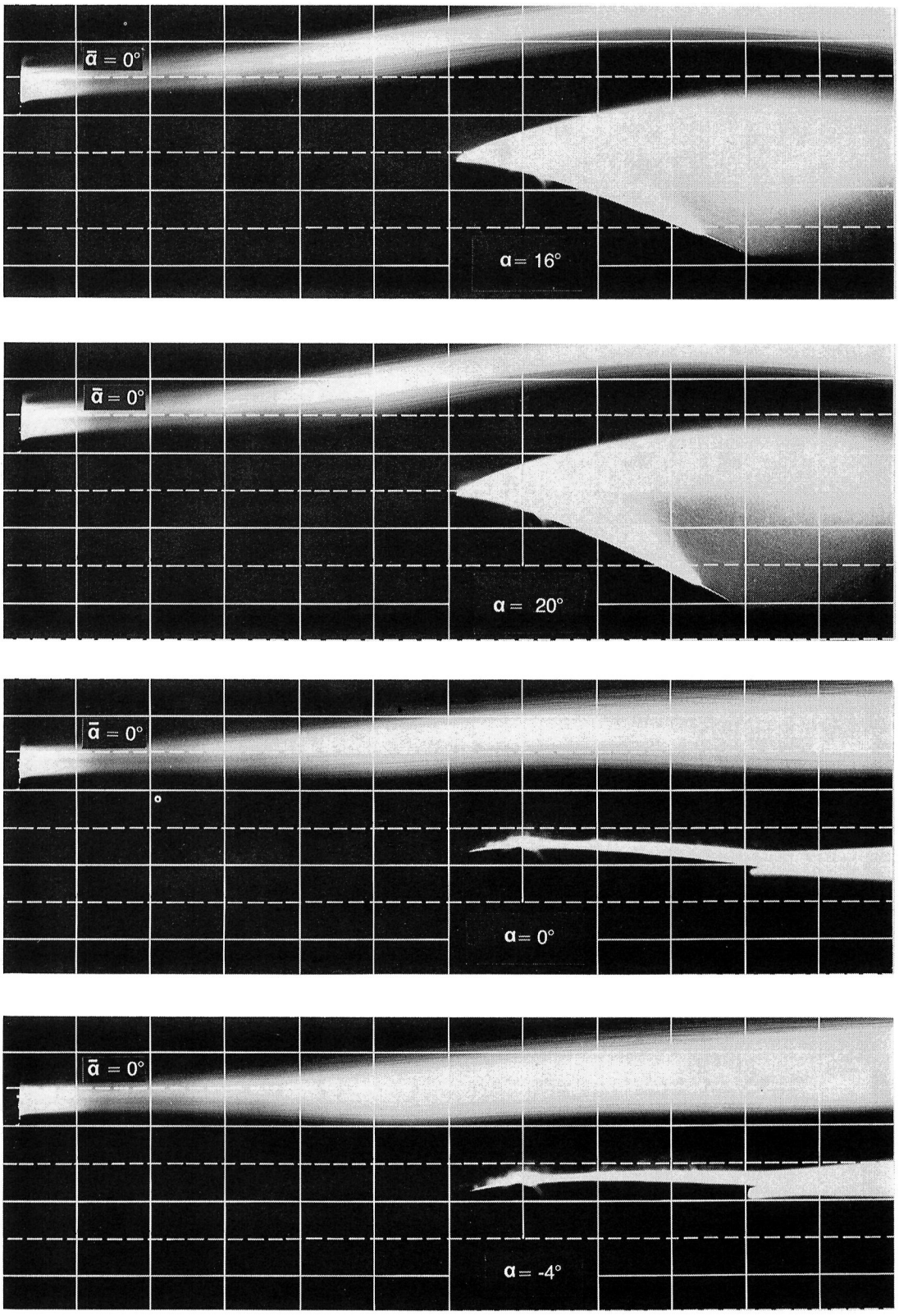

Figure 19.– Continued.

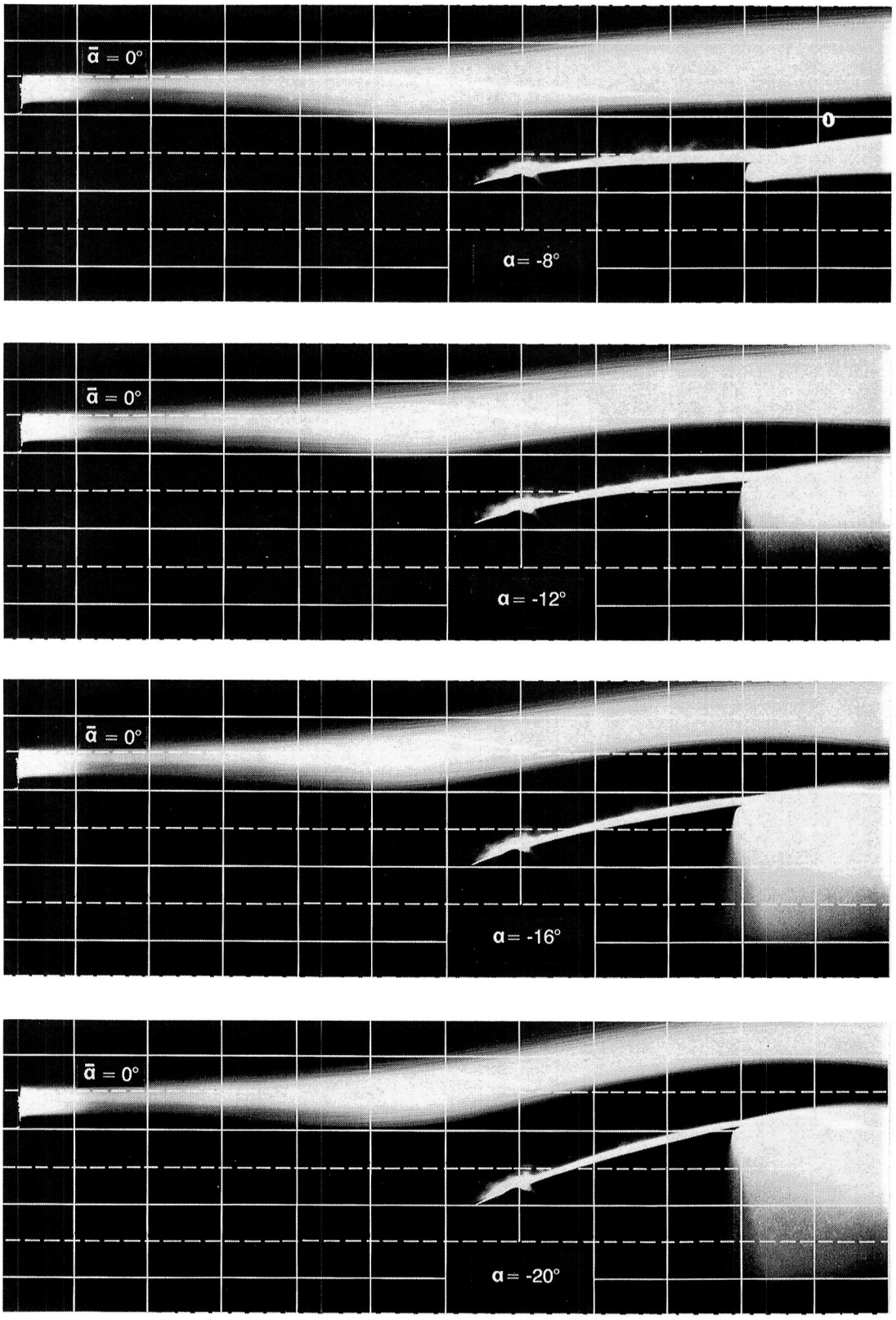

Figure 19.– Concluded.

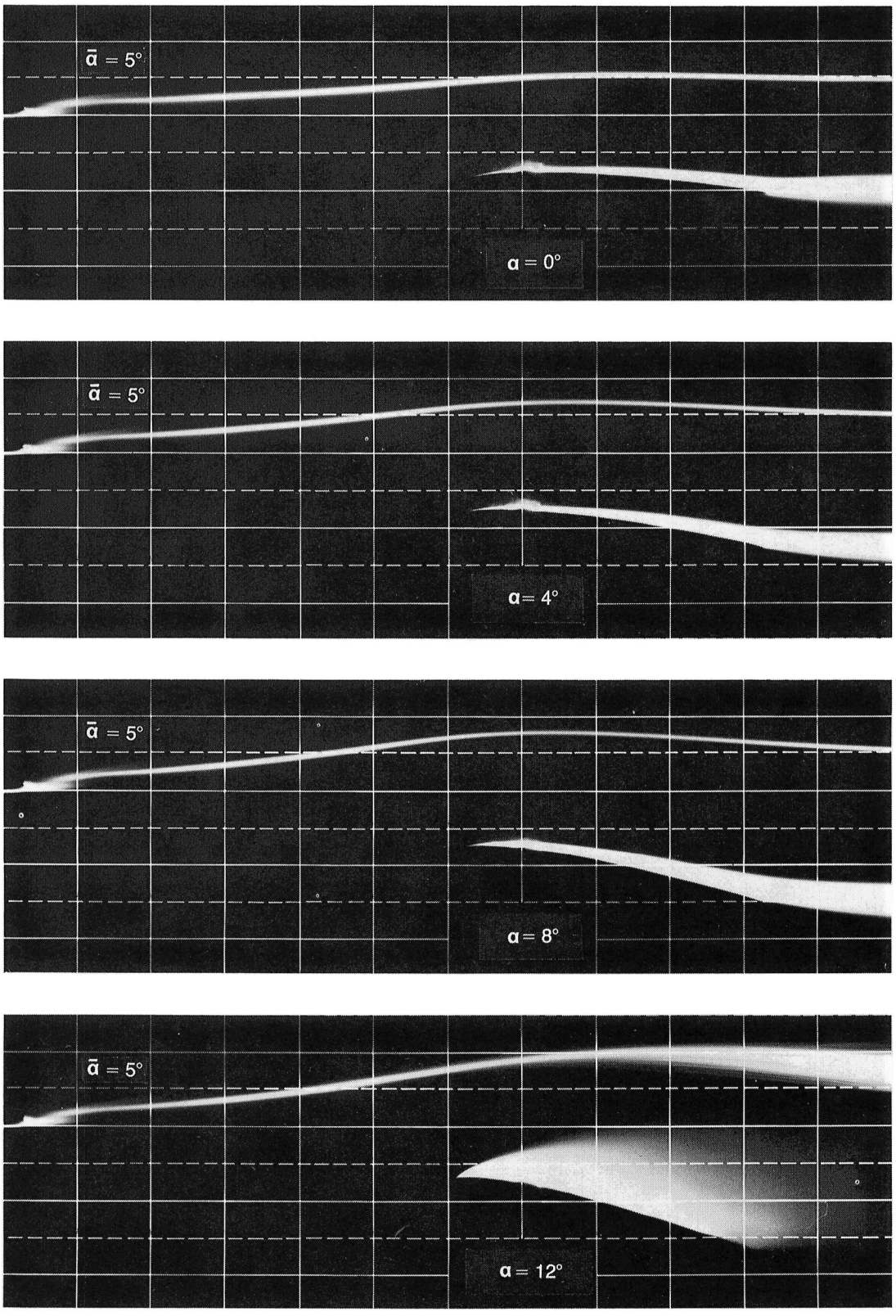

Figure 20.– Long-exposure visualization of flow at Re = 120,000 with generator off centerline and set at $\tilde{\alpha} = 5^\circ$ (weak-vortex case).

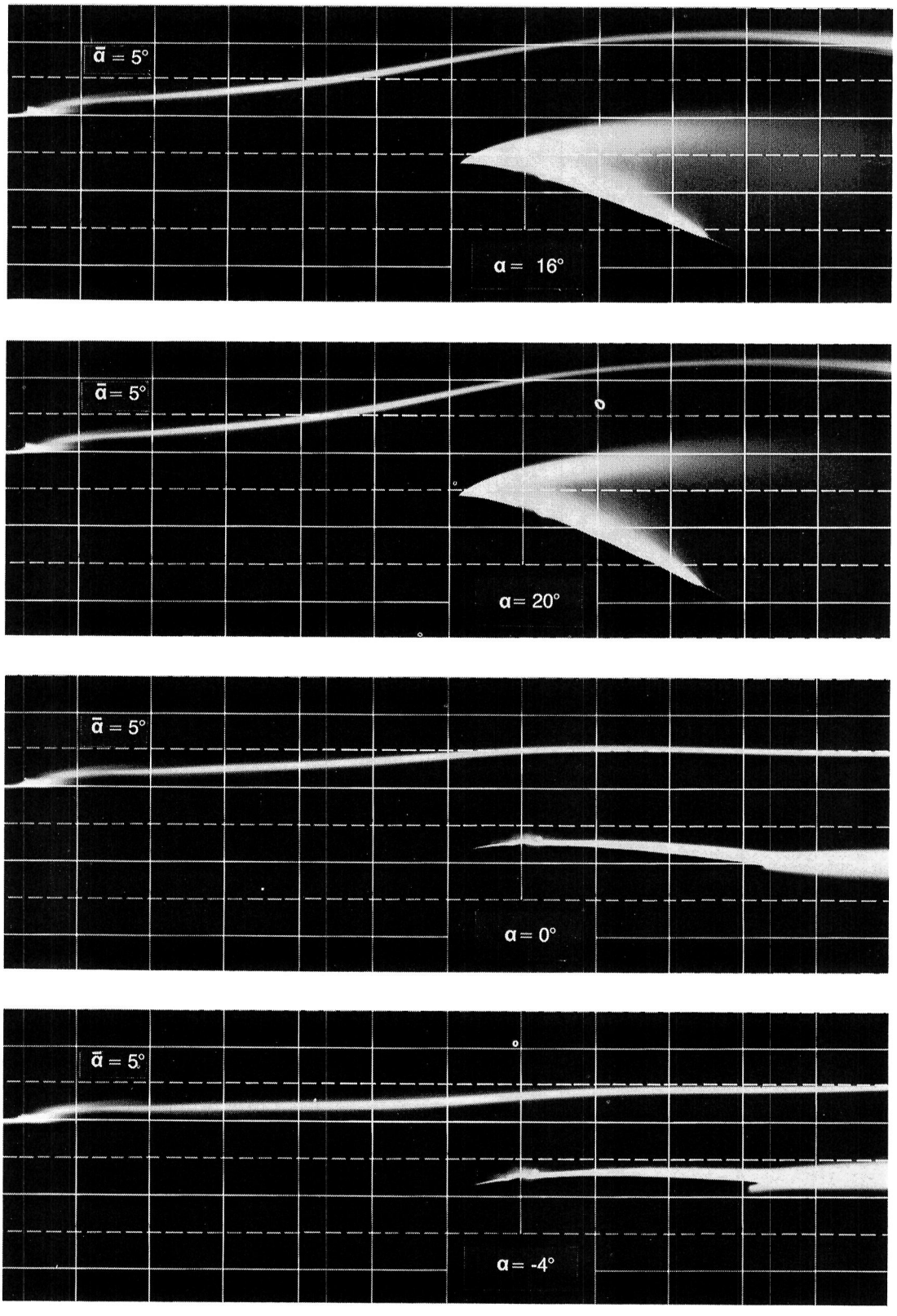

Figure 20.– Continued.

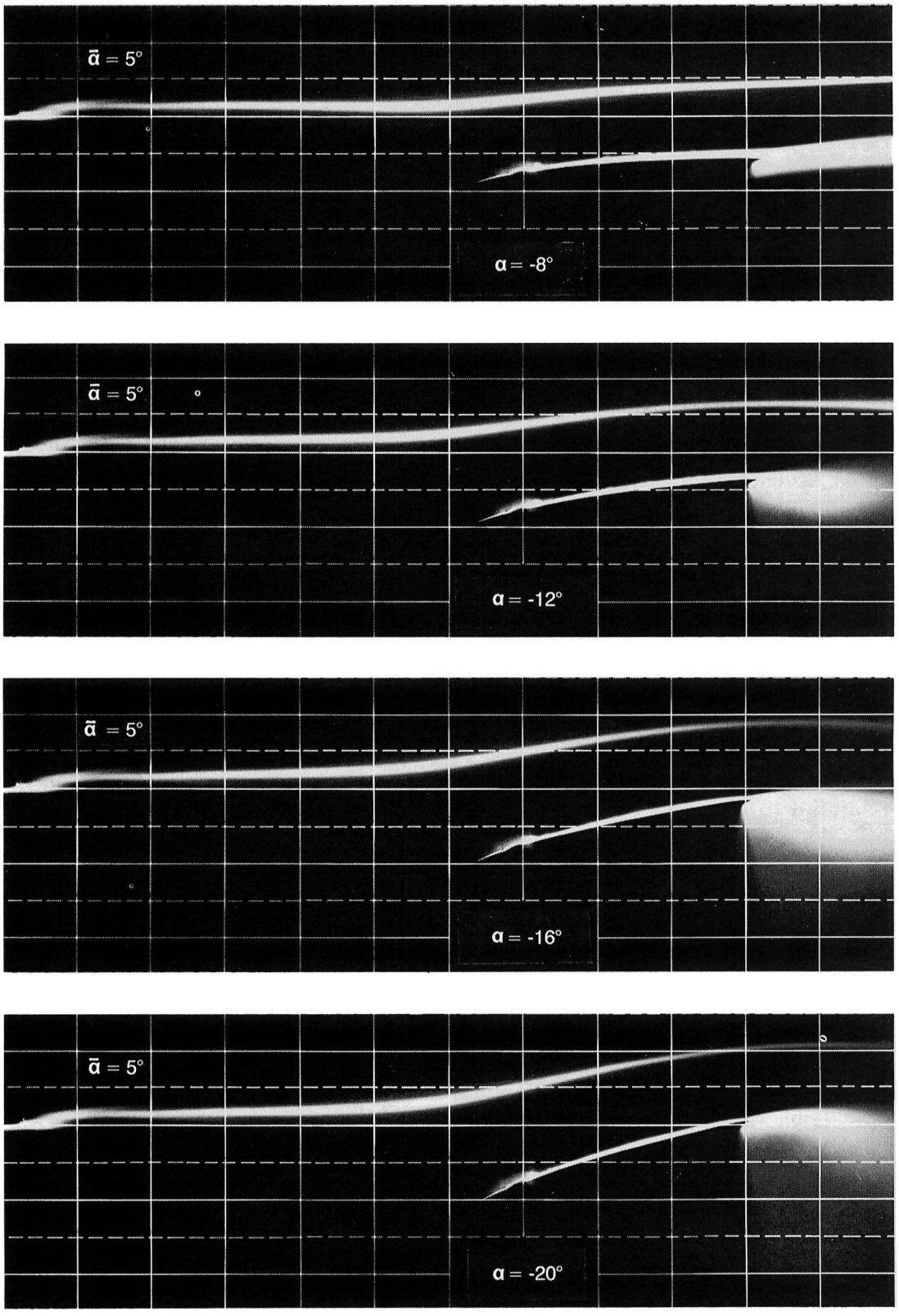

Figure 20.– Concluded.

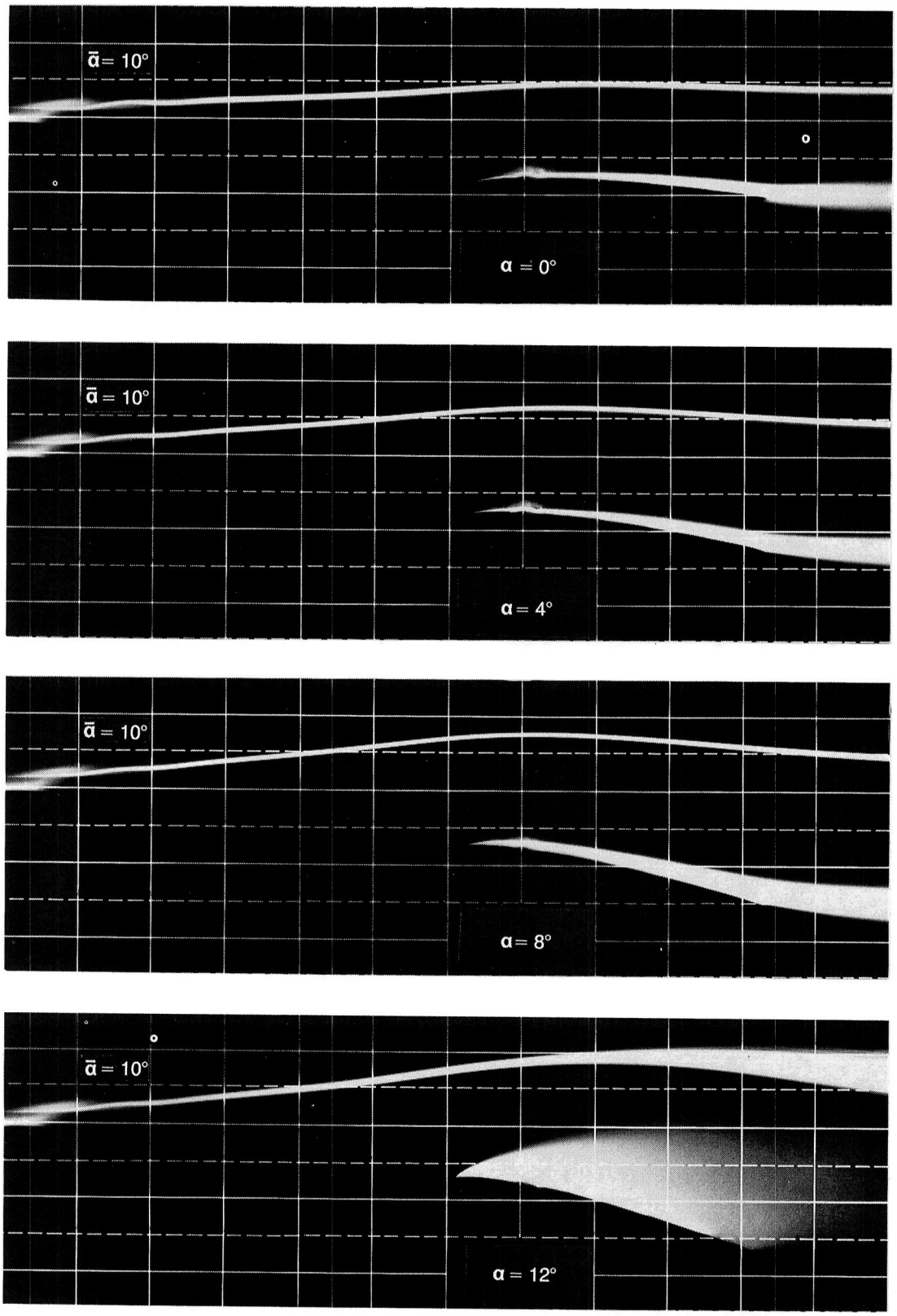

Figure 21.– Long-exposure visualization of flow at Re = 120,000 with generator off centerline and set at $\tilde{\alpha} = 10°$ (strong-vortex case).

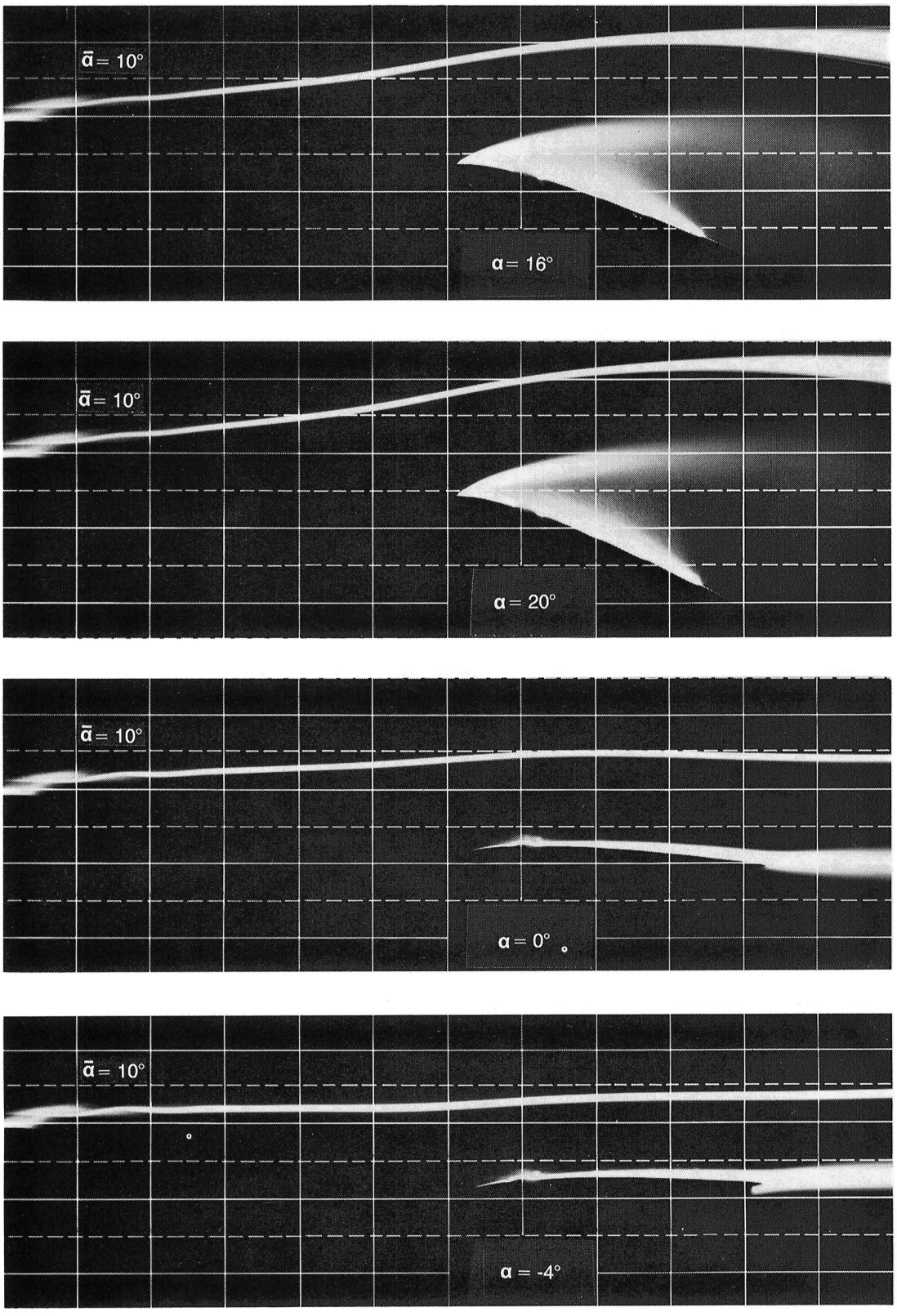

Figure 21.– Continued.

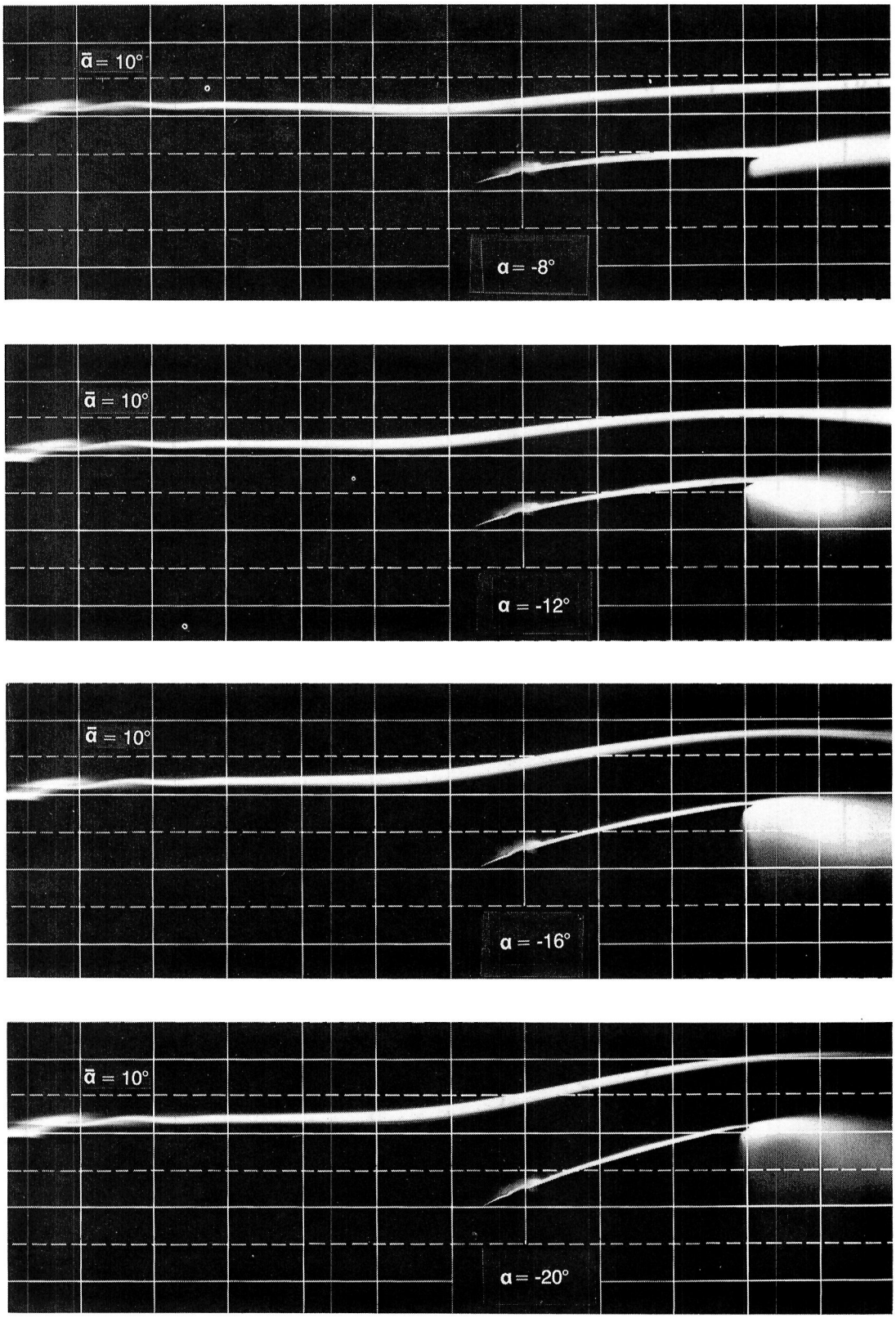

Figure 21.– Concluded.

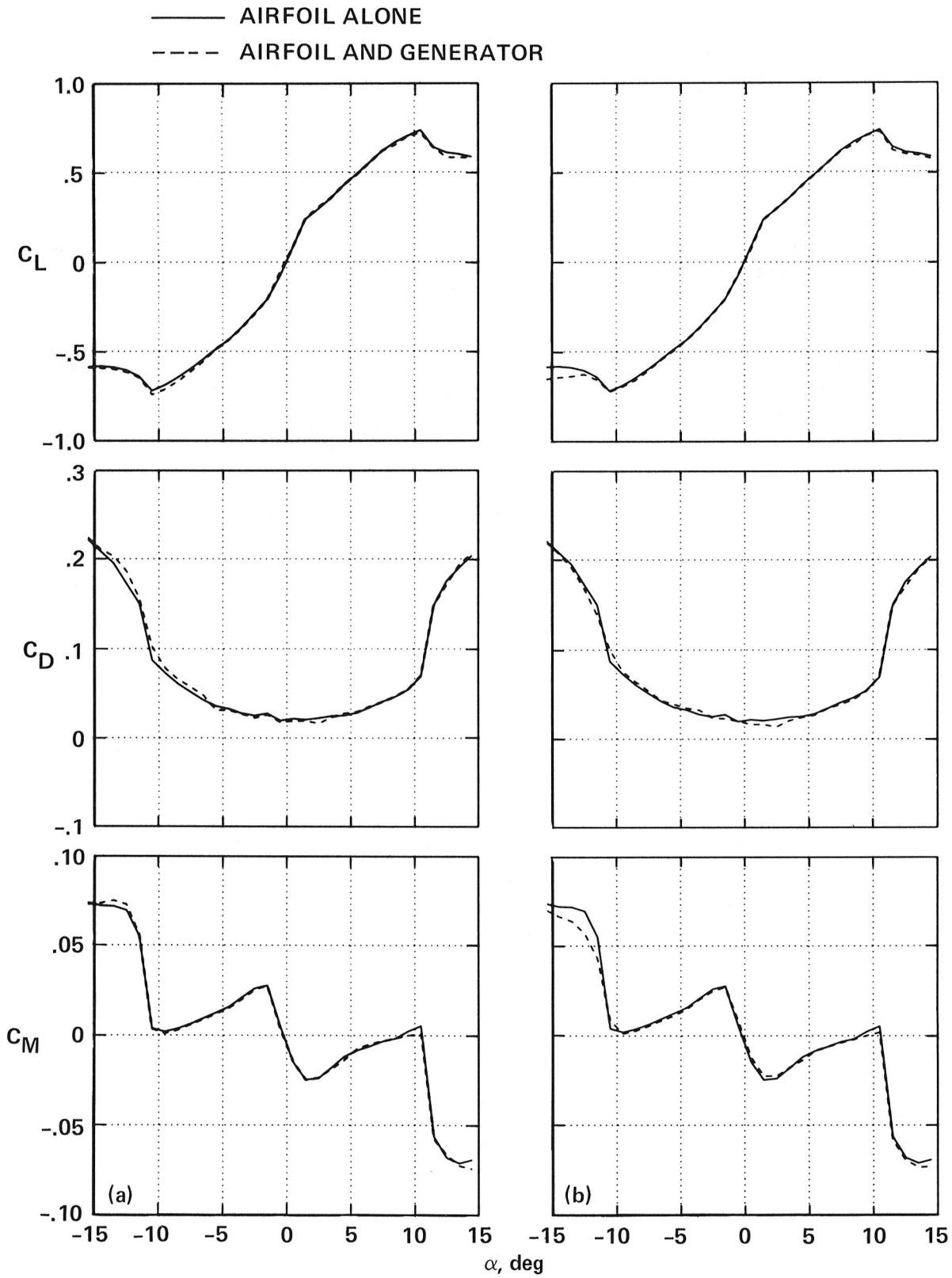

(a) Generator on centerline.

(b) Generator off centerline.

Figure 22.– Generator wake effects on airfoil loads when $\tilde{\alpha} = 0°$.

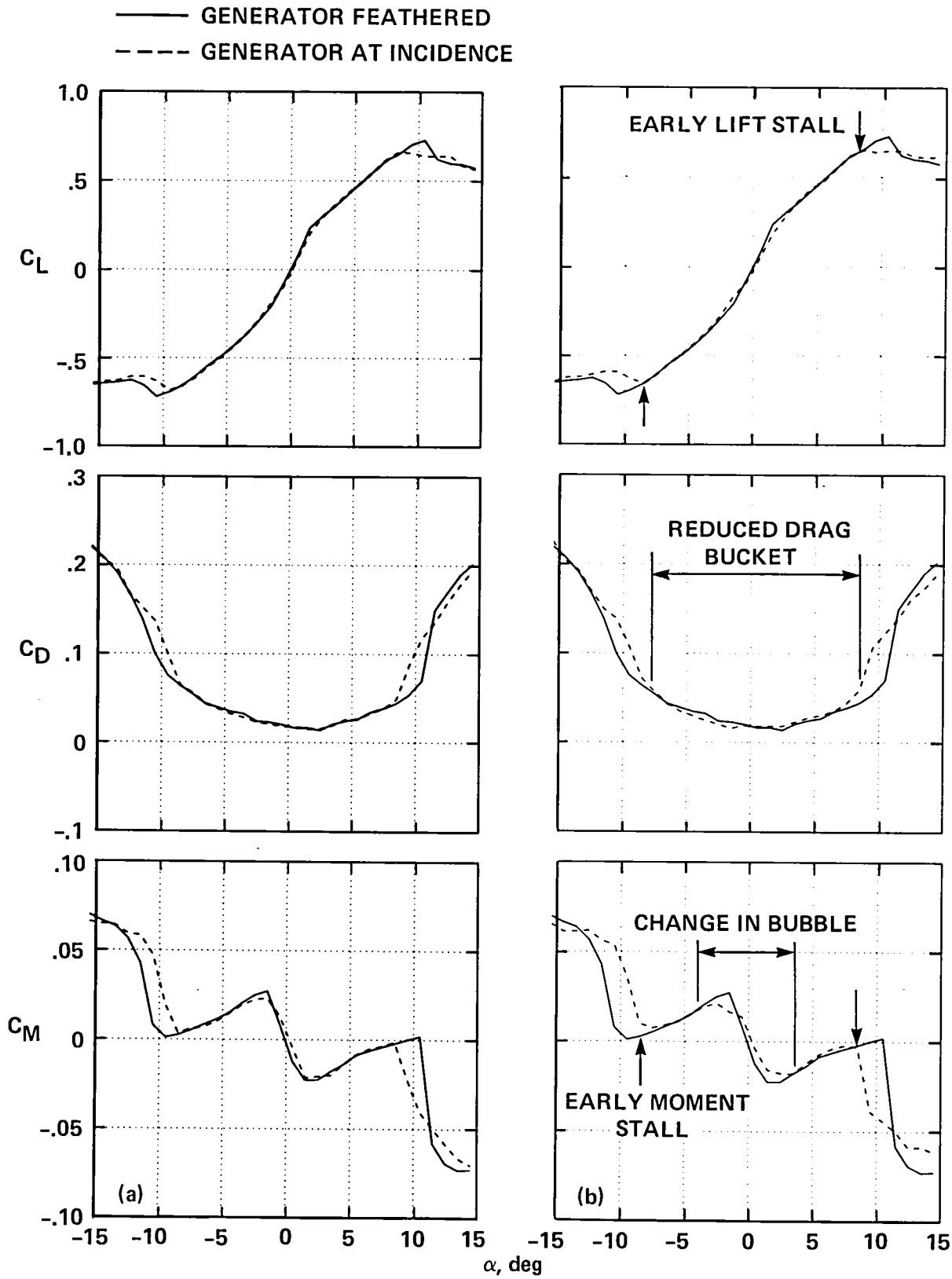

(a) $\tilde{\alpha} = 5°$.

(b) $\tilde{\alpha} = 10°$.

Figure 23.– Airfoil loads during vortex encounter with generator on centerline.

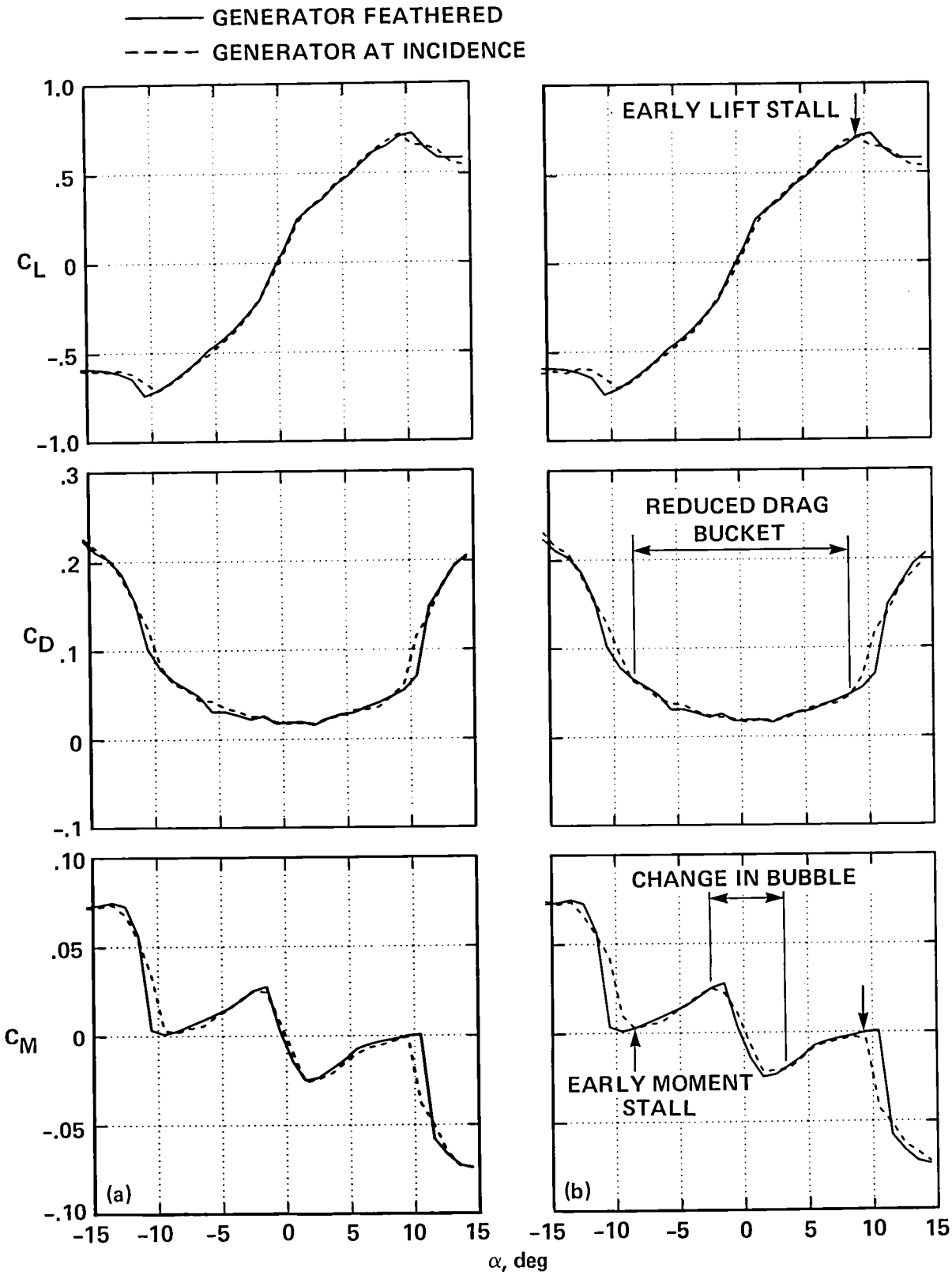

(a) $\tilde{\alpha} = 5°$.

(b) $\tilde{\alpha} = 10°$.

Figure 24.– Airfoil loads during vortex encounter with generator off centerline.

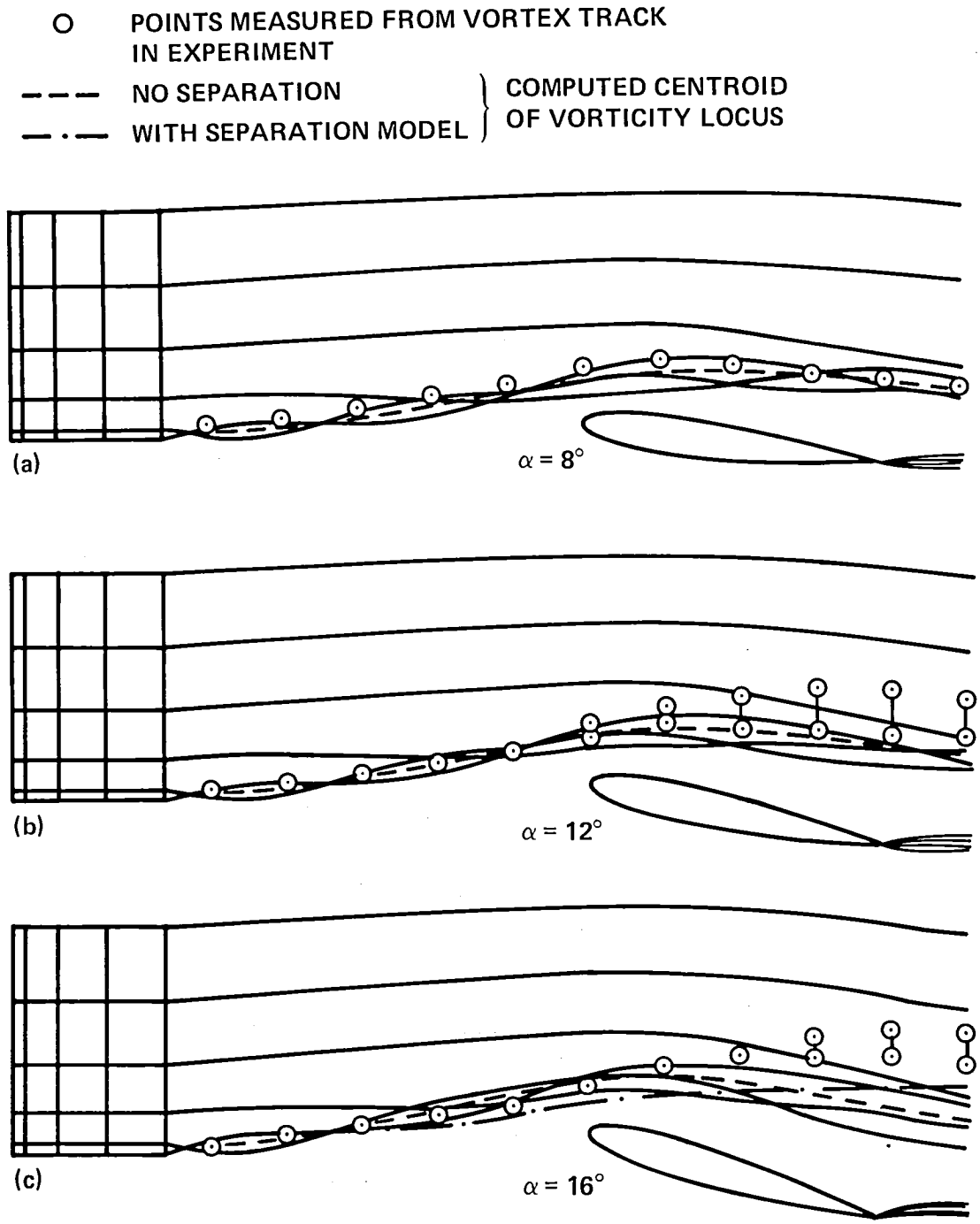

(a) $\alpha = +8°$.

(b) $\alpha = +12°$.

(c) $\alpha = +16°$.

Figure 25.– Comparison of theory and experiment.

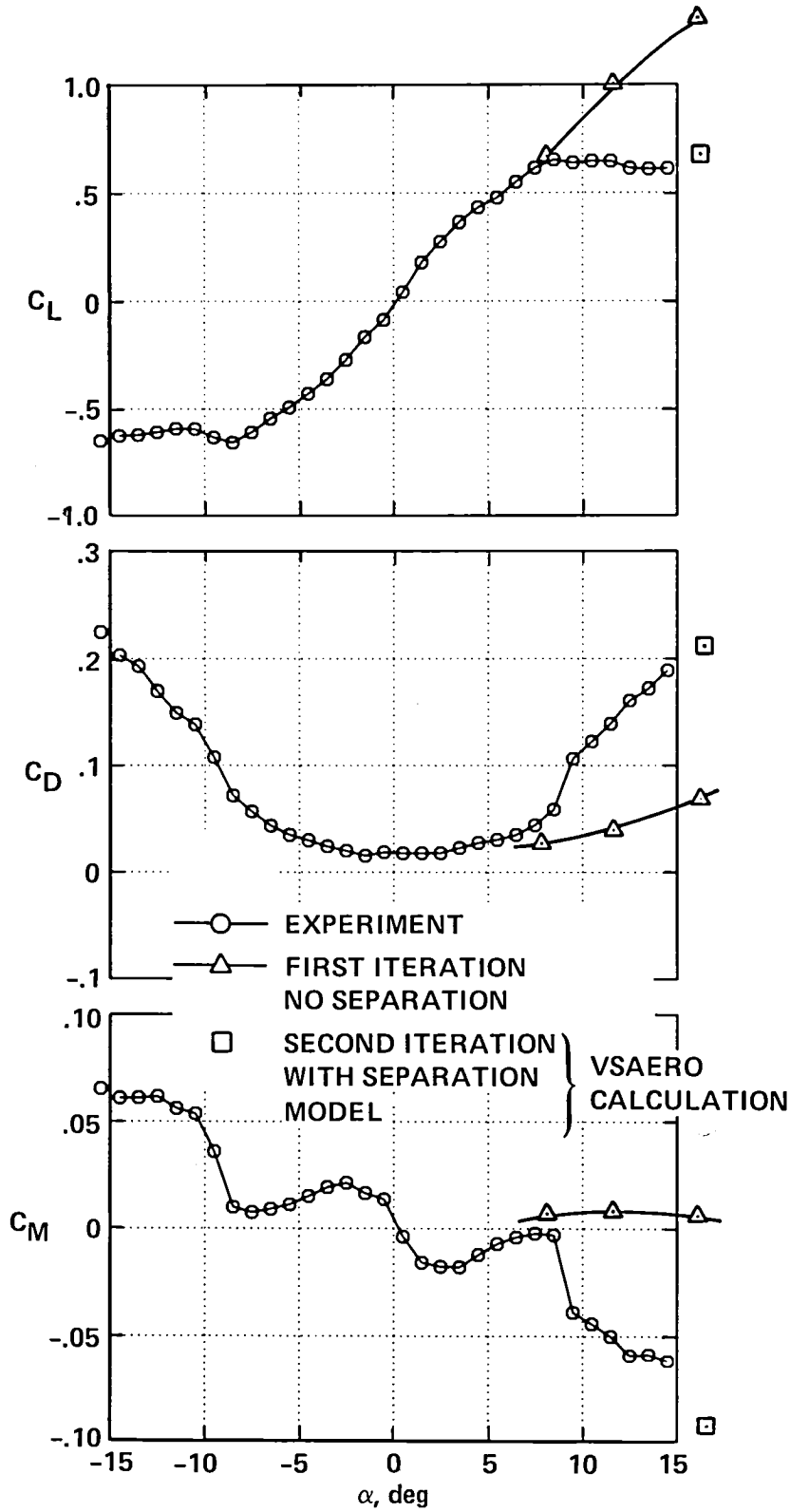

Figure 26.– Comparison of theory and experiment over separated region.

1. Report No.	2. Government Accession No.	3. Recipient's Catalog No.
NASA TP-2273 AVSCOM TR 83-A-17		

4. Title and Subtitle	5. Report Date
AIRFOIL INTERACTION WITH AN IMPINGING VORTEX	February 1984
	6. Performing Organization Code

7. Author(s)	8. Performing Organization Report No.
K. W. McAlister and C. Tung	A-9543
	10. Work Unit No. K-1585

9. Performing Organization Name and Address	11. Contract or Grant No.
Aeromechanics Laboratory USAAVSCOM Research and Technology Laboratories NASA Ames Research Center Moffett Field, CA 94035	

12. Sponsoring Agency Name and Address	13. Type of Report and Period Covered
National Aeronautics and Space Administration Washington, DC 20546 and U.S. Army Aviation Systems Command St. Louis, MO 63166	Technical Paper
	14. Sponsoring Agency Code 992-21-01

15. Supplementary Notes

K. W. McAlister and C. Tung: Aeromechanics Laboratory, USAAVSCOM Research and Technology Laboratories.

Point of Contact: K. W. McAlister, Ames Research Center, MS 215-1, Moffett Field, Calif. 94035 (415)965-5892 or FTS 448-5892

16. Abstract

The tip of a finite-span airfoil was used to generate a streamwise vortical flow, the strength of which could be varied by changing the incidence of the airfoil. The vortex that was generated traveled downstream and interacted with a second airfoil on which measurements of lift, drag, and pitching moment were made. The flow field, including the vortex core, was visualized in order to study the structural alterations to the vortex resulting from various levels of encounter with the downstream airfoil. These observations were also used to evaluate the accuracy of a theoretical model.

17. Key Words (Suggested by Author(s))	18. Distribution Statement
Vortex interaction Vortex instability Airfoil stall	Unclassified - Unlimited Subject Category: 02

19. Security Classif. (of this report)	20. Security Classif. (of this page)	21. No. of Pages	22. Price*
Unclassified	Unclassified	86	A02

*For sale by the National Technical Information Service, Springfield, Virginia 22161

NASA-Langley, 1984

NASA